THE AERONAUTICAL QUARTERLY

A Journal devoted to Aeronautics and the Allied Sciences

Volume XI FEBRUARY 1960 Part 1

CONTENTS

The Estimation of Laminar Skin Friction, including the Effects of Distributed Suction — *N. Curle*

A Theory for Flow with Axial Symmetry in Centrifugal Impellers Running at Low Speed — *R. J. Tonks and A. G. Smith*

Vibration of Rectangular Plates Point-Supported at the Corners — *Hugh L. Cox and J. Boxer*

The Pressure Distribution on a Wing with a Subsonic Leading Edge in the Presence of Anti-Symmetric Body Shaping — *J. G. Jones*

Struts with Linearly Varying Axial Loading — *J. S. Przemieniecki*

Some Properties of the Admittances of Dynamical Chains — *W. J. Duncan*

Correspondence on "Impulsive and Indicial Admittances of Simple Dynamical Chains" by W. J. Duncan — *R. J. Fitzgerald*

LONDON

ROYAL AERONAUTICAL SOCIETY

4 HAMILTON PLACE W1

15/-

THE AERONAUTICAL QUARTERLY

Editorial Board

Dr. A. M. BALLANTYNE, T.D., B.Sc., Ph.D., Hon.F.C.A.I. F.I.A.S., F.R.Ae.S. (*Chairman*)

Mr. HAYNE CONSTANT, C.B., C.B.E., M.A., F.R.S., F.R.Ae.S.

Sir HAROLD ROXBEE COX, D.Sc., D.I.C., Ph.D., F.I.A.S., F.R.Ae.S.

Sir WILLIAM FARREN, C.B., M.B.E., M.A., D.Sc., F.R.S., Hon.F.I.A.S., Hon.F.R.Ae.S.

Sir ARNOLD HALL, M.A., F.R.S., F.R.Ae.S.

Sir BENNETT MELVILL JONES, C.B.E., A.F.C., M.A., F.R.S., Hon.F.I.A.S., Hon.F.R.Ae.S.

Sir ALFRED PUGSLEY, O.B.E., D.Sc., F.R.S., F.R.Ae.S.

Sir GEOFFREY TAYLOR, M.A., D.Sc., F.R.S., Hon.F.R.Ae.S.

Dr. P. B. WALKER, C.B.E., M.A., F.R.Ae.S.

Editor—E. C. PIKE, M.A., A.F.R.Ae.S.

Editorial Referees

Aerodynamics

(a) General

Sir LEONARD BAIRSTOW
Mr. D. KEITH-LUCAS
Prof. W. A. MAIR
Mr. L. F. NICHOLSON
Dr. R. C. PANKHURST
Mr. E. F. RELF
Prof. E. J. RICHARDS
Dr. B. THWAITES

(b) Fluid Motion

Dr. G. K. BATCHELOR
Mr. A. FAGE
Dr. D. W. HOLDER
Prof. L. HOWARTH
Dr. W. P. JONES
Dr. J. W. MACCOLL
Prof. J. H. PRESTON
Prof. H. B. SQUIRE
Prof. G. TEMPLE
Prof. G. N. WARD
Prof. A. D. YOUNG

(c) Stability and Control

Mr. L. W. BRYANT
Mr. S. B. GATES
Mr. H. B. IRVING
Mr. G. H. LEE
Mr. M. B. MORGAN
Mr. H. H. B. M. THOMAS

Helicopters and Propellers

Prof. J. A. J. BENNETT
Mr. P. BRETT
Mr. L. G. FAIRHURST
Mr. R. HAFNER
Dr. G. S. HISLOP
Capt. R. N. LIPTROT

Instruments and Electrical Equipment

Dr. G. E. BAIRSTO
Sir GEORGE GARDNER
Dr. C. S. HUDSON
Mr. C. N. JAQUES
Mr. F. W. MEREDITH

Aircraft Design

Mr. R. BOORMAN
Mr. R. M. CLARKSON
Mr. A. N. CLIFTON
Mr. H. H. GARDNER
Mr. H. KNOWLER
Mr. W. E. W. PETTER
Mr. F. H. POLLICUTT
Dr. A. E. RUSSELL
Mr. R. S. STAFFORD
Mr. W. H. STEPHENS

Radio and Radar

Mr. J. F. ATHERTON
Mr. B. G. GATES
Dr. R. L. SMITH ROSE
Dr. A. M. UTTLEY
Sir ROBERT WATSON-WATT

Aviation Medicine

Dr. K. G. BERGIN
Dr. A. BUCHANAN BARBOUR

Meteorology

Sir DAVID BRUNT
Mr. J. K. HARDY
Prof. P. A. SHEPPARD

Sound

Mr. W. MAKINSON
Mr. F. B. GREATREX
Mr. N. FLEMING

Aircraft Propulsion

Mr. A. D. BAXTER
Mr. A. V. CLEAVER
Sir A. H. ROY FEDDEN
Dr. S. HOOKER
Mr. A. R. HOWELL
Mr. W. H. LINDSEY
Mr. P. LLOYD
Dr. A. W. MORLEY
Dr. E. S. MOULT
Mr. N. S. MUIR
Mr. F. NIXON
Mr. F. M. OWNER
Mr. H. PEARSON
Sir DAVID PYE
Mr. H. SAMMONS
Prof. O. A. SAUNDERS
Prof. A. G. SMITH

Air Transport

Mr. A. C. CAMPBELL ORDE
Mr. P. G. MASEFIELD
Mr. N. E. ROWE
Mr. B. S. SHENSTONE
Mr. W. TYE

Aircraft Accessories

Mr. A. E. BINGHAM
Mr. W. C. CLOTHIER
Mr. H. G. CONWAY
Sir GEORGE DOWTY
Mr. R. GRAHAM
Mr. C. D. HOLLAND

Performance

Mr. H. DAVIES
Mr. D. R. NEWMAN
Mr. A. H. YATES

Flight Testing

Mr. R. R. DUDDY
Mr. P. A. HUPTON
Mr. E. T. JONES
Mr. S. SCOTT HALL
Mr. H. L. STEVENS

Structures

Prof. J. H. ARGYRIS
Mr. A. C. BROWN
Mr. H. L. COX
Mr. D. J. FARRAR
Prof. W. S. HEMP
Prof. R. HILL
Mr. H. B. HOWARD
Col. H. T. JESSOP
Mr. E. D. KEEN
Mr. F. A. KERRY
Dr. D. M. A. LEGGETT
Mr. R. L. LICKLEY
Prof. A. J. SUTTON PIPPARD
Prof. S. C. REDSHAW
Mr. R. H. SANDIFER
Sir RICHARD SOUTHWELL

Fuels and Oils

Mr. E. L. BASS
Dr. J. W. DRINKWATER
Prof. F. H. GARNER
Prof. W. E. GARNER
Dr. K. E. W. RIDLER
Dr. C. G. WILLIAMS

Materials

Dr. L. AITCHISON
Dr. N. P. ALLEN
Mr. G. FORREST
Prof. N. F. MOTT
Mr. L. ROTHERHAM
Dr. H. SUTTON
Dr. C. SYKES

Vibration and Flutter

Mr. E. G. BROADBENT
Prof. A. R. COLLAR
Prof. W. J. DUNCAN
Mr. H. TEMPLETON
Mr. M. O. W. WOLFE

The Estimation of Laminar Skin Friction, including the Effects of Distributed Suction

N. CURLE, M.Sc., Ph.D.

(Aerodynamics Division, National Physical Laboratory)

SUMMARY: Stratford's analysis of the laminar boundary layer near separation uses two physical ideas. In the outer part of the boundary layer, where viscous effects are small, the development is given by the condition that the total head is constant along streamlines, apart from a second-order correction for viscosity. Near the wall, however, viscous forces must balance the pressure forces, and the profile adjusts itself accordingly. Quantitatively these ideas yield a simple formula for predicting separation, which has been found to be particularly accurate.

In this paper it is indicated how the same approach may be used to yield the full distribution of skin friction along the wall. Further, the effects of suction may be incorporated into the method. Physically, suction affects the outer part of the boundary layer in that the streamlines are drawn towards the wall when suction is applied. At the wall, the balance between viscous and pressure forces is influenced by the momentum of the fluid which is sucked away. When these effects are accounted for quantitatively, the resulting formula for the skin friction is still very simple.

Several examples are considered, and comparison is made with exact theory and with approximate results by other methods. It is indicated that the method has a useful range of validity.

1. Introduction

Flow in the laminar boundary layer on a solid body has been treated by numerous workers, and many methods of solution have been devised, of varying speed and accuracy. (For a detailed summary, *see* Ref. 1.) If only the position of separation is required, the best method for obtaining accurate results is probably that due to Stratford[2]. If, in addition, it is necessary to estimate the detailed distribution of skin friction or the momentum and displacement thicknesses, then the method of Thwaites[3] is very efficient. The numerical accuracy of Thwaites's method and the speed of Stratford's method were both later improved by Curle and Skan[4]. If, however, one wishes to know accurately the shape of the boundary-layer profile, as is necessary for a stability calculation, then a more powerful (and more lengthy) method must be used, such as that due to Head[5].

When one considers the boundary layer with suction (or blowing), accurate methods are hard to find and the only method in which one can really place any

Received May 1959.

[The Aeronautical Quarterly, Vol. XI, February 1960]

THE AERONAUTICAL QUARTERLY

Editorial Board

Dr. A. M. BALLANTYNE, T.D., B.Sc., Ph.D., Hon.F.C.A.I. F.I.A.S., F.R.Ae.S. (*Chairman*)

Mr. HAYNE CONSTANT, C.B., C.B.E., M.A., F.R.S., F.R.Ae.S.

Sir HAROLD ROXBEE COX, D.Sc., D.I.C., Ph.D., F.I.A.S., F.R.Ae.S.

Sir WILLIAM FARREN, C.B., M.B.E., M.A., D.Sc., F.R.S., Hon.F.I.A.S., Hon.F.R.Ae.S.

Sir ARNOLD HALL, M.A., F.R.S., F.R.Ae.S.

Sir BENNETT MELVILL JONES, C.B.E., A.F.C., M.A., F.R.S., Hon.F.I.A.S., Hon.F.R.Ae.S.

Sir ALFRED PUGSLEY, O.B.E., D.Sc., F.R.S., F.R.Ae.S.

Sir GEOFFREY TAYLOR, M.A., D.Sc., F.R.S., Hon.F.R.Ae.S.

Dr. P. B. WALKER, C.B.E., M.A., F.R.Ae.S.

Editor—E. C. PIKE, M.A., A.F.R.Ae.S.

Editorial Referees

Aerodynamics

(a) *General*

Sir LEONARD BAIRSTOW
Mr. D. KEITH-LUCAS
Prof. W. A. MAIR
Mr. L. F. NICHOLSON
Dr. R. C. PANKHURST
Mr. E. F. RELF
Prof. E. J. RICHARDS
Dr. B. THWAITES

(b) *Fluid Motion*

Dr. G. K. BATCHELOR
Mr. A. FAGE
Dr. D. W. HOLDER
Prof. L. HOWARTH
Dr. W. P. JONES
Dr. J. W. MACCOLL
Prof. J. H. PRESTON
Prof. H. B. SQUIRE
Prof. G. TEMPLE
Prof. G. N. WARD
Prof. A. D. YOUNG

(c) *Stability and Control*

Mr. L. W. BRYANT
Mr. S. B. GATES
Mr. H. B. IRVING
Mr. G. H. LEE
Mr. M. B. MORGAN
Mr. H. H. B. M. THOMAS

Helicopters and Propellers

Prof. J. A. J. BENNETT
Mr. P. BREIT
Mr. L. G. FAIRHURST
Mr. R. HAFNER
Dr. G. S. HISLOP
Capt. R. N. LIPTROT

Instruments and Electrical Equipment

Dr. G. E. BAIRSTO
Sir GEORGE GARDNER
Dr. C. S. HUDSON
Mr. C. N. JAQUES
Mr. F. W. MEREDITH

Aircraft Design

Mr. R. BOORMAN
Mr. R. M. CLARKSON
Mr. A. N. CLIFTON
Mr. H. H. GARDNER
Mr. H. KNOWLER
Mr. W. E. W. PETTER
Mr. F. H. POLLICUTT
Dr. A. E. RUSSELL
Mr. R. S. STAFFORD
Mr. W. H. STEPHENS

Radio and Radar

Mr. J. F. ATHERTON
Mr. B. G. GATES
Dr. R. L. SMITH ROSE
Dr. A. M. UTTLEY
Sir ROBERT WATSON-WATT

Aviation Medicine

Dr. K. G. BERGIN
Dr. A. BUCHANAN BARBOUR

Meteorology

Sir DAVID BRUNT
Mr. J. K. HARDY
Prof. P. A. SHEPPARD

Sound

Mr. W. MAKINSON
Mr. F. B. GREATREX
Mr. N. FLEMING

Aircraft Propulsion

Mr. A. D. BAXTER
Mr. A. V. CLEAVER
Sir A. H. ROY FEDDEN
Dr. S. HOOKER
Mr. A. R. HOWELL
Mr. W. H. LINDSEY
Mr. P. LLOYD
Dr. A. W. MORLEY
Dr. E. S. MOULT
Mr. N. S. MUIR
Mr. F. NIXON
Mr. F. M. OWNER
Mr. H. PEARSON
Sir DAVID PYE
Mr. H. SAMMONS
Prof. O. A. SAUNDERS
Prof. A. G. SMITH

Air Transport

Mr. A. C. CAMPBELL ORDE
Mr. P. G. MASEFIELD
Mr. N. E. ROWE
Mr. B. S. SHENSTONE
Mr. W. TYE

Aircraft Accessories

Mr. A. E. BINGHAM
Mr. W. C. CLOTHIER
Mr. H. G. CONWAY
Sir GEORGE DOWTY
Mr. R. GRAHAM
Mr. C. D. HOLLAND

Performance

Mr. H. DAVIES
Mr. D. R. NEWMAN
Mr. A. H. YATES

Flight Testing

Mr. R. R. DUDDY
Mr. P. A. HUFTON
Mr. E. T. JONES
Mr. S. SCOTT HALL
Mr. H. L. STEVENS

Structures

Prof. J. H. ARGYRIS
Mr. A. C. BROWN
Mr. H. L. COX
Mr. D. J. FARELL
Prof. W. S. HEMP
Prof. R. HILL
Mr. H. B. HOWARD
Col. H. T. JESSOP
Mr. E. D. KEEN
Mr. F. A. KERRY
Dr. D. M. A. LEGGETT
Mr. R. L. LICKLEY
Prof. A. J. SUTTON PIPPARD
Prof. S. C. REDSHAW
Mr. R. H. SANDIFER
Sir RICHARD SOUTHWELL

Fuels and Oils

Mr. E. L. BASS
Dr. J. W. DRINKWATER
Prof. F. H. GARNER
Prof. W. E. GARNER
Dr. K. E. W. RIDLER
Dr. C. G. WILLIAMS

Materials

Dr. L. AITCHISON
Dr. N. P. ALLEN
Mr. G. FORREST
Prof. N. F. MOTT
Mr. L. ROTHERHAM
Dr. H. SUTTON
Dr. C. SYKES

Vibration and Flutter

Mr. E. G. BROADBENT
Prof. A. R. COLLAR
Prof. W. J. DUNCAN
Mr. H. TEMPLETON
Mr. M. O. W. WOLFE

The Estimation of Laminar Skin Friction, including the Effects of Distributed Suction

N. CURLE, M.Sc., Ph.D.

(*Aerodynamics Division, National Physical Laboratory*)

SUMMARY: Stratford's analysis of the laminar boundary layer near separation uses two physical ideas. In the outer part of the boundary layer, where viscous effects are small, the development is given by the condition that the total head is constant along streamlines, apart from a second-order correction for viscosity. Near the wall, however, viscous forces must balance the pressure forces, and the profile adjusts itself accordingly. Quantitatively these ideas yield a simple formula for predicting separation, which has been found to be particularly accurate.

In this paper it is indicated how the same approach may be used to yield the full distribution of skin friction along the wall. Further, the effects of suction may be incorporated into the method. Physically, suction affects the outer part of the boundary layer in that the streamlines are drawn towards the wall when suction is applied. At the wall, the balance between viscous and pressure forces is influenced by the momentum of the fluid which is sucked away. When these effects are accounted for quantitatively, the resulting formula for the skin friction is still very simple.

Several examples are considered, and comparison is made with exact theory and with approximate results by other methods. It is indicated that the method has a useful range of validity.

1. Introduction

Flow in the laminar boundary layer on a solid body has been treated by numerous workers, and many methods of solution have been devised, of varying speed and accuracy. (For a detailed summary, *see* Ref. 1.) If only the position of separation is required, the best method for obtaining accurate results is probably that due to Stratford[2]. If, in addition, it is necessary to estimate the detailed distribution of skin friction or the momentum and displacement thicknesses, then the method of Thwaites[3] is very efficient. The numerical accuracy of Thwaites's method and the speed of Stratford's method were both later improved by Curle and Skan[4]. If, however, one wishes to know accurately the shape of the boundary-layer profile, as is necessary for a stability calculation, then a more powerful (and more lengthy) method must be used, such as that due to Head[5].

When one considers the boundary layer with suction (or blowing), accurate methods are hard to find and the only method in which one can really place any

Received May 1959.

[The Aeronautical Quarterly, Vol. XI, February 1960]

confidence is that of Head[5]. As Head points out, any one-parameter method, which may give quite reasonable answers for solid boundaries, is at a distinct disadvantage when suction is applied, whereas his two-parameter method remains almost as accurate. The reason for this is that, if finite suction is applied at some position, then the curvature of the velocity profile at the wall will change accordingly, although the momentum thickness, for example, will be continuous. These independent conditions cannot, in general, be satisfied by a one-parameter family of profiles, for which reason the methods of Thwaites[6, 7] and Schlichting's[8] adaptation of the classical Pohlhausen[9] method give only a rough indication of the effects of suction.

The purpose of this present paper is twofold. Firstly it is indicated how the method used by Stratford can be extended so as to yield not only accurate predictions of separation, but also the detailed distribution of skin friction with equal accuracy. Secondly, and simultaneously, it is shown how the effects of distributed suction may be incorporated into the theory. Stratford's method was originally designed for dealing with flows in which a large pressure gradient caused a sharp curvature of the profile near the wall, while not greatly affecting the general shape in the outer part of the layer. One might reasonably hope, therefore, that the method would deal with sharp local profile curvatures caused by suction and so lead to a particularly speedy method.

The generalisation of Stratford's theory for retarded flow is first developed (Section 2), including the allowance to be made for an initial favourable pressure gradient (Section 3). Three distinct types of example are then worked out, the solutions in each case being compared with exact solutions or with accurate solutions by other approximate methods.

For flows without suction (Section 4) it is known that Stratford's method will usually yield accurate predictions of separation.[4] The detailed distribution of skin friction is derived in this paper for the problem in which the main stream velocity u_1 decreases linearly with distance x along the boundary[10], so that

$$u_1 = u_0 (1 - x/l), \quad . \quad . \quad . \quad . \quad . \quad (1)$$

where u_0 and l are a representative velocity and length respectively. In addition the skin friction is predicted in the region of adverse pressure gradient for Schubauer's experimental velocity distribution[11]. In each case the agreement with the exact solution is good. Further, a case with a uniform favourable pressure gradient is considered, corresponding to a main stream velocity

$$u_1 = u_0 (1 + x/l)^{1/2}. \quad . \quad . \quad . \quad . \quad . \quad (2)$$

No exact solution is available for this problem, but, as Thwaites's method usually yields accurate predictions of skin friction in regions of accelerated flow, a solution by his method has accordingly been obtained for comparison, and the two solutions give values for the local skin friction which differ nowhere by more than 7 per cent.

Further, the solution for large x may be compared with the exact asymptotic solution, corresponding to one of the Falkner-Skan similarity profiles[12]. The predicted skin friction is in error by only 3 per cent.

The method is then used (Section 5) for predicting separation in problems with prescribed suction and pressure gradient. We consider the linearly retarded main stream (equation (1)), with a uniform velocity of suction w_0. The position of separation is estimated for various values of a suction parameter $\sigma = w_0 [l/(u_0 \nu)]^{1/2}$, where ν is the kinematic viscosity. The results are compared with two solutions by approximate methods due to Thwaites[6, 7], and appear to be quite reasonable. Further, an estimate is made of the suction distribution which would just prevent separation, the main stream velocity (equation (1)) again being used. No exact solution to this problem is available, but a solution by Head[13], which is almost certainly quite accurate, is compared with the prediction of this paper. The present method indicates greater suction requirements immediately downstream of where suction is first applied, but the agreement is better some distance downstream.

The method is then applied (Section 6) to flows with zero pressure gradient and prescribed suction, the distribution of skin friction being predicted. The case of uniform suction is considered, in which the profile, of the Blasius type at the leading edge, gradually deforms into the asymptotic suction profile far downstream. The solution is compared with the exact solution of Iglisch[14]. For values of $w_0 [2x/(u_0 \nu)]^{1/2}$ less than about 0·2, the predicted skin friction is in error by less than 5 per cent, at a position where it is about 30 per cent greater than in the absence of suction. The more general problem is then considered, with a solid entry length and uniform suction applied downstream of a prescribed position. Here the Blasius solution is valid up to the position where suction is applied, and deforms downstream of this position into the asymptotic suction profile.

For flow without suction the method is thus both accurate and speedy. For flows with suction, however, the shortage of accurate numerical solutions makes it difficult to assess accuracy. What evidence is available indicates that the method should in general be at least as accurate as most of the one-parameter methods, as well as being considerably quicker to use. The question of accuracy is discussed at various points in the text.

NOTATION

x, z	Cartesian co-ordinates, parallel and perpendicular to wall
u, w	velocity components parallel to x- and z-axes respectively
l, l_0	representative lengths
σ, ξ	suction parameters, defined in equations (46) and (49) respectively
p	pressure
μ	viscosity
ρ	density
ν	kinematic viscosity, $=\mu/\rho$

ψ stream function

w_s velocity of suction, $= -w(0)$

τ skin friction at wall

a a function introduced in equation (10)

n, k constants

C_p pressure coefficient, $=(p-p_0)/(\frac{1}{2}\rho u_0^2)$

$T=\tau/\tau_B$

x_L a length, defined by equation (30)

$t_1=\xi^{1/2}(1-\xi_0/\xi)^{1/3}$

Suffixes

0 values at leading edge or at start of pressure rise

1 local values in main stream

w values at the wall

B Blasius profile

j position of join of inner and outer profile

m values at pressure minimum

2. Development of General Theory for Retarded Flow

The inner and outer portions of the boundary layer are considered separately. In deriving the theory attention will first be restricted, following Stratford, to flows in which the pressure is constant between $x=0$ and $x=x_0$, with a sharp but otherwise arbitrary pressure rise starting at $x=x_0$. In addition, we shall allow an arbitrary distribution of suction when $x>x_0$. If the pressure gradient is very great, then viscous forces will be dominated by pressure forces, except in a very thin layer near the wall. Hence it is permissible to consider the development of the outer layer by first assuming inviscid flow and then adding on a secondary correction for the effects of viscosity.

If we assume nearly inviscid flow when $x \geq x_0$, $z \geq z_j$, where z is the distance measured in a direction normal to the wall and suffix " j " refers to values at the join of the inner and outer layers, then in this region the total head is nearly constant along streamlines.

Thus
$$(\tfrac{1}{2}\rho u^2)_{x,\psi}=(\tfrac{1}{2}\rho u^2)_{x_0,\psi}-(p-p_0)+\Delta H, \quad . \quad . \quad . \quad (3)$$

where the stream function ψ is given by

$$\psi=\int_{x_0}^{x} w_s\,dx+\int_{0}^{z} u\,dz, \quad . \quad . \quad . \quad . \quad (4)$$

u is the velocity parallel to the wall, ρ is the density and p the pressure of the fluid, w_s is the velocity of suction and $\triangle H$ is the change in total head due to viscosity. Now the shape of the velocity profile in the outer layer is not greatly changed by a sharp pressure rise of the type being considered or by suction. Consequently the viscous forces are given approximately as if there were no pressure rise or suction. Accordingly the change of total head due to viscosity is

$$\triangle H=(\tfrac{1}{2}\rho u_B^2)_{x,\psi}-(\tfrac{1}{2}\rho u_B^2)_{x_0,\psi}, \qquad . \quad . \quad . \quad (5)$$

where u_B is the Blasius solution for a boundary layer with no pressure gradient. If this is superimposed on equation (3), noting that $u\equiv u_B$ when $x=x_0$, then the outer layer is given by

$$(\tfrac{1}{2}\rho u^2)_{x,\psi}=(\tfrac{1}{2}\rho u_B^2)_{x,\psi}-(p-p_0),$$

which may be written

$$u^2(x,\psi)=u_B^2(x,\psi)-\frac{2(p-p_0)}{\rho} \qquad . \quad . \quad . \quad . \quad (6)$$

This result may also be deduced algebraically from the boundary-layer equations, provided that terms of order $(x-x_0)^2$ may be neglected, as Stratford showed. Further, by similar arguments, which amount essentially to the differentiation of equation (6) with respect to ψ, it may be deduced that in the outer layer

$$\left(\frac{\partial u}{\partial z}\right)_{x,\psi}=\left(\frac{\partial u_B}{\partial z}\right)_{x,\psi} \qquad . \quad . \quad . \quad . \quad . \quad (7)$$

and

$$\left(\frac{\partial^2 u}{\partial z^2}\right)_{x,\psi}=\left(\frac{u}{u_B}\frac{\partial^2 u_B}{\partial z^2}\right)_{x,\psi} \qquad . \quad . \quad . \quad . \quad . \quad (8)$$

In the inner layer, in contrast, viscous forces become very important, so that when there is no suction the resultant viscous force on an element of fluid at the wall must exactly balance the pressure-gradient force. When there is suction, momentum is being transferred across the boundary and the equation representing the balance of forces at the wall is modified. This equation, which may be obtained by letting $z\longrightarrow 0$ in the momentum equation, is

$$\rho w_s\left(\frac{\partial u}{\partial z}\right)_w+\mu\left(\frac{\partial^2 u}{\partial z^2}\right)_w=\frac{dp}{dx}. \qquad . \quad . \quad (9)$$

It is assumed, generalising Stratford's analysis, that the velocity profile in the inner layer may be adequately represented by a form

$$\mu u=\tau z+\tfrac{1}{2}\left(\frac{dp}{dx}-\frac{\tau w_s}{\nu}\right)z^2+az^n, \qquad . \quad . \quad . \quad (10)$$

Here τ is the skin friction $\mu(\partial u/\partial z)_0$ and, for the moment, a and the constant n are arbitrary. The condition (9) is, of course, identically satisfied by (10), which holds for $x \geqslant x_0$, $z \leqslant z_j$.

It is now postulated that ψ, u, $\partial u/\partial z$ and $\partial^2 u/\partial z^2$ shall be continuous at the join of the inner and outer layers. These four conditions are sufficient to determine τ, a, z_j and ψ_j, with n appearing as an arbitrary parameter. As in Stratford's theory, the simplifying assumption is made that the inner layer is sufficiently thin for the Blasius profile to be linear throughout it. This will be true provided that

$$\frac{u_B(x, \psi_j)}{u_0} \leqslant k, \qquad (11)$$

where k is, say, 0·6, and must certainly be less than unity. The implications of this restriction will be examined later. Assuming that it holds, the Blasius profile is approximated by

$$u_B(x, \psi) = \left\{\frac{2\tau_B}{\mu}\psi\right\}^{1/2}, \qquad (12)$$

$$\left(\frac{\partial u_B}{\partial z}\right)_{x,\psi} = \frac{\tau_B}{\mu}, \qquad (13)$$

and

$$\left(\frac{\partial^2 u_B}{\partial z^2}\right)_{x,\psi} = 0, \qquad (14)$$

where τ_B is the skin friction for the Blasius layer, and relations (12) to (14) hold for $\psi \leqslant \psi_j$. The joining conditions then become

$$u_j^2 = \frac{2\tau_B}{\mu}\psi_j - \frac{2(p-p_0)}{\rho}, \qquad (15)$$

$$\mu\psi_j = \mu\int_{x_0}^{x} w_s\,dx + \tfrac{1}{2}\tau z_j^2 + \frac{1}{6}\left(\frac{dp}{dx} - \frac{\tau w_s}{\nu}\right)z_j^3 + \frac{a}{n+1}z_j^{n+1}, \qquad (16)$$

$$\mu u_j = \tau z_j + \frac{1}{2}\left(\frac{dp}{dx} - \frac{\tau w_s}{\nu}\right)z_j^2 + a z_j^n, \qquad (17)$$

$$\tau_B = \tau + \left(\frac{dp}{dx} - \frac{\tau w_s}{\nu}\right)z_j + n a z_j^{n-1}, \qquad (18)$$

$$0 = \frac{dp}{dx} - \frac{\tau w_s}{\nu} + n(n-1)a z_j^{n-2}. \qquad (19)$$

The solution of these five equations is fairly straightforward, and leads to the following result.

$$x^2\left\{\frac{dC_p}{dx}-\frac{2\tau w_s}{\mu u_0{}^2}\right\}^2\left\{C_p-\frac{2\tau_B}{\mu u_0{}^2}\int_{x_0}^{x} w_s\,dx\right\}$$

$$=\frac{(n-1)^3(n^2+3)}{3n^2(n+1)(n-2)^2}\,\frac{\tau_B{}^4x^2}{\mu^2\rho^2u_0{}^6}\left(1-\frac{\tau}{\tau_B}\right)^3\left\{1+\frac{3(n^2-1)}{n^2+3}\,\frac{\tau}{\tau_B}\right\}$$

$$=\frac{0{\cdot}00405\,(n-1)^3(n^2+3)}{n^2(n+1)(n-2)^2}\left(1-\frac{\tau}{\tau_B}\right)^3\left\{1+\frac{3(n^2-1)}{n^2+3}\,\frac{\tau}{\tau_B}\right\}, \quad . \quad (2$$

where C_p is the pressure coefficient, defined as $(p-p_0)/(\frac{1}{2}\rho u_0{}^2)$.

A criterion for separation is obtained by setting $\tau=0$ in equation (20). If this is done, then for the case of solid boundaries, $w_s=0$, it follows that

$$\left[x^2\left(\frac{dC_p}{dx}\right)^2 C_p\right]_{sep}=\frac{0{\cdot}00405\,(n-1)^3(n^2+3)}{n^2(n+1)(n-2)^2} \quad . \quad . \quad . \quad (21)$$

When $n=6$ the right-hand side becomes 0·0049, and when $n=4$ it becomes 0·0065, the values obtained by Stratford. Further, when $n=3$ it becomes 0·0108. Now Curle and Skan[4] showed that the best all-round accuracy in predicting separation would be obtained by taking the right-hand side of equation (21) equal to 0·0104, which corresponds to

$$n=3{\cdot}043. \quad . \quad . \quad . \quad . \quad . \quad . \quad (22)$$

Accordingly the theory will be developed assuming this value of n, so that the equation (20) for τ becomes

$$x^2\left\{\frac{dC_p}{dx}-\frac{2\tau_B w_s}{\mu u_0{}^2}T\right\}^2\left\{C_p-\frac{2\tau_B}{\mu u_0{}^2}\int_{x_0}^{x} w_s\,dx\right\}=0{\cdot}0104\,(1-T)^3(1+2{\cdot}02T), \quad (23)$$

$$\text{where} \qquad T=\tau/\tau_B. \quad . \quad . \quad . \quad . \quad . \quad . \quad (24)$$

The method is nominally applicable, according to condition (11), when

$$\frac{u_B(x,\psi_1)}{u_0}\leqslant k, \quad . \quad . \quad . \quad . \quad . \quad (25)$$

and, by relation (12), this condition becomes

$$\frac{2\tau_B}{\mu u_0{}^2}\psi_1\leqslant k^2, \quad . \quad . \quad . \quad . \quad . \quad (26)$$

where it can be shown that

$$\frac{2\tau_B}{\mu u_0^2}\psi_1=\frac{8{\cdot}916\,(1+1{\cdot}01T)}{(1-T)\,(1+2{\cdot}02T)}\left\{C_p-\frac{2\tau_B}{\mu u_0^2}\int_{x_0}^{x} w_s\,dx\right\}+\frac{2\tau_B}{\mu u_0^2}\int_{x_0}^{x} w_s\,dx. \quad . \quad (27)$$

When there is no suction, the method should be valid at separation provided that

$$8{\cdot}916\,(C_p)_{sep}\leqslant k^2. \quad . \quad . \quad . \quad . \quad . \quad (28)$$

Since k is about 0·6, and certainly is less than unity, it follows that the method should strictly apply only when $(C_p)_{sep}$ is less than about 0·04, with an absolute upper limit of about 0·11, and for greater values of C_p it should be necessary to use the exact joining conditions rather than the simpler ones which assume the linearity of the Blasius profile. Nevertheless, it has been found that the simpler method yields accurate predictions of separation for values of C_p as great as 0·25. It will be found in this paper that the method also applies far beyond its nominal range in predictions of the skin friction τ, and for flows with suction.

3. Allowance for Initial Favourable Pressure Gradient

The theory as developed in Section 2, although it does not exclude all accelerated flows, does assume that the initial velocity profile is of the Blasius type, which will be true if the leading edge is sharp. Boundary layers beginning at a stagnation point require different treatment.

Consider, then, a flow in which the main stream velocity $u_1(x)$ increases from zero at a stagnation point $x=0$, reaching a maximum (at the pressure minimum) and then decreasing again. Stratford indicated that at the position of the pressure minimum, $x=x_m$, the velocity profile would be very similar to the Blasius profile of an equivalent distance x_m-x_L. The position $x=x_L$ of the equivalent origin is determined by equating the known momentum thickness of the equivalent Blasius profile to the true boundary-layer momentum thickness at $x=x_m$.

Now, according to Thwaites's method, which predicts momentum thickness accurately, the true momentum thickness at a position x is given by

$$\delta_2^2=0{\cdot}45\nu u_1^{-6}\int_0^x u_1^5\,dx, \quad . \quad . \quad . \quad . \quad (29)$$

from which it may be shown that

$$x_L=x_m-\int_0^{x_m}\left(\frac{u_1}{u_m}\right)^5 dx. \quad . \quad . \quad . \quad . \quad (30)$$

The development of the boundary layer in $x \geqslant x_m$ will be given by the following modified form of equation (23):—

$$(x-x_L)^2 \left\{ \frac{dC_p}{dx} - \frac{2\tau_B w_s}{\mu u_m^2} T \right\}^2 \left\{ C_p - \frac{2\tau_B}{\mu u_m^2} \int_{x_m}^{x} w_s \, dx \right\} = 0{\cdot}0104\,(1-T)^3\,(1+2{\cdot}02T), \quad . \quad . \quad . \quad . \quad (31)$$

$$\text{where} \quad \frac{\tau_B}{\mu u_m^2} = \frac{0{\cdot}33206}{\{u_m \nu\,(x-x_L)\}^{1/2}} \quad . \quad . \quad . \quad . \quad . \quad (32)$$

and C_p is also defined in terms of the pressure and velocity at $x = x_m$. This form of the equation will be used in the particular application to flow past an elliptic cylinder (Section 4.2). It is to be noted that, for flows where the boundary layer begins at a stagnation point, the method cannot deal with suction upstream of the pressure minimum. This is not a serious drawback, from a practical point of view, as suction would normally be applied only in a region of retarded flow.

4. Application to Some Flows Without Suction

When there is no suction the general formula (31) becomes

$$(x-x_L)^2 \left(\frac{dC_p}{dx}\right)^2 C_p = 0{\cdot}0104\,(1-T)^3\,(1+2{\cdot}02T). \quad . \quad . \quad . \quad (33)$$

In this section three different velocity distributions are considered, and in each case $T(x)$ is determined for comparison with exact theory.

4.1. Linearly Retarded Velocity

In this example the main stream velocity is

$$u_1 = u_0\,(1 - x/l). \quad . \quad . \quad . \quad . \quad . \quad . \quad (34)$$

Since the flow is everywhere retarded, it follows that $x_L = 0$.

$$\text{Also} \quad C_p = 1 - \frac{u_1^2}{u_0^2} = 2\frac{x}{l} - \frac{x^2}{l^2}, \quad . \quad . \quad . \quad (35)$$

so equation (33) becomes

$$\left(\frac{x}{l}\right)^3 \left(1-\frac{x}{l}\right)^2 \left(2-\frac{x}{l}\right) = 0{\cdot}0026\,(1-T)^3\,(1+2{\cdot}02T). \quad . \quad . \quad (36)$$

The values of T have been computed for several values of x/l, and values of

$$\frac{1}{u_0}\left(\frac{\nu l}{u_0}\right)^{1/2} \left(\frac{\partial u}{\partial z}\right)_w = 0{\cdot}33206 \left(\frac{x}{l}\right)^{-1/2} T$$

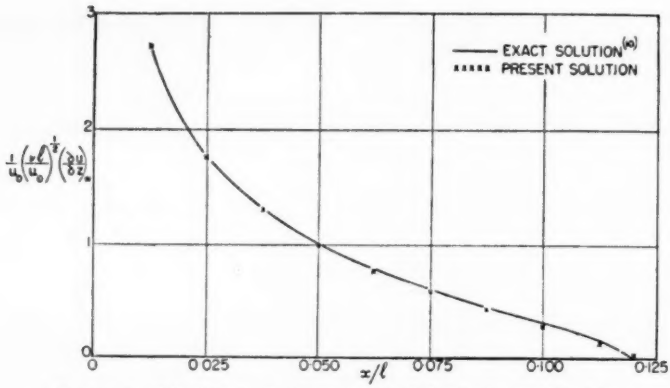

FIGURE 1. Skin friction for linearly retarded velocity distribution.

have been deduced therefrom. The results are shown in Table I and Fig. 1, as are the exact values obtained by Howarth[10]. The agreement, it will be noted, is very good, the distribution of skin friction being given accurately, except just upstream of the separation point, which, none the less, is determined to an accuracy of one per cent.

The values given by the approximate method of Thwaites[3], generally agreed to be one of the more accurate approximate methods, are of roughly the same accuracy as the present results.

4.2. SCHUBAUER'S EXPERIMENTAL DISTRIBUTION

Hartree[11] has examined the experimental pressure distribution obtained by Schubauer for flow past an elliptic cylinder. He has carried out a precise numerical integration of the boundary-layer equations, assuming Schubauer's experimentally obtained values of C_p, and prescribing dC_p/dx by numerical differentiation. With the minor axis of the ellipse as the representative length l, the pressure minimum is at $x/l = 1{\cdot}300$, and the velocity maximum is $u_m = 1{\cdot}295u_\infty$, where u_∞ is the velocity at infinity. The position of separation is $x/l = 1{\cdot}983$. The change of origin x_L, to account for the initial favourable pressure gradient, is easily calculated to be $x_L = 0{\cdot}394l$, whereupon the value of T can be obtained from equation (33) at each station $x/l \geqslant 1{\cdot}3$ for which C_p is given. From this is calculated

$$2\,(1{\cdot}295)^{3/2}\frac{1}{u_m}\left(\frac{\nu l}{u_m}\right)^{1/2}\left(\frac{\partial u}{\partial z}\right)_w = 0{\cdot}9791\left(\frac{x-x_L}{l}\right)^{-1/2}T,$$

which is equal to Hartree's "$2\partial^2\psi/\partial y^2$" in his Table 8. The results are shown in Table II, and again the agreement is extremely good. The skin friction is predicted to within 1 per cent for $1{\cdot}3 \leqslant x/l \leqslant 1{\cdot}8$, and the position of separation is also given to an accuracy of 1 per cent.

The accuracy in this case is rather better than that obtained by Thwaites's method. In general one would expect this to be so, since Stratford's method predicts the separation position even more accurately than Thwaites's method[4].

TABLE I

SKIN FRICTION FOR LINEARLY RETARDED VELOCITY
(SECTION 4.1)

x/l	$\frac{1}{u_0}\left(\frac{\nu l}{u_0}\right)^{1/2}\left(\frac{\partial u}{\partial z}\right)_w$		
	Predicted Value	*Exact Value*[10]	*Thwaites*[3]
0	∞	∞	
0·0125	2·733	2·739	
0·0250	1·762	1·772	1·765
0·0375	1·295	1·309	
0·0500	0·995	1·011	1·019
0·0625	0·772	0·790	
0·0750	0·591	0·613	0·631
0·0875	0·435	0·459	
0·1000	0·289	0·315	0·348
0·1125	0·140	0·163	
0·1200	0·029	0·000	0·072

TABLE II

SKIN FRICTION FOR SCHUBAUER'S PRESSURE DISTRIBUTION
(SECTION 4.2)

x/l	$2\,(1{\cdot}295)^{3/2}\frac{1}{u_m}\left(\frac{\nu l}{u_m}\right)^{1/2}\left(\frac{\partial u}{\partial z}\right)_w$		
	Predicted Value	*Exact Value*[11]	*Thwaites*[3]
1·30	1·029		
1·40	0·958	0·943	0·912
1·50	0·829		
1·60	0·685	0·687	0·643
1·70	0·542		
1·80	0·399	0·395	0·346
1·85	0·314		
1·90	0·230		
1·95	0·143		
2·00	0·033		

TABLE III

SKIN FRICTION FOR UNIFORM FAVOURABLE PRESSURE GRADIENT
(SECTION 4.3)

x/l	*Values of T*		x/l	*Values of T*	
	Equation (39)	*Thwaites*[3]		*Equation* (39)	*Thwaites*[3]
0	1·000	1·000	0·7	2·718	2·616
0·1	1·298	1·263	0·8	2·923	2·810
0·2	1·568	1·519	0·9	3·124	3·004
0·3	1·820	1·735	1·0	3·318	3·194
0·4	2·058	1·915	1·1	3·509	3·378
0·5	2·287	2·133	1·2	3·697	3·561
0·6	2·507	2·377			

4.3. Uniform Favourable Pressure Gradient

We consider now the accelerated velocity distribution

$$u_1 = u_0 (1 + x/l)^{1/2}, \quad . \quad . \quad . \quad . \quad . \quad . \quad (37)$$

which corresponds to a pressure coefficient

$$C_p = -x/l. \quad . \quad . \quad . \quad . \quad . \quad . \quad (38)$$

Although the flow is everywhere accelerated, $x_L = 0$, nevertheless, since there is no stagnation point. So equation (33) becomes

$$(x/l)^5 = 0{\cdot}0104\,(T-1)^5\,(1+2{\cdot}02T), \quad . \quad . \quad . \quad . \quad (39)$$

from which T may be deduced as a function of x/l, as shown in Table III. No exact solution is available for purposes of comparison, but it may be deduced from equation (39) that, for small x/l, T may be expanded in a series

$$T = 1 + 3{\cdot}17x/l \ldots\ldots, \quad . \quad . \quad . \quad . \quad (40)$$

and that, for large x/l, the asymptotic form is

$$T = 2{\cdot}627\,(x/l)^{3/4} \ldots\ldots \quad . \quad . \quad . \quad . \quad (41)$$

Now the exact values of the numerical coefficients in relations (40) and (41) may be found as follows. The coefficient of x/l in (40) is found from Howarth's results, and is 3·07. The coefficient of $(x/l)^{3/4}$ in (41) is deduced from the Falkner-Skan similarity solutions, and is 2·705. It would therefore seem a reasonable conclusion that the skin friction predicted by the present method is nowhere in error by more than about 3 per cent. This conclusion is reinforced by comparison with a solution which the author has obtained by Thwaites's method[3], usually accurate for accelerated flow. If the Thwaites solution is expanded as in (40), then the coefficient of x/l is 2·91, so that for small x the error in the present solution should be about five-eighths of the error in Thwaites's solution. As shown in Table III, the greatest discrepancy between the two solutions is about 7·5 per cent; one would conclude that at worst the predicted skin friction becomes 3 per cent too high before tending to its asymptotic value of 3 per cent too low.

It is worthy of note that, in each of the three examples considered in this section, the method applies far beyond its nominal range of application. In the first two examples the pressure coefficient at separation is about 0·23 and 0·09 respectively, compared with the nominal limit of about 0·04. In the third example, the function which should be less than $k^2 \simeq 0{\cdot}36$ increases from about 1·87 at the leading edge to about 1·70 $(x/l)^{1/4}$ for large x/l. One can only conclude that in some fortuitous manner the errors caused by the various approximations made in

the theory, namely the approximation to the outer profile and the assumption of a linear Blasius régime throughout the inner profile, must cancel out, at any rate as regards the prediction of skin friction.

5. Predictions of Separation for Some Flows with Suction

5.1. The Simplified Equation

This section is concerned only with separation properties, the assumption being made that separation occurs where the skin friction is zero. The general equation (23) accordingly simplifies to

$$x^2\left(\frac{dC_p}{dx}\right)^2\left\{C_p-\frac{2\tau_B}{\rho u_0^2}\int_{x_0}^{x} w_s\,dx\right\}=0{\cdot}0104, \quad . \quad . \quad . \quad (42)$$

provided that the velocity distribution is everywhere retarded. Further, we consider only cases of a linearly retarded velocity

$$u_1=u_0\,(1-x/l), \quad . \quad . \quad . \quad . \quad . \quad (43)$$

for which C_p is given in equation (35). Hence equation (42) becomes

$$\frac{x^2}{l^2}\left(1-\frac{x}{l}\right)^2\left\{2\,\frac{x}{l}-\frac{x^2}{l^2}-\frac{0{\cdot}66412}{(u_0\nu x)^{1/2}}\int_0^x w_s\,dx\right\}=0{\cdot}0026. \quad . \quad . \quad (44)$$

5.2. Uniform Suction

When uniform suction w_0 is applied from the leading edge, then equation (44) indicates that separation occurs where

$$\frac{x^2}{l^2}\left(1-\frac{x}{l}\right)^2\left\{2\,\frac{x}{l}-\frac{x^2}{l^2}-0{\cdot}66412\sigma\left(\frac{x}{l}\right)^{1/2}\right\}=0{\cdot}0026, \quad . \quad . \quad (45)$$

where σ is the suction parameter

$$\sigma=w_0\left(\frac{l}{u_0\nu}\right)^{1/2}. \quad . \quad . \quad . \quad . \quad . \quad (46)$$

The solution of equation (46), giving the relationship between the suction parameter σ and the position of separation, is shown in Table IV and Fig. 2. It may be noted from Table IV that as σ increases the position of separation moves back, from $x/l=0{\cdot}12$ when $\sigma=0$ to $x/l=0{\cdot}18$ when $\sigma=0{\cdot}74$, and then to $x/l=0{\cdot}22$ when $\sigma=0{\cdot}974$ and to $x/l=0{\cdot}30$ when $\sigma=1{\cdot}240$. Beyond this point the position of

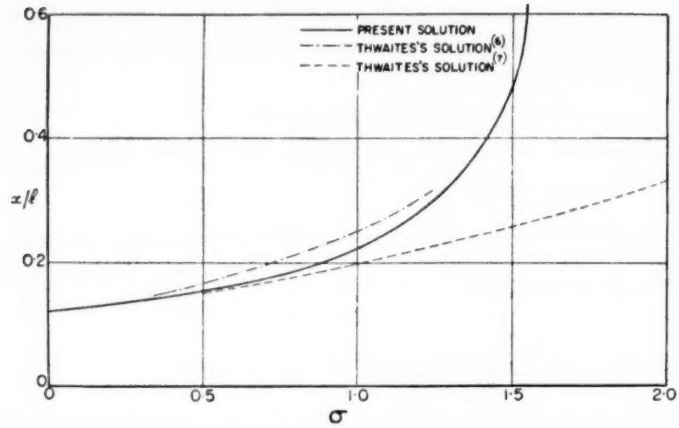

FIGURE 2. Position of separation for linearly retarded velocity, with uniform suction.

separation moves back very rapidly as σ increases, so that an increase in σ from 1·240 to 1·545 results in separation being delayed from 0·30 to 0·60. When $\sigma = 1{\cdot}5466$ separation just occurs at $x/l = 0{\cdot}62$, and separation is completely suppressed when $\sigma > 1{\cdot}5466$.

The result that separation is completely suppressed for large enough σ is not new. For example, Thwaites[7] suggested a critical value $\sigma = 4$, and earlier Prandtl[15] and Preston[16] had suggested 2·18 and 1·61 respectively. The correct value of σ for complete suppression of separation will, of course, depend upon the pressure distribution. The possibility that Thwaites's value may be too high can be reasonably inferred from some of the results of Head. In Fig. 10 of Ref. 13 Head shows the results of his method and Thwaites's method for the problem (to be considered in Section 5.3) of what suction distribution would be required to produce a zero-skin-friction layer with a linearly retarded velocity distribution. Thwaites's curve of $v_s\star$, which is just the local value of σ, is tending to the limiting value 4 as $x/l \longrightarrow 1$, as would be expected. On the other hand, Head's values are smaller when $x/l > 0{\cdot}16$, and appear to be tending to a limit of about 2. This suggests that possibly the critical value $\sigma \simeq 1{\cdot}55$, as given by the present method, may not be too wildly in error.

It is interesting to note the manner in which suppression of separation is predicted to arise. As σ increases, separation moves back to $x/l = 0{\cdot}62$ when $\sigma = 1{\cdot}5466$, and no separation occurs if σ is further increased; separation in $0{\cdot}62 < x/l < 1{\cdot}00$ cannot be achieved with uniform suction. Whether or not this really happens will presumably only be decided when an exact solution is obtained.

In Fig. 2 the predictions of the present theory are compared with the results of two theories due to Thwaites[6, 7]. It is seen that the present results agree reasonably with both when $\sigma \leqslant 1{\cdot}2$, so presumably they are accurate in this range of σ at least.

TABLE IV

POSITION OF SEPARATION FOR LINEARLY RETARDED VELOCITY, WITH UNIFORM SUCTION

(SECTION 5.2)

σ	x/l	σ	x/l
0	0·121	1·240	0·30
0·326	0·14	1·416	0·40
0·566	0·16	1·509	0·50
0·739	0·18	1·545	0·60
0·870	0·20	1·5466	0·62
0·974	0·22		

TABLE V

SUCTION REQUIRED FOR ZERO SKIN FRICTION LAYER

(SECTION 5.3)

x/l	$(u_0\nu l)^{-1/2}\int_0^x w_s dx$		$w_s(l/u_0\nu)^{1/2}$	
	Equation (44)	*Head*[13]	*Equation* (44)	*Head*[13]
0·12	−0·004	0·000		
0·13			2·48	0·65
0·14	0·046	0·013		
0·15			2·25	0·88
0·16	0·091	0·030		
0·17			2·12	1·08
0·18	0·133	0·051		
0·19			2·05	1·23
0·20	0·174	0·076		
0·25	0·273	—	1·98	—
0·30	0·372	—		

5.3. Suction Required to Preserve Zero Skin Friction

In the absence of suction the boundary layer with external velocity (equation (43)) separates where $x/l=0{\cdot}120$, the solution of equation (44) being $x/l=0{\cdot}121$ when $w_s\equiv 0$. If the correct amount of suction is applied downstream of this position it is possible to maintain zero skin friction. The required suction velocity w_s is given as a function of x by equation (44).

By solving this equation, the value of $(u_0\nu l)^{-1/2}\int_0^x w_s\,dx$ was obtained as a function of x/l, and then $w_s\,[l/(u_0\nu)]^{1/2}$ by differentiation. The results are shown in Table V and Figs. 3 and 4, where they are compared with the results obtained by Head[13].

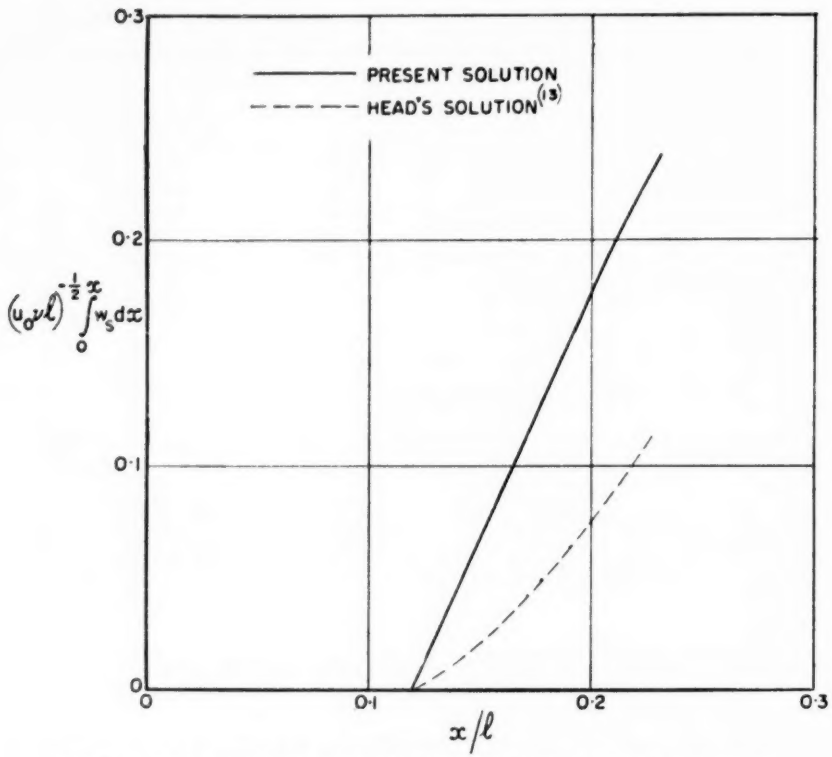

FIGURE 3. Suction quantity for zero skin friction with linearly retarded main stream.

It is noted that the present method agrees with Head's in predicting that a non-zero suction must be applied at the position where separation would otherwise occur, namely $x/l \simeq 0{\cdot}12$. The magnitude, however, is overestimated by the present method, by a factor of 4. Downstream, however, the results in Fig. 4 are in much better agreement. For example, at $x/l \simeq 0{\cdot}17$, the predicted suction is twice Head's value, and, by extrapolating Head's results it is estimated that the predicted suction is only 25 per cent too high when $x/l \simeq 0{\cdot}25$ and about 7 per cent too high when $x/l \simeq 0{\cdot}30$.

The results for the suction quantity $\int_0^x w_s\,dx$ behave appropriately, the curves in Fig. 3 being roughly parallel when $x/l > 0{\cdot}25$.

It is not absolutely certain just how accurate Head's results are, but it is quite certain that, in the absence of an extremely lengthy numerical integration of the full boundary-layer equations, they constitute the most reliable solution available.

Further, it seems almost certain that the required suction velocity w_s should increase with distance, as the following argument suggests. If uniform suction were applied in $x \geqslant 0{\cdot}12l$, then presumably separation would still occur at some downstream position where greater suction would be required if separation is to be further delayed. This argument is not conclusive, of course, since the magnitude of the adverse pressure gradient is decreasing in the present example, but it does strengthen the case for accepting Head's results rather than those of the present paper in the region $0{\cdot}12 \leqslant x/l \leqslant 0{\cdot}25$, where there is a discrepancy between them. Accordingly it is concluded that the present method does not yield accurate predictions of suction near the position where suction begins, for this example at any rate, but does so farther downstream.

A possible explanation of the initial discrepancy lies in the fact that the inner profile is rather thick in this example, so that the quantity of equation (27), which should be less than $(0{\cdot}6)^2$ if the method is theoretically applicable at separation, is equal to 2·01 at the initial point of zero skin friction. Now Head points out that the main drawback of one-parameter methods lies in their implicit assumption that

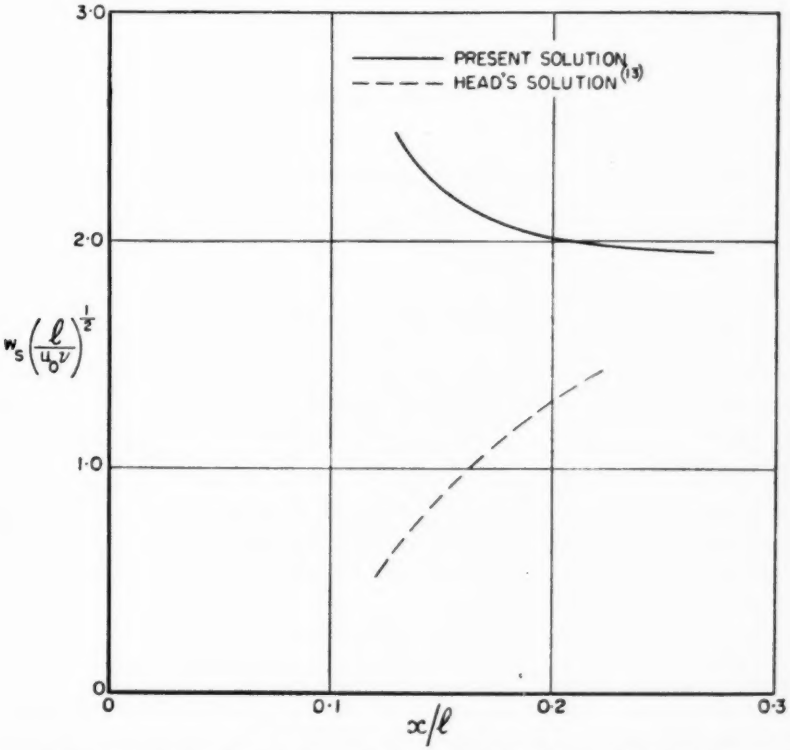

FIGURE 4. Suction velocity for zero skin friction with linearly retarded main stream.

changes in suction velocity affect the whole boundary layer, whereas in fact the effects can only be felt as they diffuse outwards. Similarly, in the present method it is implicitly assumed that the whole of the inner profile is affected by changes in suction velocity. This assumption will perhaps be quite acceptable when the inner layer is truly thin and when the suction varies slowly with position. In the present example, however, the application of a large amount of suction is probably responsible for the initial discrepancy, with the downstream improvement due to the outward diffusion effect.

In spite of these criticisms it should be pointed out that the method predicts, with Head, that non-zero suction is required immediately, whereas the various one-parameter methods (e.g., Refs. 7, 8) would predict that zero suction is required initially.

6. Applications to Some Flows with Zero Pressure Gradient

In this section some examples are considered in which there is no pressure gradient, departures from the Blasius régime being determined entirely by the suction applied. In such circumstances, equation (23) for the skin friction may be simplified to give

$$w_s\left(\frac{x}{u_0\nu}\right)^{1/2}\left\{\frac{1}{w_s x}\int_0^x w_s\,dx\right\}^{1/3}=0{\cdot}32867\,(T-1)\left\{\frac{1+2{\cdot}02T}{T^2}\right\}^{1/3} \quad . \quad (47)$$

Suppose there is uniform suction downstream of a solid entry length l_0; then equation (47) becomes

$$T=1 \text{ when } x\leqslant l_0,$$

$$w_0\left(\frac{x}{u_0\nu}\right)^{1/2}\left(1-\frac{l_0}{x}\right)^{1/3}=0{\cdot}32867\,(T-1)\left\{\frac{1+2{\cdot}02T}{T^2}\right\}^{1/3} \quad \text{when } x\geqslant l_0. \quad . \quad (48)$$

$$\xi=\frac{w_0{}^2x}{u_0\nu}, \quad . \quad . \quad . \quad . \quad . \quad . \quad (49)$$

then equation (48) becomes

$$\xi^{1/2}\left(1-\frac{\xi_0}{\xi}\right)^{1/3}=0{\cdot}32867\,(T-1)\left\{\frac{1+2{\cdot}02T}{T^2}\right\}^{1/3}, \quad . \quad . \quad . \quad (50)$$

$$\text{where} \quad \xi_0=\frac{w_0{}^2l_0}{u_0\nu}. \quad . \quad . \quad . \quad . \quad . \quad (51)$$

This result indicates that the non-dimensional skin friction T is purely a function of $t_1=\xi^{1/2}(1-\xi_0/\xi)^{1/3}$. If this were exactly true then it would be the same function of t_1 as in the case $\xi_0=0$, studied by Iglisch[14]. In fact it is not exactly true, but holds over a range of t_1 which increases with ξ_0.

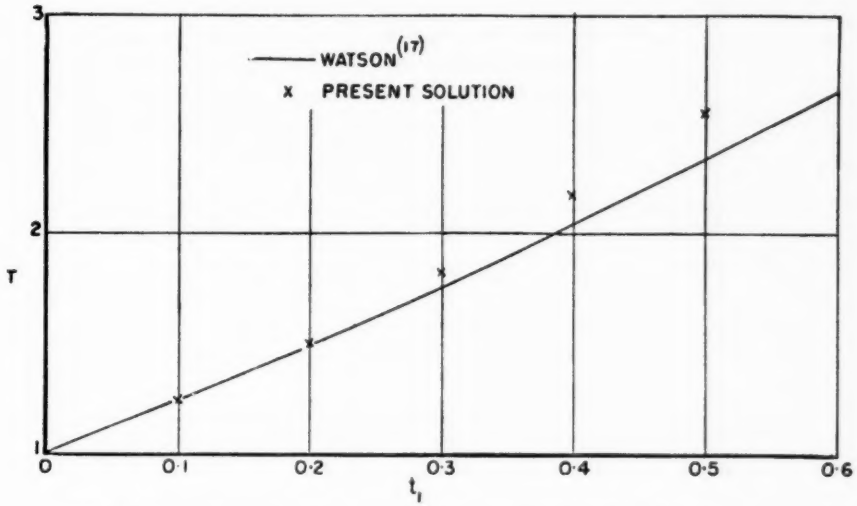

FIGURE 5. Skin friction for flat plate with uniform suction and solid entry length.

Theoretically the range of validity of the present results is easily deduced from equation (27) and is

$$t_1 \leqslant \tfrac{1}{2}\,\xi_0^{1/2}. \qquad . \quad . \quad . \quad . \quad . \quad (52)$$

Now Watson[17] has derived an analytic solution for this problem, which may be written in the form

$$T = 1 + 2{\cdot}2183t_1 + 1{\cdot}0215t_1^2 - 0{\cdot}1376t_1^3 + (0{\cdot}0446 - 0{\cdot}3083\xi_0^{-3/2})\,t_1^4. \quad . \quad (53)$$

This series supports the conclusion of the present method that, within the restricted range of values of t_1 given by condition (52), T is a function of t_1 only. Quantitatively it can easily be verified that the predictions of the present method agree well with the series (53) throughout the range over which each should be valid. As an example, the results for the case $\xi_0 = 1$ are plotted in Fig. 5. We note that the agreement is within 6 per cent when $t_1 \leqslant 0{\cdot}4$, and when $t_1 = 0{\cdot}5$ the agreement is to about 9 per cent. For values of t_1 greater than this value, Watson's series does not appear to converge quickly enough to enable any firm conclusions to be reached.

TABLE VI

RESULTS FOR FLAT PLATE WITH UNIFORM SUCTION

(SECTION 6)

t_1	0	0·0455	0·0877	0·1643	0·2332	0·2962	0·3550	0·4876
T	1·0	1·1	1·2	1·4	1·6	1·8	2·0	2·5

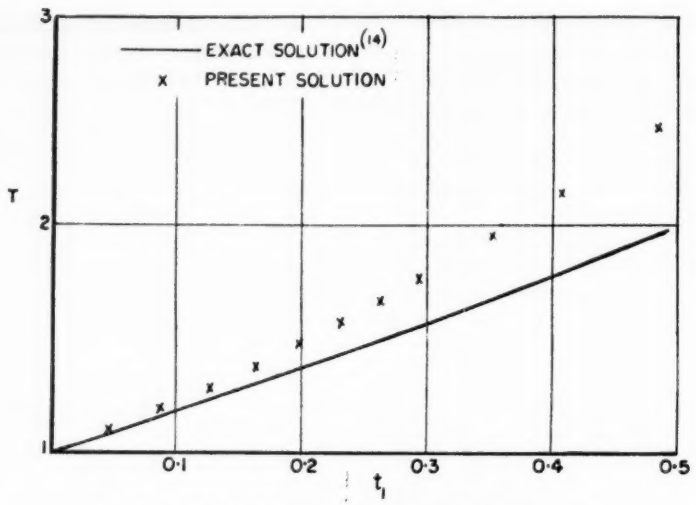

FIGURE 6. Skin friction for flat plate with uniform suction.

Further, the results for the case $\xi_0 = 0$ are shown in Table VI and compared with those obtained by Iglisch in Fig. 6.

ACKNOWLEDGMENTS

The computations which are given in this paper were carried out by Miss B. A. Foster of the Aerodynamics Division of the National Physical Laboratory. The author is indebted to Dr. B. Stratford for many valuable comments and suggestions. The paper describes work carried out in the Aerodynamics Division of the National Physical Laboratory. It is published on the recommendation of the Aeronautical Research Council and by permission of the Director of the Laboratory.

REFFRENCES

1. GADD, G. E., JONES, C. W. and WATSON, E. J. *Laminar Boundary Layers.* Chapter VI. Unpublished manuscript.

2. STRATFORD, B. S. Flow in the Laminar Boundary Layer near Separation. R. & M. 3002, November 1954.

3. THWAITES, B. Approximate Calculation of the Laminar Boundary Layer. *Aeronautical Quarterly*, Vol. I, p. 245, November 1949.

4. CURLE, N. and SKAN, S. W. Approximate Methods for Predicting Separation Properties of Laminar Boundary Layers. *Aeronautical Quarterly*, Vol. VIII, p. 257, August 1957.

5. HEAD, M. R. An Approximate Method of Calculating the Laminar Boundary Layer in Two-Dimensional Incompressible Flow. R. & M. 3123, March 1957.

6. THWAITES, B. Investigations into the Effect of Continuous Suction on Laminar Boundary-Layer Flow under Adverse Pressure Gradients. R. & M. 2514, April 1946.

7. THWAITES, B. The Development of Laminar Boundary Layers under Conditions of Continuous Suction. Part II. Approximate Methods of Solution. A.R.C. 12,699, F.M.1296a, November 1949.

8. SCHLICHTING, H. Ein Näherungsverfahren zur Berechnung der laminaren Grenzschicht mit Absaugung bei beliebiger Körperform. Aerodynamisches Institut der Technischen Hochschule, Braunschweig. Bericht 43/13, 1943. Translation N.A.C.A. T.M. 1216, 1949.

9. POHLHAUSEN, K. Zur Integration der Differential-gleichung der laminaren Grenzschicht. *Zeitschrift für angewandte Mathematik und Mechanik*. Vol. I, p. 252, 1921.

10. HOWARTH, L. On the Solution of the Laminar Boundary Layer Equations. *Proc. Roy. Soc.* A. 164, p. 542, 1938.

11. HARTREE, D. R. The Solution of the Equations of the Laminar Boundary Layer for Schubauer's Observed Pressure Distribution for an Elliptic Cylinder. R. & M. 2427, April 1939.

12. FALKNER, V. M. and SKAN, S. W. Some Approximate Solutions of the Boundary Layer Equations. R. & M. 1314, 1930.

13. HEAD, M. R. Approximate Calculations of the Laminar Boundary Layer with Suction, with Particular Reference to the Suction Requirements for Boundary Layer Stability on Aerofoils of Different Thickness/Chord Ratios. R. & M. 3124, September 1957.

14. IGLISCH, R. Exakte Berechnung der laminaren Grenzschicht an der längsangeströmten ebenen Platte mit homogener Absaugung. Schriften der Deutschen Akademie der Luftfahrtforschung, Band 8B, 1944. Translation N.A.C.A. T.M. 1205, 1949.

15. PRANDTL, L. *The Mechanics of Viscous Fluids. Vol. III, Aerodynamic Theory*, p. 118, Springer, Berlin, 1935.

16. PRESTON, J. H. The Boundary Layer Flow over a Permeable Surface through which Suction is Applied. R. & M. 2244, February 1946.

17. WATSON, E. J. Private Communication.

A Theory for Flow with Axial Symmetry in Centrifugal Impellers*

R. J. TONKS†, B.Sc., Ph.D. and A. G. SMITH‡, B.Sc., A.F.R.Ae.S.

SUMMARY: A theory of incompressible flow with axial symmetry through the impeller of a centrifugal compressor is given more fully and more accurately that by previous writers. The theory is applied to compute the flow through two different impellers. For each design the experimental axial velocity distribution at the impeller eye is in good agreement with that computed numerically from the theory. This means that for the impeller assembly—not untypical of modern designs—considered here, theoretical calculation of intake axial velocity should provide a useful guide to designers.

1. Introduction

In certain respects one-dimensional theory does not describe the flow through a centrifugal impeller adequately. In particular, at the impeller eye, designers have been in the habit of modifying the blade angles predicted from one-dimensional flow theory, either to fit experimentally determined flow angles, or on a "cut-and-try" basis. Many writers have therefore felt it worthwhile to advance a little beyond one-dimensional flow theory.

The actual flow in a centrifugal impeller is complex and, at present, intractable. It is usual therefore to make certain simplifications, namely, to assume the fluid to be inviscid and also to limit the flow to two dimensions. This two-dimensional limitation may be imposed in two ways:—

(*i*) By assuming the flow to be completely constrained by the impeller vanes (*i.e.* axially symmetric flow) and then considering the flow referred to the meridional plane passing through the axis of the compressor (*see* Fig. 1(*a*)).

(*ii*) By assuming the flow limited to two dimensions on surfaces of revolution generated by rotating the meridional streamlines of (*i*) about the axis of the compressor (the so-called "blade-to-blade" solution, *see* Figure 1(*b*)).

---

*Most of this work was done in the course of Ph.D. research at City and Guilds College, London University.

†Research Engineer, Austin Motor Company.

‡Professor of Aircraft Propulsion, College of Aeronautics.

Received April 1959.

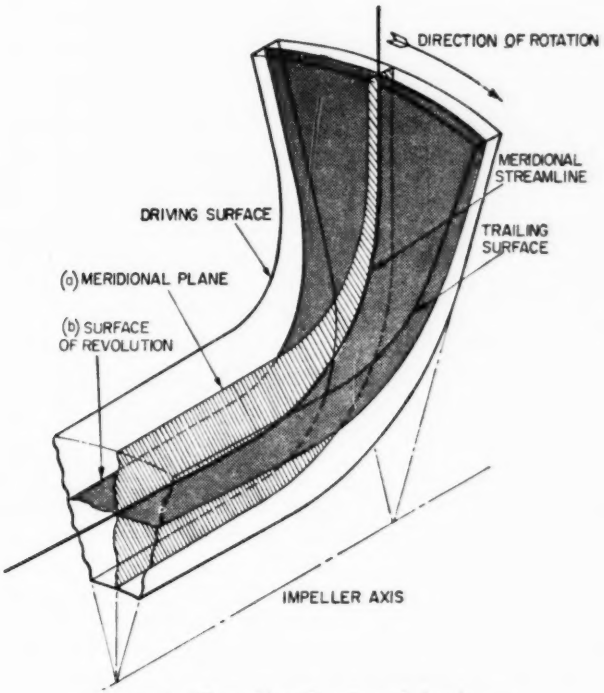

FIGURE 1. View of impeller channel showing:—

(*a*) meridional plane,
(*b*) surface of revolution, generated by rotating a meridional streamline about axis of impeller.

These simplifications permit the description of the flow in terms of a stream function, the distribution of which can be determined with reasonable ease. From the distribution of the stream function, velocities may be deduced.

A combination of (*i*) and (*ii*) constitutes the "quasi-three-dimensional" solution of the problem under consideration.

Stanitz and Ellis[1] have investigated theoretically the case of two-dimensional, non-viscous flow. The analysis was restricted to impellers in which the centre line of the passage between impeller blades generated a right circular cone when rotated about the axis of the compressor. The two-dimensional flow was then considered to lie on the surface of this cone. A further restriction confined the region investigated to that unaffected by the inlet configuration of the impeller and by the diffuser vanes. It is this latter restriction which is the main limitation on using the results for precise quantitative application. Later these two investigators extended their analysis[2] to include channels whose centre lines generated arbitrary surfaces of revolution when rotated about the axis of the compressor. In this treatment a

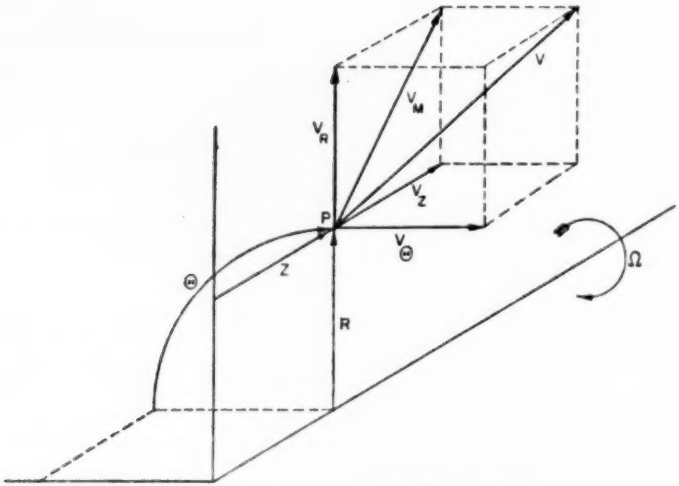

FIGURE 2. Cylindrical polar co-ordinates and velocity components relative to rotating impeller.

knowledge of the streamline pattern in a meridional plane was assumed (*i.e.* an axial-symmetry solution had already been determined) and the mean streamlines were used to generate surfaces of revolution. Once again the effects of blade curvature at inlet were, of necessity, omitted.

A rather interesting analysis developed by Stanitz and his colleagues[3] considered axial-symmetry solutions for incompressible flow in an impeller fitted with curved inducer vanes. The analysis was limited to blade shapes which were composed wholly of radial fibres. With such blades no radial force is exerted on the fluid and the absence of this radial force simplified the analysis considerably.

A comparison between a "quasi-three-dimensional" solution and a general three-dimensional solution has been made by the same author[4]. He has concluded that the "quasi-three-dimensional" solution gives a sufficiently accurate description of the flow for engineering purposes.

Marble and his co-workers[5] have considered axially-symmetric flow through blades of arbitrary shape. Radial body forces arising from the blade geometry were taken into account. The results of his analysis are considered in Section 3.

NOTATION

r, θ, z cylindrical polar co-ordinates

R, Θ, Z dimensionless cylindrical polar co-ordinates (*see* Fig. 2)

$\hat{\mathbf{n}}$ unit normal to vane surface

$\mathbf{v}$ absolute velocity

$\mathbf{V}$ velocity relative to impeller

$\boldsymbol{\Omega}$ angular velocity of impeller

$\mathbf{U}$ tangential velocity of impeller

$\mathbf{w}$ absolute vorticity

$\mathbf{F}$ vane (blade) force

V_{zm} mean (dimensionless) axial velocity at intake

p fluid static pressure

ρ fluid mass density

H fluid total pressure ($=p+\frac{1}{2}\rho v^2$)

$I=p+\frac{1}{2}\rho V^2-\frac{1}{2}\rho U^2$

ψ stream function, defined by equation (8)

Ψ dimensionless stream function

$\overline{\Psi}$ stream function ratio ψ/ψ_S

λ angle defining the vane curvature (*see* Fig. 3)

μ angle whose tangent is n_z/n_θ

ν angle whose tangent is n_r/n_θ

P arbitrary points on vane surface

h relaxation net size

F_0, F_A, F_B residual errors associated with finite-difference equations

Suffixes

r, θ, z components in the r-, θ-, z- directions, respectively

T impeller tip

H hub

S shroud

0, 1, 2, 3, 4 grid points associated with relaxation net

Note:

$r=Rr_T, \qquad z=Zr_T$

$V_r=V_RU_T, \qquad V_z=V_ZU_T$ etc.

2. Equation of Motion

The equation of motion for incompressible flow, in vector notation, is

$$\frac{\partial \mathbf{v}}{\partial t}+\frac{1}{\rho}\nabla H=\mathbf{v}_A\mathbf{w}-\nu\,\mathrm{curl}\,\mathbf{w}+\mathbf{F}. \quad . \quad . \quad . \quad (1)$$

The equation of continuity is

$$\operatorname{div} \mathbf{v} = 0. \quad . \quad . \quad . \quad . \quad . \quad . \quad (2)$$

For steady inviscid flow with axial symmetry, the equation of motion reduces to

$$\frac{1}{\rho} \nabla H = \mathbf{v}_A \mathbf{w} + \mathbf{F}. \quad . \quad . \quad . \quad . \quad . \quad (3)$$

In the present problem it is essential to work as many kinematic terms as possible into the equation of motion, since many of the boundary conditions are specifications of fluid direction. For this reason the "vortex" form of the equation of motion (equation (3)) is the most useful, since it lends itself better to kinematic boundary conditions in the sense that $\mathbf{v}_A \mathbf{w}$ is essentially a velocity term and hence related directly to the boundary conditions. Further, $(1/\rho)\nabla H$ is often a simple quantity and indeed is zero in many problems.

When rotary flows are considered, a more convenient, though less well-known, form is

$$\frac{1}{\rho} \nabla I = \mathbf{V}_A \mathbf{w} + \mathbf{F}. \quad . \quad . \quad . \quad . \quad . \quad (4)$$

This has the virtue that in many rotary flows $(1/\rho)\nabla I$ is zero and thus the equation only contains the terms $\mathbf{F}$ and $\mathbf{V}_A \mathbf{w}$, both quite closely related to the kinematic boundary conditions.

When v_θ is zero upstream of an impeller, as it is for compressors without prewhirl, ∇I is also zero upstream. Since I is constant along a streamline in inviscid flow, if ∇I is zero upstream it is zero everywhere, and equation (4) becomes

$$\mathbf{V}_A \mathbf{w} = -\mathbf{F}. \quad . \quad . \quad . \quad . \quad . \quad (5)$$

Any method of throwing this equation into one in terms of the Stokes stream function must essentially incorporate relations between the tangential component of velocity and the axial and radial velocities, since the stream function itself is related to the axial and radial components only. These relations can be found by considering that the relative velocity $\mathbf{V}$ is tangential to the surface of the vane; in fact

$$\mathbf{V} \cdot \hat{\mathbf{n}} = 0,$$

$$\text{whence} \quad V_\theta = -V_r \cdot \frac{n_r}{n_\theta} - V_z \cdot \frac{n_z}{n_\theta} \quad . \quad . \quad . \quad . \quad (6)$$

n_r, n_θ and n_z are geometrical properties of the impeller and may be obtained from the vane configuration (*see* Fig. 3). Use of equation (6) permits the left hand side of equation (5) to be thrown into "stream function" form.

It is as well to note at this juncture that

$$\hat{\mathbf{F}} = \hat{\mathbf{n}},$$

$$\text{so that} \quad \frac{F_r}{n_r} = \frac{F_\theta}{n_\theta} = \frac{F_z}{n_z} \quad . \quad . \quad . \quad . \quad . \quad . \quad (7)$$

For axisymmetrical flows, the stream function ψ may be defined by

$$V_z = \frac{1}{r}\frac{\partial \psi}{\partial r} \quad \text{and} \quad V_r = -\frac{1}{r}\frac{\partial \psi}{\partial z} \quad . \quad . \quad . \quad . \quad (8)$$

$$\text{Also} \quad w_r = -\frac{\partial v_\theta}{\partial z}, \quad w_z = \frac{1}{r}\frac{\partial}{\partial r}(r v_\theta) \quad \text{and} \quad w_\theta = -\frac{1}{r} D^2\psi.$$

Now $\mathbf{V} \wedge \mathbf{w} \,.\, \mathbf{w} = 0.$

Therefore, from (5), $\mathbf{F} \,.\, \mathbf{w} = 0.$

Hence $w_r n_r + w_\theta n_\theta + w_z n_z = 0,$

$$\text{or} \quad w_\theta = -w_r \frac{n_r}{n_\theta} - w_z \frac{n_z}{n_\theta} \quad . \quad . \quad . \quad . \quad . \quad . \quad (9)$$

Substitution from equations (6) and (8) into (9) yields

$$D^2\psi - 2\Omega r \frac{n_z}{n_\theta} + \left(\frac{n_z}{n_\theta}\right)^2 \frac{\partial^2 \psi}{\partial r^2} + \frac{n_z}{n_\theta}\frac{\partial \psi}{\partial r}\frac{\partial}{\partial r}\left(\frac{n_z}{n_\theta}\right) + \frac{n_z}{n_\theta}\frac{n_r}{n_\theta} V_r + r\frac{n_z}{n_\theta}\frac{n_r}{n_\theta}\frac{\partial}{\partial r}(V_r) +$$

$$+ r V_r \frac{n_z}{n_\theta}\frac{\partial}{\partial r}\left(\frac{n_r}{n_\theta}\right) = r V_r \frac{n_r}{n_\theta}\frac{\partial}{\partial z}\left(\frac{n_r}{n_\theta}\right) + r\left(\frac{n_r}{n_\theta}\right)^2 \frac{\partial}{\partial z}(V_r) + \frac{n_r}{n_\theta}\frac{n_z}{n_\theta} r \frac{\partial}{\partial z}(V_z) + r V_z \frac{n_r}{n_\theta}\frac{\partial}{\partial z}\left(\frac{n_z}{n_\theta}\right)$$

$$. \quad . \quad . \quad (10)$$

In equation (10), which is the governing equation for the idealised flow, the first, third and fourth terms of the left hand side of the equation have been put in terms of the stream function, for reasons which will be apparent later.

It is customary to specify blade shape in terms of certain angles rather than in terms of the components of the unit normal vector and it is necessary, therefore, to determine the relation between these components, which are needed for putting in equation (10), and the angles which will normally be known for a given design. These parameters are depicted in Fig. 3. The curvature of the guiding surface is, of course, purely arbitrary but, in the interests of clarity, has been depicted as being of constant chord, untwisted and extending to the impeller axis. This enables the angles λ and ν (essentially design parameters) to be clearly defined at any point P on the guiding surface. In fact such a surface is utilised in a common form of inducer vane, being very easily generated and consequently reducing the machining

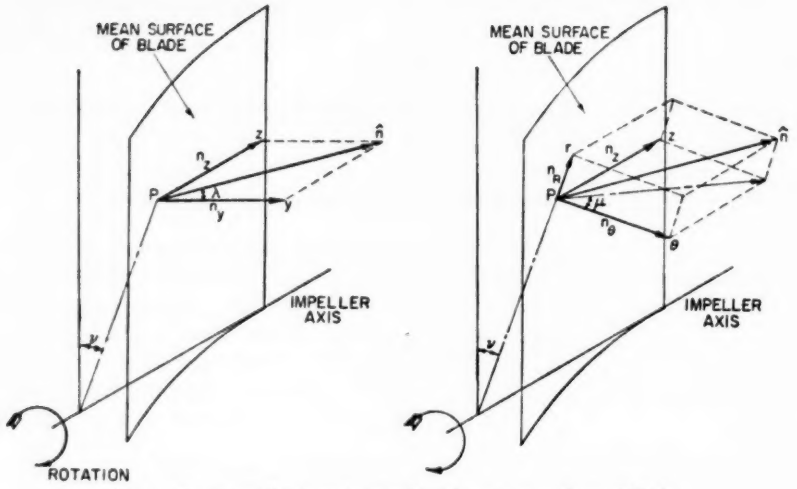

FIGURE 3. Co-ordinate systems referred to mean surface of blade.

difficulties in manufacture. For a twisted vane the angles λ and ν are not quite so readily accessible but, nevertheless, may be determined. It is easily shown that

$$\frac{n_z}{n_\theta} = \frac{\tan\lambda}{\cos\nu} = \tan\mu \quad \text{and} \quad \frac{n_r}{n_\theta} = \tan\nu. \qquad (11)$$

It will be seen that μ defines the angle normally associated with radially-fibred vanes.

3. Comparison with Existing Theories

For impellers having radially-fibred vanes, $n_r = F_r = 0$ and equation (10) reduces to

$$(1+\tan^2\mu)\frac{\partial^2\psi}{\partial r^2} + \left\{\frac{\tan^2\mu}{r} - \frac{1}{r}\right\}\frac{\partial\psi}{\partial r} + \frac{\partial^2\psi}{\partial z^2} - 2\Omega r\tan\mu = 0.$$

$$\text{Substitution of } \tan\mu = \frac{n_z}{n_\theta} = -\frac{V_\theta}{V_z} = -\tan\varepsilon,$$

and use of the non-dimensional form, gives

$$(1+\tan^2\varepsilon)\frac{\partial^2\Psi}{\partial R^2} + \frac{\partial^2\Psi}{\partial Z^2} + \frac{(\tan^2\varepsilon - 1)}{R}\frac{\partial\Psi}{\partial R} + 2R\tan\varepsilon = 0, \qquad (12)$$

which is identical with the equation derived by Stanitz[3].

Similarly, for axial turbo-machines—also for impellers fitted with inducer vanes sufficiently far upstream for them to be regarded as the initial row of rotating blades

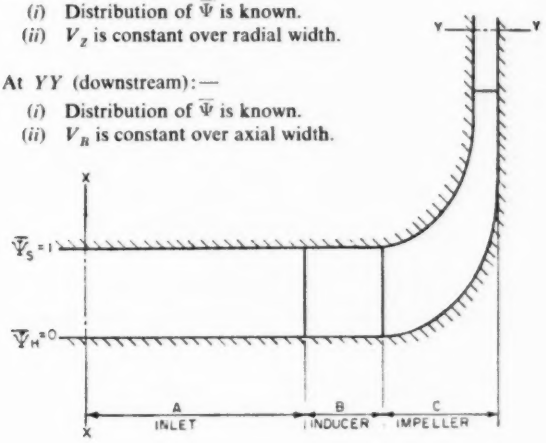

In region A:

$$\frac{\partial^2\bar{\Psi}}{\partial R^2}+\frac{\partial^2\bar{\Psi}}{\partial Z^2}-\frac{1}{R}\frac{\partial\bar{\Psi}}{\partial R}=0$$

In region B:

$$(1+\tan^2\mu)\frac{\partial^2\bar{\Psi}}{\partial R^2}+\frac{\partial^2\bar{\Psi}}{\partial Z^2}-\left[\frac{1}{R}+\tan\nu\frac{\partial}{\partial Z}(\tan\mu)\right]\frac{\partial\bar{\Psi}}{\partial R}-\frac{2R}{0{\cdot}102\,V_{Zm}}\tan\mu=0$$

In region C:

$$\frac{\partial^2\bar{\Psi}}{\partial R^2}+\frac{\partial^2\bar{\Psi}}{\partial Z^2}-\frac{1}{R}\frac{\partial\bar{\Psi}}{\partial R}=0$$

FIGURE 4. Governing equations and regions of application.

in an axial compressor—the stream surfaces are practically circular cylinders and consequently the radial component of velocity may be ignored as a first approximation in equation (10). Also, because of the small magnitude of the radial body force F_r, it seems justifiable to approximate the local axial velocity V_z (which is unknown) to the mean axial velocity V_{Zm} (which will be a known design parameter).

Thus equation (10) reduces to

$$\frac{\partial^2\psi}{\partial r^2}-\frac{1}{r^2}\frac{\partial\psi}{\partial r}+\frac{\partial^2\psi}{\partial z^2}=2\Omega r\frac{n_z}{n_\theta}+V_{Zm}r\frac{n_r}{n_\theta}\frac{\partial}{\partial z}\left(\frac{n_z}{n_\theta}\right)-\frac{n_z}{n_\theta}\frac{\partial}{\partial r}\left(r\frac{n_z}{n_\theta}V_z\right), \qquad (13)$$

which is identical with the equation derived by Marble's method[5].

4. Simplifying Assumptions

For the common type of impeller assembly used in the experimental verification of this theory, V_r and ν are both found to be small in the inducer vane region and

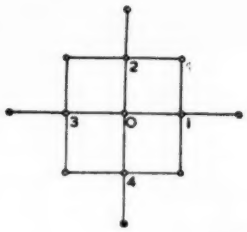

$$\left[\frac{\partial^2\overline{\Psi}}{\partial R^2}\right]_0 = \frac{\overline{\Psi}_2+\overline{\Psi}_4-2\overline{\Psi}_0}{h^2}$$

$$\left[\frac{\partial^2\overline{\Psi}}{\partial Z^2}\right]_0 = \frac{\overline{\Psi}_1+\overline{\Psi}_3-2\overline{\Psi}_0}{h^2}$$

$$\left[\frac{1}{R}\frac{\partial\overline{\Psi}}{\partial R}\right]_0 = \frac{1}{R_0}\left[\frac{\overline{\Psi}_2-\overline{\Psi}_4}{2h}\right]$$

FIGURE 5. Finite-difference approximations.

hence it is reasonable to ignore terms in equation (10) which contain combinations of V_r and tan ν (or their derivatives) and also $\partial V_z/\partial z$, since these will be of third order of smallness.

Thus equation (10) reduces to

$$(1+\tan^2\mu)\frac{\partial^2\psi}{\partial r^2} - \left[\frac{1}{r} - \tan\mu\frac{\partial}{\partial r}(\tan\mu) + \tan\nu\frac{\partial}{\partial z}(\tan\mu)\right]\frac{\partial\psi}{\partial r} + \frac{\partial^2\psi}{\partial z^2} - 2\Omega r\tan\mu = 0 \quad . \quad . \quad . \quad (14)$$

or, in non-dimensional form,

$$(1+\tan^2\mu)\frac{\partial^2\Psi}{\partial R^2} + \left[\tan\mu\frac{\partial}{\partial R}(\tan\mu) - \tan\nu\frac{\partial}{\partial Z}(\tan\mu) - \frac{1}{R}\right]\frac{\partial\Psi}{\partial R} + \frac{\partial^2\Psi}{\partial Z^2} - 2R\tan\mu = 0. \quad . \quad . \quad . \quad (15)$$

Upstream and downstream of the impeller the tangential component of vorticity is zero and, therefore,

$$\frac{\partial^2\Psi}{\partial R^2} + \frac{\partial^2\Psi}{\partial Z^2} - \frac{1}{R}\frac{\partial\Psi}{\partial R} = 0. \quad . \quad . \quad . \quad . \quad (16)$$

It is convenient to introduce a stream-function ratio $\overline{\Psi}=\Psi/\Psi_S$ into these equations. The modified equations and their regions of application are shown in Fig. 4.

5. Numerical Solution

With the finite-difference approximations indicated in Fig. 5, equations (15) and (16) may be written, respectively,

$$\overline{\Psi}_1+\overline{\Psi}_3+\left[1+\tan^2\mu_0-\frac{h}{2R_0}-\frac{h}{2}\tan\nu_0\frac{\partial}{\partial Z}(\tan\mu_0)\right]\overline{\Psi}_2-2(2+\tan^2\mu_0)\overline{\Psi}_0+$$

$$+\left[1+\tan^2\mu_0+\frac{h}{2R_0}+\frac{h}{2}\tan\nu_0\frac{\partial}{\partial Z}(\tan\mu_0)\right]\overline{\Psi}_4-\frac{4R_0h^2\tan\mu_0}{V_{Zm}(R_S^2-R_H^2)}\equiv F_0 \quad . \quad (17)$$

and

$$\overline{\Psi}_1+\overline{\Psi}_3+\left(1-\frac{h}{2R_0}\right)\overline{\Psi}_2+\left(1+\frac{h}{2R_0}\right)\overline{\Psi}_4-4\overline{\Psi}_0\equiv F_0. \quad . \quad . \quad (18)$$

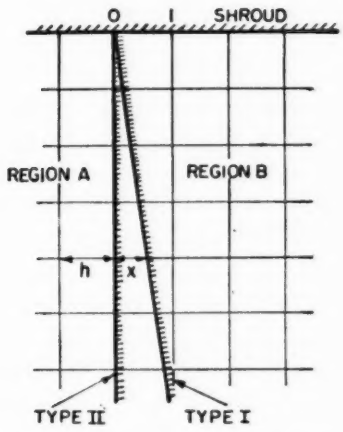

FIGURE 6. Leading edge modification.

It is a physical impossibility for a discontinuity to exist in the stream-function distribution at the leading edge of the inducer vane, although there is an abrupt change in the form of the governing equation at this point. Hence a method is required for blending the finite-difference equations (17) and (18) in the proximity of the leading edge, in order to ensure continuity of streamlines at this point. The method used was the derivation of a "weighed-mean" finite-difference equation applying at the leading edge. This is explained quite simply with reference to Fig. 6.

Let F_B and F_A represent the residuals of equations (17) and (18) respectively.

Let y be the significant fraction of F_B applying at any given node; then $(1-y)$ is the significant fraction of F_A applying at the same node.

Hence the net residual at this node is

$$F_0 = (1-y)F_A + yF_B.$$

The modified equation then becomes

$$\bar{\Psi}_1 + \bar{\Psi}_3 + \left[1 - \frac{h}{2R_0} + y\left\{\tan^2\mu_0 - \frac{h}{2}\tan\nu_0\frac{\partial}{\partial Z}(\tan\mu_0)\right\}\right]\bar{\Psi}_2 - 2(2+\tan^2\mu_0)\bar{\Psi}_0 +$$

$$+\left[1 + \frac{h}{2R_0} + y\left\{\tan^2\mu_0 + \frac{h}{2}\tan\nu_0\frac{\partial}{\partial Z}(\tan\mu_0)\right\}\right]\bar{\Psi}_4 - \frac{4yh^2R_0}{V_{zm}(R_S^2 - R_H^2)}\tan\mu_0 \equiv F_0. \quad (19)$$

and this will apply on grid lines (0) and (1).

Note: For the impeller design considered in this numerical solution.

$$\tfrac{1}{2}(R_S^2 - R_H^2) = 0{\cdot}102$$

For nodes lying along grid line (0), $y = \dfrac{h-x}{2h}$.

For nodes lying along grid line (1), $y = \dfrac{2h-x}{2h}$.

Using equations (17), (18) and (19) a solution may readily be obtained, using relaxation methods, for the stream function distribution within an impeller, since the boundary conditions are known.

6. Computation of Axial Velocity Distribution at Impeller Eye

A numerical solution on the lines of Section 5 was obtained for a radial impeller with a tip radius of 4·00 in., rotating at 7,500 r.p.m. A mean axial velocity of 75 ft./sec. (nominal mass flow = 1,500 lb./hr) was assumed upstream of the eye.

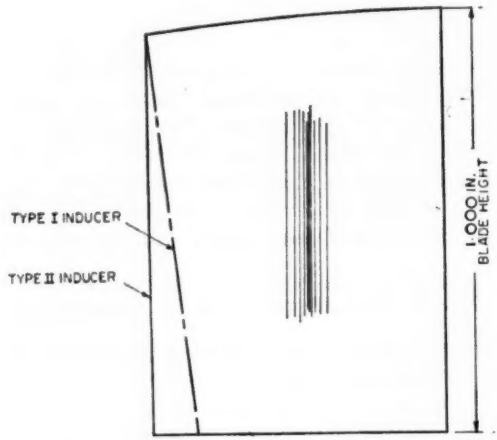

FIGURE 7.
Inducer vane geometry.

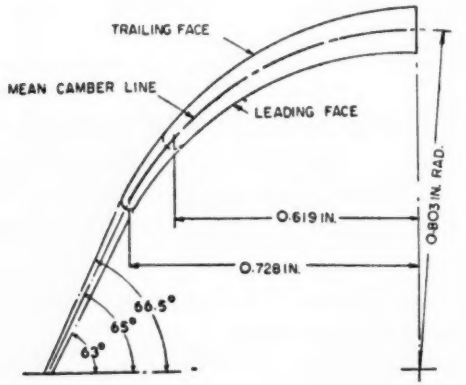

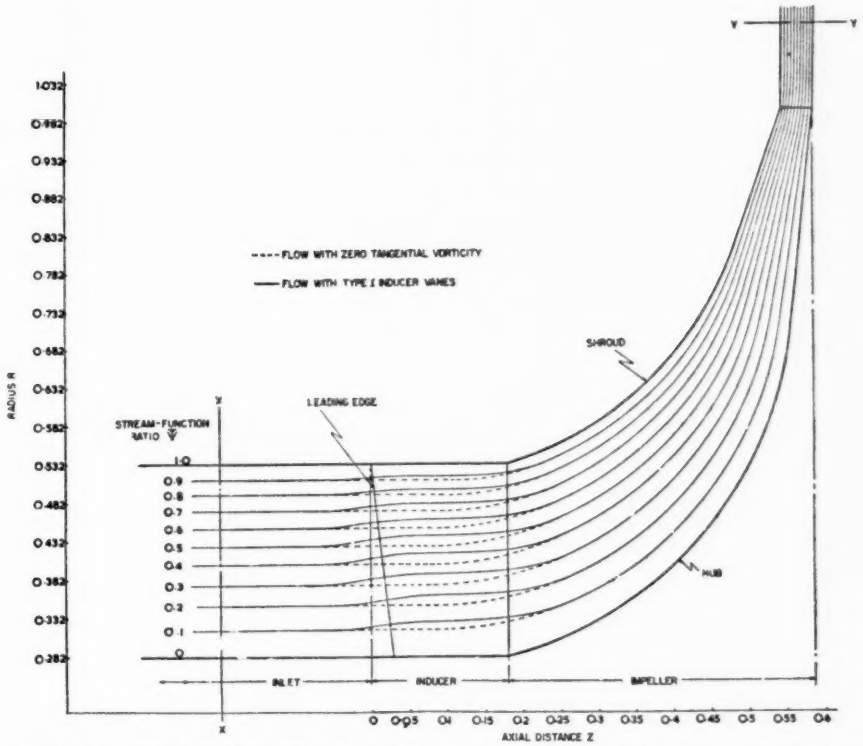

FIGURE 8. Streamline distribution in meridional plane—Type I inducer vanes. (Streamline designation indicates proportion of flow through impeller between streamline and hub.)

Two types of inducer vane (*see* Fig. 7) were considered. Each was of constant chord and untwisted, the mean camber line being defined by

$$\tan\lambda = \left| \frac{1}{\sqrt{\left\{ \frac{0{\cdot}0403}{(z-0{\cdot}182)^2} - 1 \right\}}} \right| .$$

Both types were identical except that the leading edge of Type I was "cut back" in order to give approximate matching at the eye. It will be noted that such vanes are essentially non-radial and hence a radial body force is manifested.

The fundamental flow between the hub and shroud of an impeller might be regarded as that with zero tangential vorticity everywhere. This is the flow that would be obtained if there were no blades on the impeller at all, and no pre-whirl in the air going through between hub and shroud. The distortion of the streamlines when an impeller and set of inducer vanes is present can then be judged relative to this fundamental case. A zero-vorticity solution was therefore obtained in the

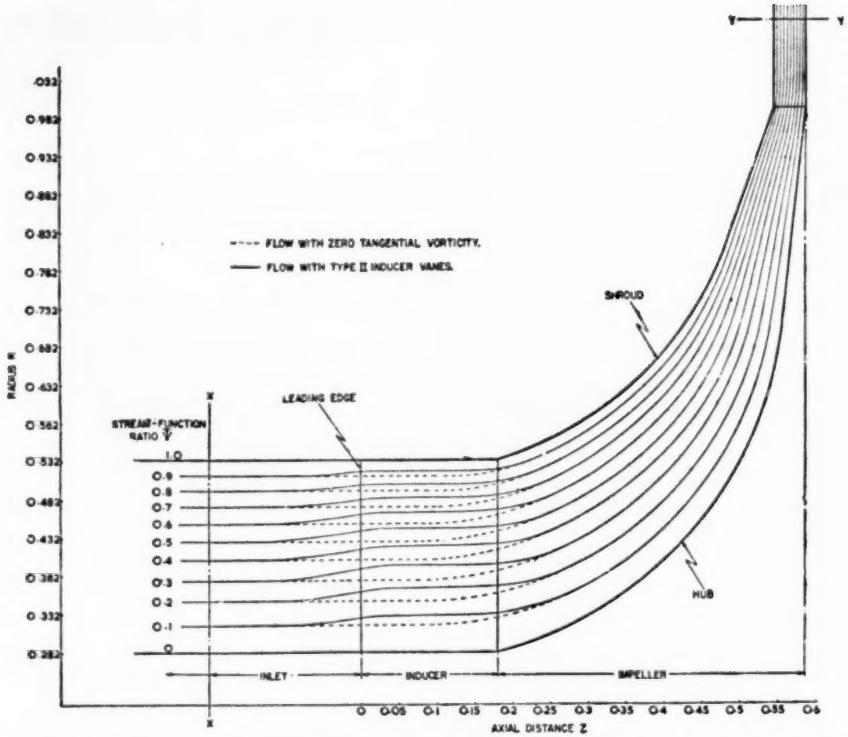

FIGURE 9. Streamline distribution in meridional plane—Type II inducer vanes. (Streamline designation indicates proportion of flow through impeller between streamline and hub.)

present case, since this provided a good basis for comparison with the non-radial inducer vanes. This solution is presented in Figs. 8 and 9, which show the streamline distribution in the meridional plane. Similar solutions are presented for the Type I and Type II inducer vanes.

Axial velocity distributions deduced from the stream-function distributions for Types I and II are presented in Figs. 10, 11, and 12.

7. Experimental Measurement of Axial Velocity Distribution at Impeller Eye

To confirm the theory developed, an experimental investigation of the air flow in the vicinity of the impeller eye was undertaken and compared with the theoretical conclusions.

A 26-vaned radial impeller, fitted with 13 inducer vanes, was utilised and the two types of inducer vane discussed in Section 6 were considered. The compressor

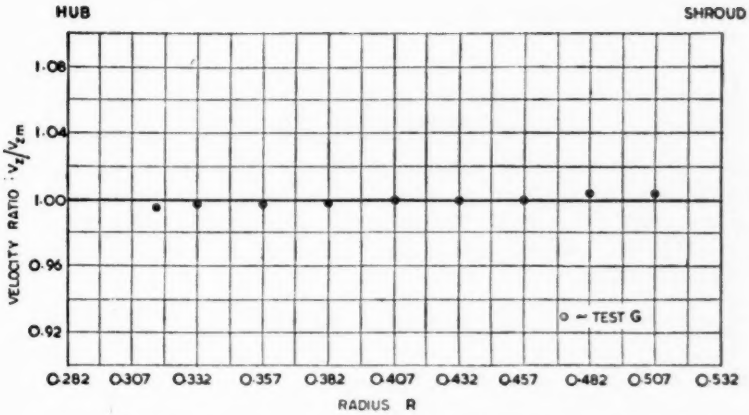

FIGURE 10. **Axial** velocity distribution 0·875 in. upstream of impeller eye — Type I inducer vanes.

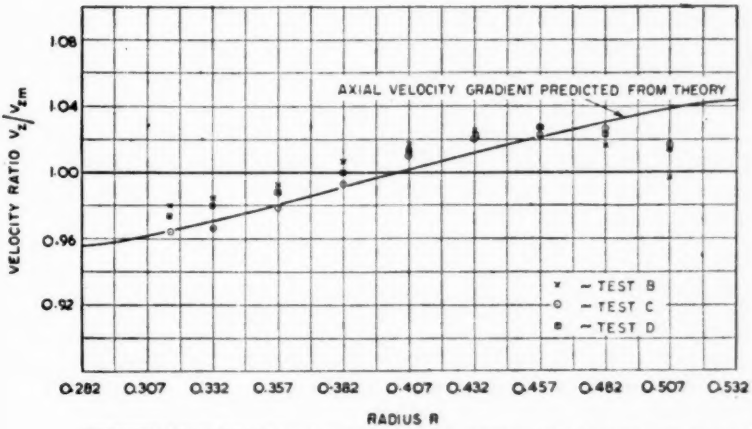

FIGURE 11. **Axial** velocity distribution 0·150 in. upstream of impeller eye — Type I inducer vanes.

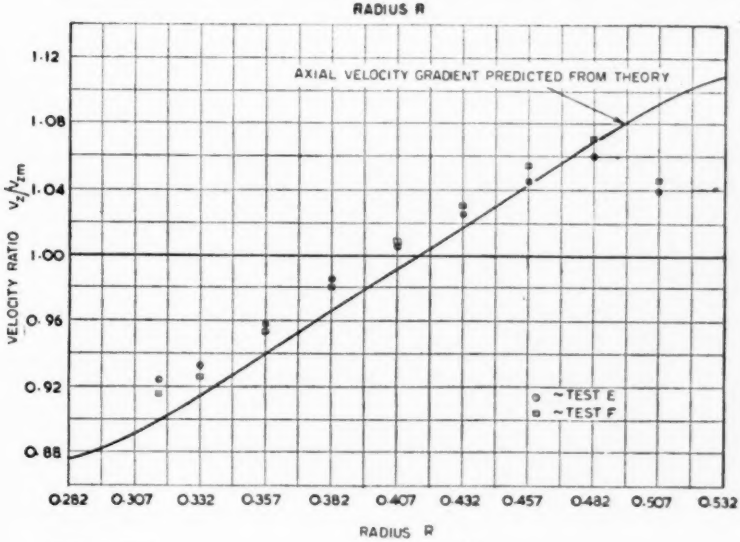

FIGURE 12. Axial velocity distribution 0·150 in. upstream of impeller eye — Type II inducer vanes.

was fitted with adjustable diffuser vanes which enabled the mass-flow rate, and hence the upstream axial velocity V_{z_m}, to be varied.

The accurate measurement of the dynamic pressure so close to the rotating leading edges of the diffuser vanes presented certain difficulties which were overcome by the use of yaw-sensitive disc probes. The probes had previously been calibrated and were mounted on the intake shroud in such a way as to facilitate radial traversing and yaw determination.

The rig layout is shown in Fig. 13 and the probe traversing mechanism can be seen in Fig. 14.

Since the main preoccupation was the determination of the axial velocity distribution in the proximity of the eye due to the radial body forces imposed by the non-radial vanes, it was considered desirable to ensure that no velocity gradient existed by virtue of the upstream hub/shroud profile. A preliminary investigation was therefore undertaken far upstream from the eye; a radial traverse in the plane $z = -0{\cdot}875$ in. showed the absence of any velocity gradient across the intake at this point (*see* Fig. 10). Similar radial traverses were made as close as possible to the leading edges of the inducer vanes (at $z = -0{\cdot}150$ in.) for various values of upstream axial velocity. These demonstrated the presence of gradients for both types of inducer vane used (*see* Figs. 11 and 12).

8. Analysis of Results

From the results obtained in the investigation of flow conditions prevailing at the measuring station, situated 0·875 in. upstream of the eye, it was concluded that the assumptions of uniform axial velocity far upstream (*see* Fig. 10), also of zero pre-whirl, were both perfectly valid.

The agreement between the mean axial velocity obtained from flow measurements at the Venturi meter and that obtained from measurements at the eye was quite reasonable (*see* Table I), there being less than 3 per cent difference in most cases. The very close agreement for upstream measurements ($z = -0{\cdot}875$ in.) suggests that the difference is probably due to slight disturbances in the flow near the eye which were reflected in the probe readings. This is further verified by the fact that, for very low diffuser vane settings where there was a 6 per cent difference in the estimated values of mean velocity, wool-tuft observation indicated the presence of continuous blow-back at the eye tip.

The absence of pre-rotation just upstream of the eye (due to drag from the rotating leading edges) was apparent from the negligible yaw angles obtained.

The values of the velocity ratio included in Table II are also plotted on Figs. 11 and 12. It can be seen that good agreement was obtained over three-quarters of the radial length for both types of inducer vane. Near the shroud, however, a disparity existed between the experimental and calculated values, the former being lower than anticipated. The experimental and calculated gradients are in good agreement, the plotted points lying above the calculated curves. This result was to

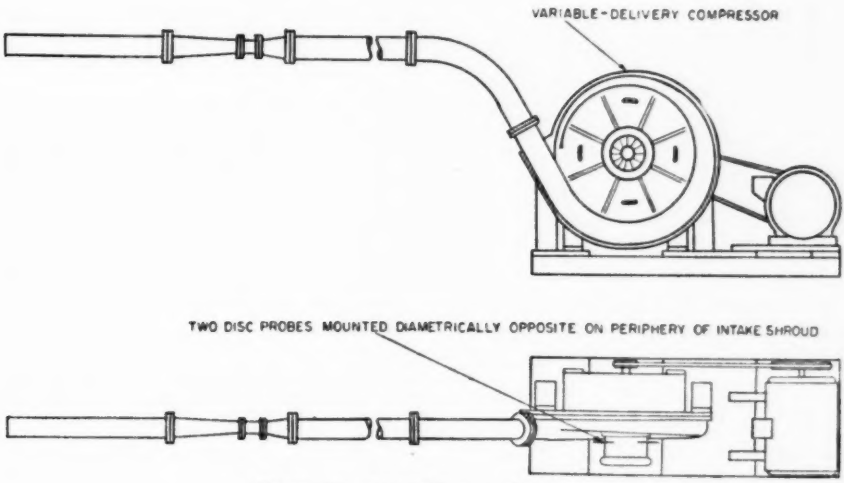

FIGURE 13. General layout of test rig.

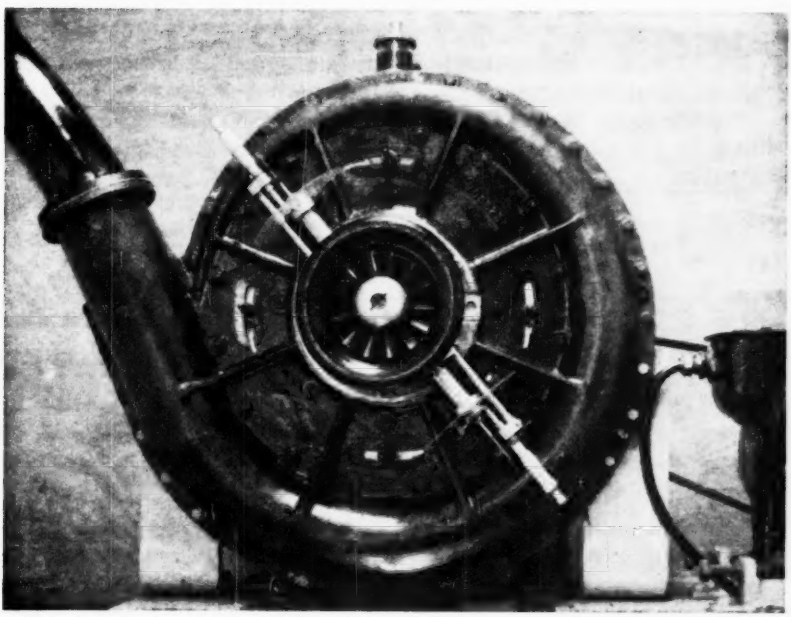

FIGURE 14. Front view of compressor showing disc-probe transversing mechanism.

TABLE I

SUMMARY OF FLOW AT IMPELLER EYE

$-z$ (*in.*)	*Test*	$(r-r_{II})$ (in.)									v_{zm} (*a*)	v_{zm} (*b*)	*Percentage Error* $\frac{(a)-(b)}{(b)} \times 100$
		0·14	0·20	0·30	0·40	0·50	0·60	0·70	0·80	0·90			
0·150	A	58·8	58·3	58·0	57·2	56·0	54·1	50·9	47·5	42·5	51·6	48·7	+5·96
	B	65·3	65·5	66·1	67·0	67·8	68·3	68·5	67·8	66·3	66·6	65·0	+2·46
	C	73·8	74·0	75·0	76·0	77·4	78·2	78·8	78·7	77·8	76·6	73·9	+3·66
	D	89·5	89·0	90·8	91·9	92·9	93·6	94·1	94·1	93·3	91·9	89·5	+2·68
0·150	E	65·1	65·7	67·5	69·3	70·6	72·3	73·6	74·7	73·4	70·5	68·8	+2·48
	F	68·0	68·7	70·8	72·7	74·8	76·6	78·3	79·4	77·5	74·2	72·0	+3·06
0·875	G	65·2	65·3	65·3	65·4	65·5	65·5	65·5	65·7	65·7	65·5	65·3	+0·31
		Velocity v_z determined experimentally.											

Notes

(*See* Table III for details of Tests A-G)

Velocities in ft./sec.
Negligible yaw in all cases.

$-z$ is the position of the measuring station upstream of the eye.
v_{zm} (*a*) is the mean axial velocity deduced from velocity measurements at the eye.
v_{zm} (*b*) is the mean axial velocity deduced from Venturi readings.

TABLE II

SUMMARY OF VELOCITY GRADIENT DATA

$-Z$	*Test*	*Radius R*								
		0·316	0·332	0·357	0·382	0·407	0·432	0·457	0·482	0·507
	A	1·140	1·130	1·123	1·108	1·084	1·049	0·987	0·921	0·824
	B	0·981	0·984	0·993	1·007	1·017	1·025	1·027	1·017	0·996
0·0375	C	0·964	0·966	0·979	0·993	1·010	1·020	1·027	1·027	1·016
	D	0·974	0·979	0·988	1·000	1·011	1·020	1·024	1·024	1·014
	E	0·924	0·932	0·958	0·983	1·005	1·026	1·045	1·060	1·040
0·0375	F	0·917	0·926	0·954	0·980	1·008	1·032	1·054	1·070	1·044
0·2187	G	0·996	0·997	0·997	0·998	1·000	1·000	1·000	1·004	1·004
		Velocity ratio V_z/V_{zm} determined experimentally.								

TABLE III

DETAILS OF TESTS IN TABLES I AND II

Test	*Air Flow* (lb./hr.)	*Inducer Vane*
A	965	Type I
B	1300	Type I
C	1500	Type I
D	1800	Type I
E	1380	Type II
F	1450	Type II
G	1300	Type I

be expected since the fall-off in velocity near the eye-tip results in a smaller mean axial velocity, and hence increased values of the velocity ratio V_z/V_{zm}, resulting in the aforementioned displacement.

Various values of mean axial velocity at intake were considered when using Type I inducer vanes. These ranged from 13 per cent below to 21 per cent above the value taken as a basis for the numerical solution. Such variations did not result in any substantial alterations in the experimentally determined gradients. This is useful, since it means that a numerical solution obtained for some basic throughput (provided that this is not too small) may be applied with a good degree of accuracy to other throughputs of about the same magnitude.

The disparity between calculated and experimental velocities near the shroud was almost certainly due to disturbances in the flow originating within the impeller channels or even as far downstream as the diffuser vanes. Benser[6] has confirmed that, at low capacity, flow reversal at the eye-tip originating inside the impeller channel may occur—a condition which was encountered by the authors when operating the compressor at low diffuser vane settings and which represents the extreme case of flow disturbance inside the impeller influencing the upstream flow, particularly near the shroud.

9. Conclusions

The theory developed in Section 2 is considered verified in view of the results discussed. Although its development was restricted to idealised flow, it may be applied in the case of a real fluid flowing through an impeller in order, say, to predict the probable axial velocity distribution obtaining at the eye for a given set of design, and operating, parameters. In such a case, reasonable agreement may be expected over approximately three-quarters of the inducer vane height, but the velocity in the vicinity of the eye-tip is likely to be over-estimated and an inducer vane designed for the theoretical axial velocity will operate at a positive angle of attack.

The numerical solution obtained demonstrates that distortion in the fluid stream will occur in the region of non-radial inducer vanes due to the imposition of radial body forces. Such distortion is unlikely to extend far beyond the inducer-vane region. As a result of this distortion, a significant axial velocity gradient may occur at the eye, with consequent mis-matching of the fluid flow at the leading edges of the

inducer vanes, if these are designed on the assumption of zero axial velocity gradient.

ACKNOWLEDGMENTS

The authors are grateful to the Austin Motor Company Limited, and to Dr. J. H. Weaving of that organisation, for considerable help with the manufacture of special items of the equipment and for the loan of substantial parts of the equipment for this research.

REFERENCES

1. STANITZ, J. D. and ELLIS, G. O. Two-Dimensional Compressible Flow in Centrifugal Compressors With Straight Blades. N.A.C.A. T.N. 1932, 1949.

2. STANITZ, J. D. and ELLIS, G. O. Two-Dimensional Flow on General Surfaces of Revolution in Turbomachines. N.A.C.A. T.N. 2654, 1952.

3. ELLIS, G. O., STANITZ, J. D. and SHELDRAKE, L. J. Two Axial-Symmetry Solutions for Incompressible Flow through a Centrifugal Compressor with and without Inducer Vanes. N.A.C.A. T.N. 2464, 1951.

4. ELLIS, G. O. and STANITZ, J. D. Comparison of Two- and Three-Dimensional Potential-Flow Solution in Rotating Impeller Passage. N.A.C.A. T.N. 2806, 1952.

5. MARBLE, F. E. and MICHELSON, I. Analytical Investigation of Some Three-Dimensional Flow Problems in Turbomachines. N.A.C.A. T.N. 2614, 1952.

6. BENSER, W. A. and MOSES, J. J. An Investigation of Back-Flow Phenomenon in Centrifugal Compressors. N.A.C.A. Report 806, 1945.

Vibration of Rectangular Plates Point-Supported at the Corners

HUGH L. COX and JACK BOXER

(The Martin Company, Denver, Colorado)

SUMMARY: The fundamental frequencies of flexural vibration are determined for uniform isotropic rectangular plates that have free edges and pinpoint supports at the four corners. For the particular case of a square plate the lowest five frequencies and mode shapes have been determined. The second frequency is most unusual, since an infinite number of mode shapes exist with identical frequencies. Finite difference expressions, which simplify the treatment of the free boundaries for definite values of Poisson's ratio, are used in conjunction with extrapolation procedures to obtain the approximate solutions.

1. Introduction

An exact solution of the differential equation of a vibrating uniform elastic plate that is point-supported at the four corners may be difficult to obtain; consequently an approximate solution has been determined through the use of finite difference expressions and an electronic digital computer. The finite difference approach was selected over other approximate methods such as Rayleigh-Ritz, collocation, influence coefficients, and so on, because the formulation time required for setting up the problem for machine solution is much shorter with the finite difference method.

The usual assumptions regarding the bending of thin elastic plates are made. The effects of rotatory inertia and shear are assumed to be negligible. Poisson's ratio μ is taken as 0·3 for rectangular plates and $0 \leqslant \mu \leqslant 0{\cdot}3$ for square plates. The plate under consideration is shown in Fig. 1. If the static lateral loads on the plate are replaced with equivalent inertia forces when the plate is vibrating freely, the governing differential equation for the plate is

$$\nabla^2 \nabla^2 w - \frac{\rho t \omega_i^2}{D} w = 0, \qquad (1)$$

where w is the plate deflection, D is the plate stiffness, ρ is the plate mass per unit volume, t is the plate thickness, and ω_i is a natural frequency in radians per second. Equation (1) may be expressed in finite difference form at a selected number of points. First-order operators, which include Poisson's ratio, for points on and

Revised version received October 1959.

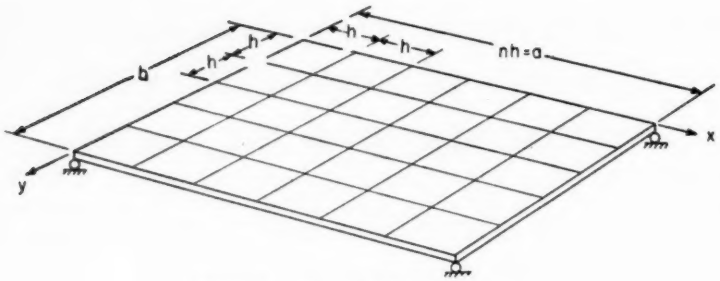

FIGURE 1. Types of plate considered.

adjacent to the free boundaries have been tabulated by Jensen[1] and Livesley and Birchall[2]. If equation (1) is written in difference form at each mesh point for a particular plate, the resulting simultaneous linear algebraic equations may be written matrically as

$$(n^4A-\lambda_i I)\,W=0 \quad . \quad . \quad . \quad . \quad . \quad (2)$$

where n is the plate length divided by the grid spacing ($n=a/h$), A is a matrix of coefficients of the $\nabla^2\nabla^2 w$ terms in equation (1), I is a unit matrix, W is a column matrix of deflections, and

$$\lambda_i=\frac{\rho t\omega_i^2 a^4}{D} \quad . \quad . \quad . \quad . \quad . \quad . \quad (3)$$

$$\text{Thus} \quad \omega_i=n^2\sqrt{(\lambda_i)}\sqrt{\left(\frac{D}{\rho t a^4}\right)}=k_i\sqrt{\left(\frac{D}{\rho t a^4}\right)} \quad . \quad . \quad . \quad . \quad (4)$$

Equation (2) is in standard eigenvalue form and the lowest roots λ_i may be determined rapidly on an electronic digital computer for any representative matrix A of a particular plate grid.

NOTATION

μ	Poisson's ratio
E	Young's modulus
a, b	plate length and plate width, respectively
h	grid spacing
$n=a/h$	
w	plate deflection
D, ρ, t	plate stiffness, density and thickness, respectively
ω_i	natural frequency (rad./sec.)

(*see* Fig. 1)

$\lambda_i = \rho t \omega_i^2 a^4 / D$

k_i vibration coefficient, $= n^2 \sqrt{(\lambda_i)}$

A, I, W matrices defined just after equation (2)

K elastic foundation modulus per length cubed.

2. Fundamental Frequencies and Mode Shapes

Plates with values of a/b of 1·0, 1·5, 2·0, and 3·0 have been considered. For each ratio of a/b the plate width has been taken as both four and six grid spacings, so that extrapolation could be used. Fig. 2 shows plan views of the plates that are six grid spacings wide. The fundamental mode shape will be symmetric about the two centre lines, as shown by the numbering system. Equation (2) has been solved on an electronic digital computer for each value of a/b, where $b = 4h$ and $b = 6h$. Richardson's h^2 extrapolation formulae[3],

$$\frac{36\,(\lambda_1 n^4)_6 - 16\,(\lambda_1 n^4)_4}{36 - 16} = k_1^2,$$

have been used to compute the vibration coefficients k_1 in equation (4). The calculations are tabulated in Table I. Values of k_1 for other values of n lower than those given in Table I indicate that k_1 is approaching the true value monotonically in each case; consequently, extrapolation should give very accurate results[3]. The values for k_1 given in Table I probably deviate from the "exact" answers by less than one per cent.

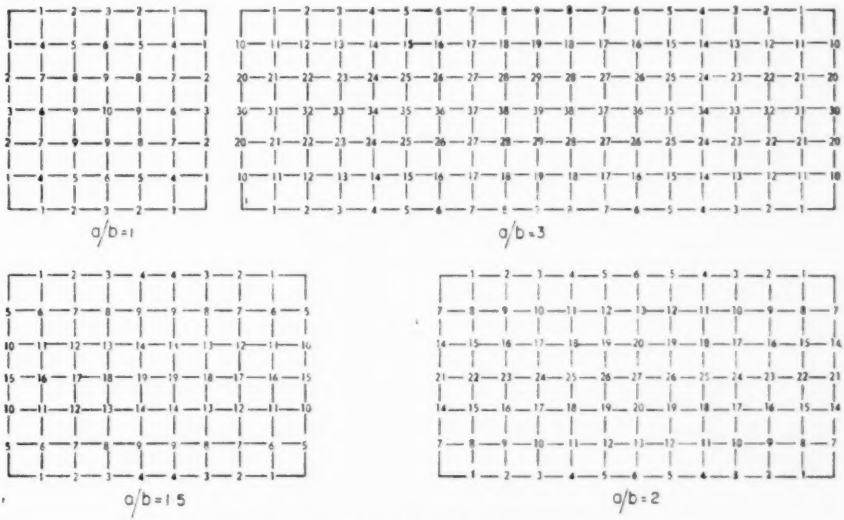

FIGURE 2. Symmetric grid for fundamental modes.

TABLE I

EXTRAPOLATION FOR FUNDAMENTAL FREQUENCIES
($\mu = 0{\cdot}3$)

a/b	n	λ_1	$\lambda_1 n^4$	*Extrapolation* k_1^2	k_1
1	4	0·190281	48·7119	50·6467	7·117
	6	0·038416	49·7868		
1·5	6	0·059568	77·1995	79·6967	8·927
	9	0·011978	78·5868		
2·0	8	0·020605	84·3988	86·3570	9·293
	12	0·004123	85·4867		
3·0	12	0·004225	87·6041	88·8982	9·429
	18	0·000841	88·3230		

The mode shapes for the grid system shown in Fig. 2 are given in Table II. Note that for the square plate the deflection at the mid-point of an edge is about two-thirds of the maximum centre deflection. For the other non-square plates it is interesting to note that the maximum deflection occurs at the mid-points of the long edges; a slightly arched condition occurs along the centre line parallel to the width.

When $a/b = \infty$ the plate frequency reduces to the familiar simply-supported fundamental beam frequency for which $k_1 = \pi^2$. Fig. 3 gives a plot of k_1 against a/b.

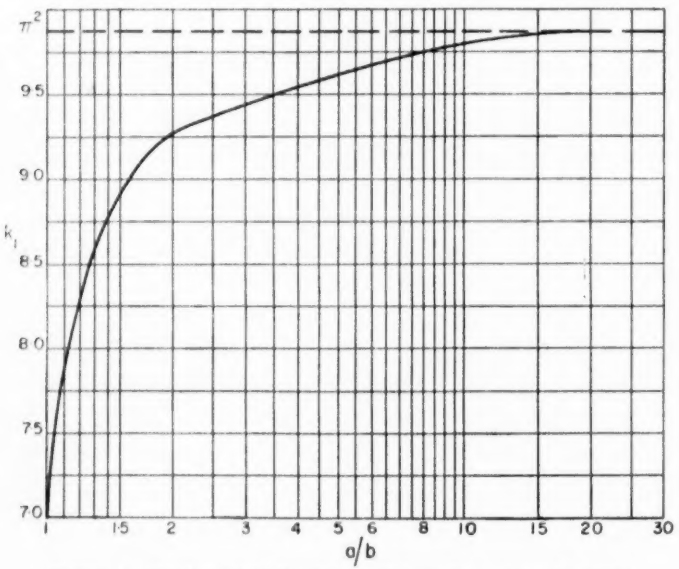

FIGURE 3. Fundamental vibration coefficients for rectangular plates.

TABLE II

FUNDAMENTAL MODE SHAPES FOR PLATES SHOWN IN FIGURE 2
($\mu = 0{\cdot}3$)

Grid Location	*a/b*			
	1·0	1·5	2·0	3·0
1	0·34407	0·35177	0·26141	0·17474
2	0·58825	0·65713	0·50327	0·34364
3	0·67600	0·88141	0·70970	0·50168
4	0·58026	1·0	0·86743	0·64423
5	0·75981	0·11297	0·96631	0·76711
6	0·82616	0·41240	1·0	0·86668
7	0·75981	0·67951	0·04188	0·94000
8	0·89905	0·87885	0·28042	0·98489
9	0·95183	0·98513	0·50445	1·0
10	1·0	0·19186	0·69753	0·01135
11		0·45973	0·84592	0·17900
12		0·70293	0·93928	0·34210
13		0·88653	0·97113	0·49540
14		0·98502	0·07094	0·63408
15		0·21992	0·29562	0·75387
16		0·47731	0·50849	0·85106
17		0·71244	0·69315	0·92268
18		0·89066	0·83569	0·96655
19		0·98649	0·92561	0·98132
20			0·95632	0·01919
21			0·08124	0·18251
22			0·30131	0·34197
23			0·51040	0·49228
24			0·69218	0·62855
25			0·83274	0·74642
26			0·92148	0·84216
27			0·95181	0·91275
28				0·95600
29				0·97057
30				0·02196
31				0·18384
32				0·34205
33				0·49135
34				0·62681
35				0·74403
36				0·83927
37				0·90952
38				0·95257
39				0·96707

3. The Square Plate

A similar approach has been used to find the first five frequencies and mode shapes of a square plate. Values of $n = 5$ and $n = 6$ have been taken so that extrapolation could be used. Fig. 4 shows the grid numbering system used for $n = 6$. Table III gives the results of the solutions of equation (2) when $\mu = 0{\cdot}3$. Table IV gives the corresponding mode shapes for the grid shown in Fig. 4. The mode shapes

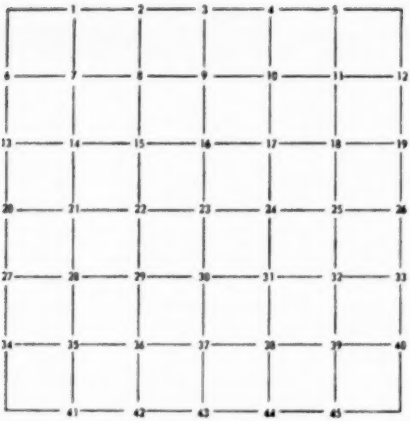

FIGURE 4. Grid pattern for square plate for higher modes.

have been plotted in Figs. 5 and 6 to illustrate the surfaces; dotted lines refer to node lines.

It is most interesting and unusual that there are an infinite number of mode shapes with identical frequencies for the second frequency*. The lower part of Fig. 6 shows how two modes of the (*a*) type may be combined to obtain more basic

TABLE III

FREQUENCY EXTRAPOLATIONS FOR A SQUARE PLATE
($\mu = 0{\cdot}3$)

Mode Number	n	λ_i	$\lambda_i n^4$	*Extrapolation* k_i^2	k_i
2	5	0·362601	226·625	247·549	15·73
	6	0·179798	233·019		
3	5	0·453258	283·286	366·007	19·13
	6	0·238087	308·562		
4	5	2·02722	1267·01	1476·40	38·42
	6	1·02700	1330·99		
5	5	2·39991	1499·95	1896·68	43·55
	6	1·25090	1621·17		

modes (*b*) and (*c*). The computer printed out the (*a*) type modes. As a check, case (*b*) was also obtained using finite difference expressions with a hinge (zero deflection) down the diagonal and case (*c*) was obtained with a hinge across

*It could be possible that this phenomenon is a result of the numerical method of solution.

TABLE IV

HIGHER MODE SHAPES FOR SQUARE PLATES

($\mu = 0.3$)

Grid Location	*Mode Number*					
	2*a*	2*b*	2*c*	3	4	5
1	0·52207	0·42800	0·50302	0·48159	0·82466	−0·49310
2	0·88521	0·79707	0·86736	0·85688	0·79791	−0·73475
3	1·0	1·0	1·0	1·0	0	−0·78861
4	0·84951	0·93765	0·86736	0·85688	−0·79791	−0·73475
5	0·48397	0·57804	0·50302	0·48159	−0·82466	−0·49310
6	0·20274	−0·42800	0·07502	−0·48159	0·82466	−0·49310
7	0·47548	0	0·37920	0	1·0	−0·35047
8	0·66279	0·39652	0·60887	0·36362	0·73369	−0·13858
9	0·69381	0·69381	0·69381	0·50055	0	−0·02813
10	0·55495	0·82122	0·60887	0·36362	−0·73369	−0·13858
11	0·28292	0·75841	0·37920	0	−1·0	−0·35047
12	−0·05269	0·57804	0·07502	−0·48159	−0·82466	−0·49310
13	0·29050	−0·79707	0·07029	−0·85688	0·79791	−0·73475
14	0·36694	−0·39652	0·21235	−0·36362	0·73369	−0·13858
15	0·40496	0	0·32296	0	0·47978	0·44086
16	0·36438	0·36438	0·36438	0·13585	0	0·69261
17	0·24096	0·64592	0·32296	0	−0·47978	0·44086
18	0·05776	0·82122	0·21235	−0·36362	−0·73369	−0·13858
19	−0·14994	0·93765	0·07029	−0·85688	−0·79791	−0·73475
20	0·25390	−1·0	0	−1·0	0	−0·78861
21	0·17616	−0·69381	0	−0·50055	0	−0·02813
22	0·09251	−0·36438	0	−0·13585	0	0·69261
23	0	0	0	0	0	1·0
24	−0·09251	0·36438	0	−0·13585	0	0·69261
25	−0·17616	0·69381	0	−0·50055	0	−0·02813
26	−0·25390	1·0	0	−1·0	0	−0·78861
27	0·14994	−0·93765	−0·07029	−0·85688	−0·79791	−0·73475
28	−0·05776	−0·82122	−0·21235	−0·36362	−0·73369	−0·13858
29	−0·24096	−0·64592	−0·32296	0	−0·47978	0·44086
30	−0·36438	−0·36438	−0·36438	0·13585	0	0·69261
31	−0·40496	0	−0·32296	0	0·47978	0·44086
32	−0·36694	0·39652	−0·21235	−0·36362	0·73369	−0·13858
33	−0·29050	0·79707	−0·07029	−0·85688	0·79791	−0·73475
34	0·05269	−0·57804	−0·07502	−0·48159	−0·82466	−0·49310
35	−0·28292	−0·75841	−0·37920	0	−1·0	−0·35047
36	−0·55495	−0·82122	−0·60887	0·36362	−0·73369	−0·13858
37	−0·69381	−0·69381	−0·69381	0·50055	0	−0·02813
38	−0·66279	−0·39652	−0·60887	0·36362	0·73369	−0·13858
39	−0·47548	0	−0·37920	0	1·0	−0·35047
40	−0·20274	0·42800	−0·07502	−0·48159	0·82466	−0·49310
41	−0·48397	−0·57804	−0·50302	0·48159	−0·82466	−0·49310
42	−0·84951	−0·93765	−0·86736	0·85688	−0·79791	−0·73475
43	−1·0	−1·0	−1·0	1·0	0	−0·78861
44	−0·88521	−0·79707	−0·86736	0·85688	0·79791	−0·73475
45	−0·52207	−0·42800	−0·50302	0·48159	0·82466	−0·49310

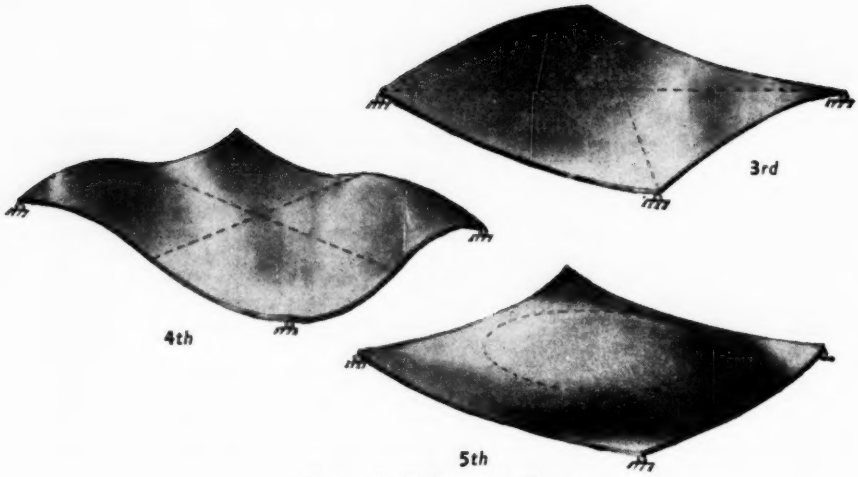

FIGURE 5. Higher mode shapes.

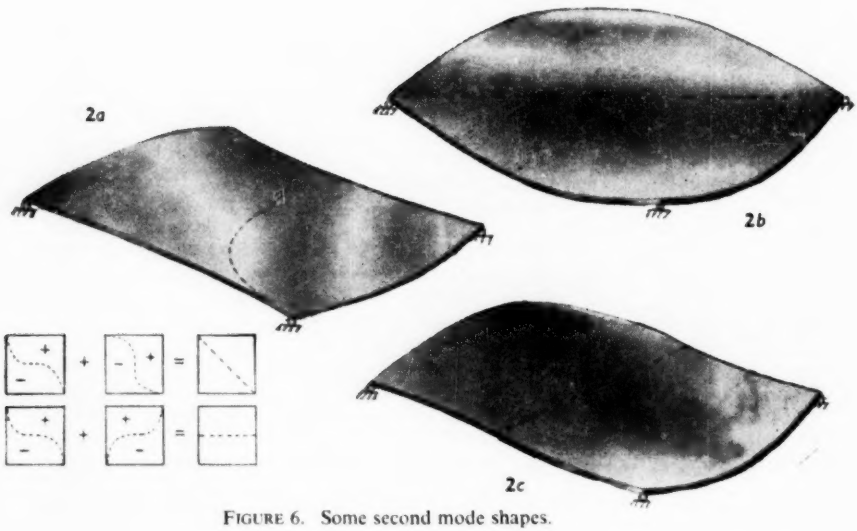

FIGURE 6. Some second mode shapes.

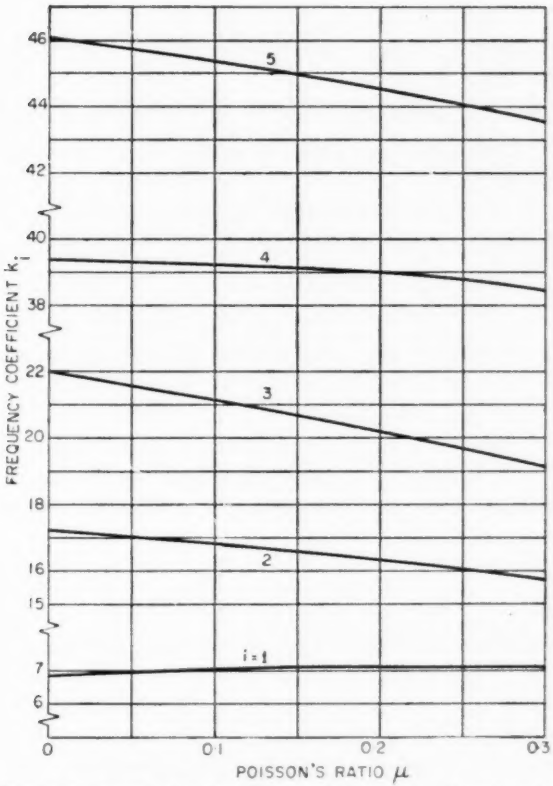

FIGURE 7. Square plate frequency variations with Poisson's ratio.

mid-span. These mode shapes agreed excellently (to six significant figures) with those obtained by the addition process of case (*a*) shown in the lower part of Fig. 6. Also, the frequencies agreed to eight significant figures. Of course, for the hinged cases (*b*) and (*c*) the first frequency corresponds to the second frequency for case (*a*), which is basically the problem under consideration.

The first five natural frequencies for values of Poisson's ratio of zero and 0·225 also were obtained in order to construct Fig. 7. The fundamental frequency coefficient increases slightly with an increase in Poisson's ratio; however, the other frequency coefficients decrease with an increase in Poisson's ratio.

Notice that the third mode shape of the plate under consideration is the same as the second mode shape of a free-free plate. Ritz[4] obtained an upper bound $k_3 = 20{\cdot}56$ for this mode for a value of Poisson's ratio of 0·225. The finite difference solution gave a value $k_3 = 19{\cdot}92$ for this mode (*see* Fig. 7). There is approximately three per cent difference beween the solutions. This frequency decreases almost linearly with increasing values of Poisson's ratio. This phenomenon has been

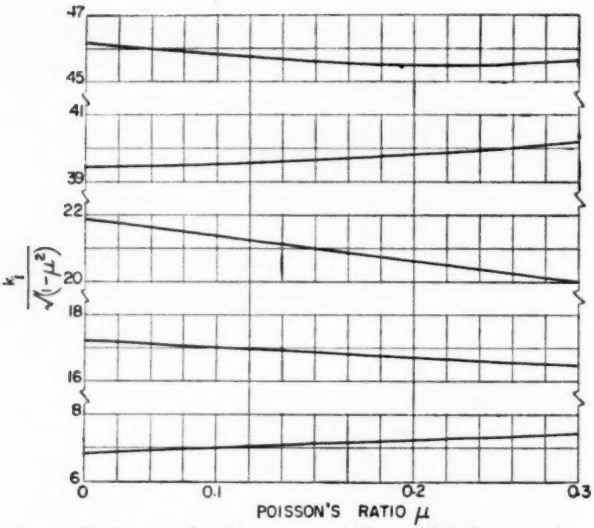

FIGURE 8. Square plate frequency variations with Poisson's ratio.

observed in tests previously[5]. The data shown in Fig. 7 is presented in a form compatible with most other published work on plates. It may be more reasonable, however, to factor out Poisson's ratio from the plate stiffness parameter and to determine the frequency variation with Poisson's ratio as (*see* Fig. 8)

$$\omega_i = \frac{k_i}{\sqrt{(1-\mu^2)}}\sqrt{\left(\frac{Et^2}{12\rho a^4}\right)} \quad . \quad . \quad . \quad . \quad . \quad (5)$$

If the plate in Fig. 1 rests on a uniform elastic foundation,

$$\omega_i = \sqrt{\left[\frac{1}{\rho t}\left(\frac{k_i^2 D}{a^4}K\right)\right]} \quad . \quad . \quad . \quad . \quad . \quad (6)$$

where K represents the elastic foundation modulus per length cubed.

REFERENCES

1. JENSEN, V. P. Analysis of Skew Slabs. University of Illinois Engineering Experimental Station Bulletin No. 332, pp. 48-49, 1941.

2. LIVESLEY, R. K. and BIRCHALL, P. C. Analysis of a Loaded Cantilever Plate by Finite Difference Methods. Royal Aircraft Establishment Technical Note M.S. 26, p. 15, June 1956.

3. SALVADORI, M. G. Numerical Computation of Buckling Loads by Finite Differences. *Transactions of the American Society of Civil Engineers*, Vol. 116, pp. 590-624, 1951.

4. RITZ, W. Theorie der Transversalschwingungen einer quadratischen Platten mit freien Randern. *Annalen der Physik*, Leipzig, Vol. 28, p. 737, 1909.

5. WALLER, MARY D. Vibrations of Free Square Plates: Part 1—Normal Vibrating Modes. *Proceedings of the London Physical Society*, Vol. 51, p. 835 and p. 843, 1939.

The Pressure Distribution on a Wing with a Subsonic Leading Edge in the Presence of Anti-symmetric Body Shaping

J. G. JONES

(Royal Aircraft Establishment, Bedford)

SUMMARY: The pressure distribution on the wing of a centrally mounted wing-body combination due to anti-symmetrical body shaping (with respect to the wing plane) can be calculated in the case where the wing leading edge is supersonic by using the fact that the upper and lower halves of the flow field are independent and that each half can be treated by quasi-cylinder theory. When the leading edge is subsonic the anti-symmetric body shaping produces flow round the leading edge. This paper is concerned with wing pressure distributions including the effect of this flow round the leading edge.

1. Introduction

The configuration considered is a lifting wing-body combination comprising a wing, with a leading edge subsonic over at least part of the span, centrally mounted on a quasi-cylindrical body. The body shape is obtained by adding small distortions to a basic circular cylinder; the distortions may be considered as the sum of two parts, one symmetrical and the other anti-symmetrical with respect to the wing plane.

This paper is concerned with the pressure distribution on the wing due to the anti-symmetric part of the body distortion, including the interaction with the subsonic leading edge.

Within the limitations of linearised theory the effects of anti-symmetric body distortions are independent of the effects due to

(*a*) wing thickness, camber, and incidence,

(*b*) body incidence,

(*c*) symmetric body distortions.

The pressure-fields due to all these effects are simply additive. Consequently it is sufficient to consider a quasi-cylindrical body with anti-symmetric body distortions in combination with a flat plate wing at zero incidence. The results are then applicable to more general wing-body combinations.

Received August 1959.

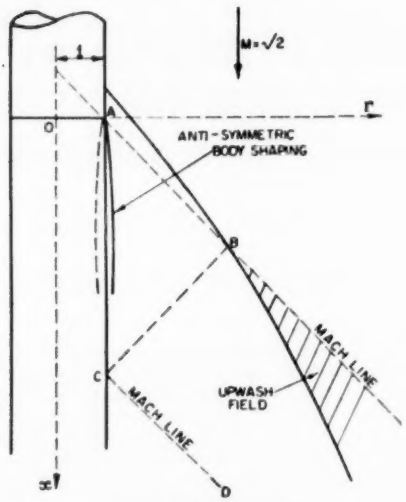

FIGURE 1. General configuration.

The configuration is illustrated in Fig. 1. In the first place it is assumed that the upstream limit AB of the pressure field due to body shaping meets the leading edge at a point B away from the body side. This implies that either the leading edge is supersonic at the root or that the body shaping starts downstream of the root leading edge. Consideration is later given to an approximate solution when this condition is violated.

Upstream of BC the pressure on the wing is that due to the direct effect of body shaping on the same side only. This pressure field is given by quasi-cylinder theory[1].

Downstream of BC the pressure on the wing is influenced by the body shaping on both sides of the combination.

Downstream of BC, but upstream of CD, the pressure on the wing is that due to the direct effect of body shaping on the same side, together with the effect of the upwash field between the leading edge and the upstream limit of the effect of body shaping. The theory of this paper applies exactly to this region and involves the application of Evvard's method[2] to the upwash field. (The treatment of Evvard's method is derived from that in Ref. 3.)

The solution of problems of this type has been generally discussed in Ref. 4. This paper is concerned with two particular cases in which explicit expressions involving tabulated functions for the pressure distribution due to the upwash field can be obtained. The two cases are

(*i*) body distortions in which the cross sections are circular,

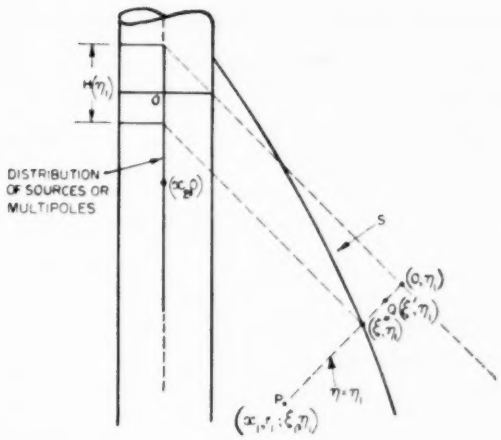

FIGURE 2. Illustration of theory.

(*ii*) body distortions of arbitrary cross section, but with the restriction that the leading edge is "nearly-sonic" (this expression is defined precisely later).

Downstream of *CD* the reflection by the body of the pressure field due to the upwash must be taken into account. The problem of finding the reflected pressure field is not treated here. However, an estimate of the order of magnitude of this reflected pressure field can be obtained by finding the flow due to the upwash across the body side downstream of *C* in the wing plane.

The effect of an upwash field on the opposite wing involves diffraction of its pressure field around the body. This problem is not treated here. In many practical problems the effect is negligible.

A particular example of the case in which the subsonic leading edge extends right into the body side and anti-symmetric shaping starts at the root leading edge is discussed in Section 3. The leading edge is straight and swept behind the Mach line by a small angle, and the pressure coefficient on the wing is found to the first order in this small angle. Conditions at the wing root leading edge are discussed in detail.

NOTATION

x, r
x, y, z } rectangular co-ordinates

θ meridian angle

ξ, η characteristic co-ordinates

$\zeta = \xi/\eta$, conical variable

Φ disturbance velocity potential

$\Phi_1(x, y) = \Psi_1(\xi, \eta)$, velocity potential, deflected wall

$\phi_1(x, r)=\psi_1(\xi, \eta)$, velocity potential, quasi-cylinder theory

$\phi_2(x, r)=\psi_2(\xi, \eta)$, velocity potential, flow round leading edge

$t(x, r)=g(\xi, \eta)$, upwash distribution

$\eta=F(\xi)$, equation of leading edge

$A_{2n}(x)$ multipole strength

$H(\eta)$ function illustrated in Fig. 2

$M_{2n}(x)$ influence function

R body radius

τ parameter in definition of body shaping

$g_{2n}(x)$ function in definition of body shaping

V free stream velocity

$W_{2n}(x, r)$ influence function

$P=-(2/V)\,\partial\Phi/\partial x$, linearised pressure coefficient

P_1 pressure coefficient, quasi-cylinder theory

P_2 pressure coefficient, flow round leading edge

a_i, b_i functions in definition of pressure coefficient

α angle defining leading edge sweep

S, S_1, S_2 regions of upwash field

$\Sigma, \Sigma_1, \Sigma_2$ regions of upwash field in characteristic co-ordinates

2. General Theory

2.1. The Application of Evvard's Method

Figure 1 illustrates the configuration considered and the cylindrical co-ordinate system. Anti-symmetric shaping starts at $x=0$. For simplicity, restriction is made to the case $\beta=(M^2-1)^{1/2}=1$ throughout. Other Mach numbers can be treated by the usual transformation known as Gothert's rule.

At present attention is confined to the region *BCD*. Then the disturbance velocity potential Φ (with $\mathbf{u}=\nabla\Phi$) may be expressed as the sum of the potential ϕ_1 due to the shaping on the same side of the wing, given by quasi-cylinder theory, and the potential ϕ_2 due to a source distribution over the upwash field, given by Evvard's method.

Then Φ is anti-symmetric and continuous upstream of the leading edge.

So, over the upwash field, $\Phi=0$. . . . . (1)

Characteristic co-ordinates are now defined by

$$\left.\begin{aligned}\xi&=x-r+1\\ \eta&=x+r+1\end{aligned}\right\}. \quad . \quad . \quad . \quad . \quad . \quad . \quad (2)$$

The body radius is taken as the unit of length.

Consider a point $P(x_1, r_1; \xi_1, \eta_1)$ on the wing and suppose

$$\left.\begin{aligned} \Phi(x_1, r_1) &= \Psi(\xi_1, \eta_1) \\ \phi_1(x_1, r_1) &= \psi_1(\xi_1, \eta_1) \\ \phi_2(x_1, r_1) &= \psi_2(\xi_1, \eta_1) \end{aligned}\right\} \quad . \quad . \quad . \quad . \quad . \quad (3)$$

The upwash distribution is denoted by

$$t(x_0, r_0) = g(\xi_0, \eta_0), \quad . \quad . \quad . \quad . \quad . \quad (4)$$

Then $$\Phi(x_1, r_1) = \phi_1(x_1, r_1) + \phi_2(x_1, r_1), \quad . \quad . \quad . \quad (5)$$

where $$\phi_2(x_1, r_1) = \frac{1}{\pi} \int_S \frac{t(x_0, r_0)\, dx_0 dr_0}{\{(x_1 - x_0)^2 - (r_1 - r_0)^2\}^{1/2}} \quad . \quad . \quad . \quad (6)$$

(S is the part of the upwash field within the upstream Mach cone from P.)

In terms of characteristic co-ordinates (6) becomes

$$\psi_2(\xi_1, \eta_1) = \frac{1}{2\pi} \int_\Sigma \frac{g(\xi_0, \eta_0)\, d\xi_0 d\eta_0}{\{(\xi_1 - \xi_0)(\eta_1 - \eta_0)\}^{1/2}} = \frac{1}{2\pi} \int_0^{\xi''} \frac{d\xi_0}{(\xi_1 - \xi_0)^{1/2}} \left\{ \int_{F(\xi_0)}^{\eta_1} \frac{g(\xi_0, \eta_0)\, d\eta_0}{(\eta_1 - \eta_0)^{1/2}} \right\}, \quad . \quad (7)$$

where $\eta = F(\xi)$ is the equation of the leading edge and the other quantities are defined in Fig. 2.

We now consider a point Q in the upwash field on the Mach line $\eta = \eta_1$ through P. Q has characteristic co-ordinates (ξ', η_1) where $0 \leqslant \xi' \leqslant \xi''$.

From equation (1), we have

$$\Phi_Q = \Psi(\xi', \eta_1) = 0.$$

Then relation (5) gives

$$0 = \psi_1(\xi', \eta_1) + \frac{1}{2\pi} \int_0^{\xi'} \frac{d\xi_0}{(\xi' - \xi_0)^{1/2}} \left\{ \int_{F(\xi_0)}^{\eta_1} \frac{g(\xi_0, \eta_0)\, d\eta_0}{(\eta_1 - \eta_0)^{1/2}} \right\} \quad . \quad . \quad (8)$$

for all $0 \leqslant \xi' \leqslant \xi''$.

Equation (8) may be regarded as an Abel integral equation of which the solution is

$$\int_{F(\xi_0)}^{\eta_1} \frac{g(\xi_0, \eta_0)\, d\eta_0}{(\eta_1 - \eta_0)^{1/2}} = -2 \frac{d}{d\xi_0} \int_0^{\xi_0} \frac{\psi_1(t, \eta_1)\, dt}{(\xi_0 - t)^{1/2}} \quad . \quad . \quad . \quad (9)$$

for $0 \leqslant \xi_0 \leqslant \xi''$.

Substitution of equation (9) in equation (7) gives $\phi_2(x_1, r_1)\,(=\psi_2(\xi_1, \eta_1))$ in terms of integrals over the upwash field.

The rest of this paper is concerned with cases in which the expression for $\phi_2(x_1, r_1)$ takes a particularly simple form.

2.2. Representation of Body Shaping by Sources and Multipoles Along the Body Axis

Quasi-cylindrical body shaping can be represented by sources and multipoles distributed along the body axis[1]. We consider the representation of the shaping on the upper half of the configuration. Body shaping, and corresponding pressure distributions, on the lower half are equal in magnitude and opposite in sign.

Then it is sufficient[1] to consider only multipoles of which the potential is given by

$$\phi_1(x_1, r_1) = \frac{1}{2\pi}\cos 2n\theta \int_{-1}^{x_1 - r_1} \frac{A_{2n}(x_2)\cosh\left[2n\cosh^{-1}\{(x_1 - x_2)/r_1\}\right]dx_2}{\{(x_1 - x_2)^2 - r_1^2\}^{1/2}}, \qquad (10)$$

where θ is the meridian angle and equals zero in the plane of the wing, and $A_{2n}(-1) = 0$.

2.3. Body Shaping with Semi-Circular Cross Sections

In this case the body shaping can be represented by a line of simple sources. The potential is then given by

$$\phi_1(x_1, r_1) = \frac{1}{2\pi}\int_{-1}^{x_1 - r_1} \frac{A_0(x_2)\,dx_2}{\{(x_1 - x_2)^2 - r_1^2\}^{1/2}}. \qquad (11)$$

In terms of characteristic co-ordinates

$$\psi_1(\xi_1, \eta_1) = \frac{1}{2\pi}\int_0^{\xi_1} \frac{A_0(\xi_2)\,d\xi_2}{\{(\xi_1 - \xi_2)(\eta_1 - \xi_2)\}^{1/2}}, \qquad (12)$$

where $\xi_2 = x_2 + 1$.

Then equation (8) becomes

$$0 = \frac{1}{2\pi}\int_0^{\xi'} \frac{d\xi_0}{(\xi' - \xi_0)^{1/2}}\left\{\frac{A_0(\xi_0)}{(\eta_1 - \xi_0)^{1/2}} + \int_{F(\xi_0)}^{\eta_1} \frac{g(\xi_0, \eta_0)\,d\eta_0}{(\eta_1 - \eta_0)^{1/2}}\right\} \qquad (13)$$

for $0 \leqslant \xi' \leqslant \xi''$.

Equation (13) may be regarded as an Abel integral equation of which the solution is

$$\frac{A_0(\xi_0)}{(\eta_1-\xi_0)^{1/2}}+\int_{F(\xi_0)}^{\eta_1}\frac{g(\xi_0,\eta_0)\,d\eta_0}{(\eta_1-\eta_0)^{1/2}}=0 \quad . \quad . \quad . \quad . \quad (14)$$

for $0\leqslant\xi_0\leqslant\xi''$.

Substituting from equation (14) into equation (7)

$$\begin{aligned}\phi_2(x_1,r_1)&=\psi_2(\xi_1,\eta_1)\\&=-\frac{1}{2\pi}\int_0^{\xi''}\frac{d\xi_0}{(\xi_1-\xi_0)^{1/2}}\,\frac{A_0(\xi_0)}{(\eta_1-\xi_0)^{1/2}}\\&=-\frac{1}{2\pi}\int_{-1}^{H(\eta_1)-1}\frac{A_0(x_2)\,dx_2}{\{(x_1-x_2)^2-r_1^2\}^{1/2}} \quad . \quad . \quad . \quad (15)\end{aligned}$$

where the function $H(\eta)$ depends on the shape of the leading edge and is illustrated in Fig. 2.

Substitution from equations (11) and (15) into relation (5) gives

$$\Phi(x_1,r_1)=\frac{1}{2\pi}\int_{H(\eta_1)-1}^{x_1-r_1}\frac{A_0(x_2)\,dx_2}{\{(x_1-x_2)^2-r_1^2\}^{1/2}} \quad . \quad . \quad . \quad (16)$$

Equation (16) expresses a result exactly analogous to Evvard's result for a planar distribution of sources. In words: "the potential at P due to the upwash field is cancelled by the potential of the linear distribution of sources that produces the upwash field." The potential at P is just that due to the remaining source distribution.

This result does not hold for a distribution of higher multipoles. However, for a combination with a "nearly-sonic" leading edge, simple analytical results are still obtained (Section 2.6).

2.4. Disturbance Velocities

In this section are presented the values of $\partial\phi_2/\partial x_1$ (from which the linearised pressure coefficient due to the upwash field is deduced) and $[\partial\phi_2/\partial r_1]_{r_1=1}$ (which gives the flow across the body side due to the upwash field).

Equation (15) gives, after simplification,

$$\frac{\partial\phi_2(x_1,r_1)}{\partial x_1}=\frac{1}{2\pi}\,\frac{A_0(H(\eta_1)-1)(1-H'(\eta_1))}{\{(x_1-H(\eta_1)+1)^2-r_1^2\}^{1/2}}-\frac{1}{2\pi}\int_{-1}^{H(\eta_1)-1}\frac{A_0'(x_2)\,dx_2}{\{(x_1-x_2)^2-r_1^2\}^{1/2}}. \quad (17)$$

$$\left[\frac{\partial \phi_2(x_1, r_1)}{\partial r_1}\right]_{r_1=1} = \frac{1}{2\pi} \frac{A_0(H(\eta_1)-1)(-H'(\eta_1)-x_1+H(\eta_1)-1)}{\{(x_1-H(\eta_1)+1)^2-1\}^{1/2}} + \\ + \frac{1}{2\pi} \int_{-1}^{H(\eta_1)-1} \frac{A_0'(x_2)(x_1-x_2)\,dx_2}{\{(x_1-x_2)^2-1\}^{1/2}} \quad . \quad (18)$$

where, in equation (18), $\eta_1 = x_1 + 2$. (It is convenient to integrate equation (15) by parts before differentiating.)

Equations (17) and (18) hold for $H(\eta_1) \geqslant 0$. For $H(\eta_1) < 0$, both $\partial\phi_2/\partial x_1$ and $[\partial\phi_2/\partial r_1]_{r_1=1}$ vanish.

Note that, for points (x_1, r_1) on the leading edge, $\xi_1 = x_1 - r_1 + 1 = H(\eta_1)$.

So $\partial\phi_2/\partial x_1$, and hence the linearised pressure coefficient, has a square root singularity on the leading edge for $H(\eta_1) > 0$.

2.5. Relation Between Source Strength and Body Shape

The relation between source strength and quasi-cylindrical body shape with semi-circular sections is given in Ref. 1 and is

$$A_0(x_2-1) = 2\pi V\tau \int_0^{x_2} g_0(t)\, M_0(x_2-t)\,dt, \quad . \quad . \quad . \quad (19)$$

where the body shape is given by

$$\frac{\partial R}{\partial x} = \tau g_0(x) \quad . \quad . \quad . \quad . \quad . \quad . \quad . \quad (20)$$

and $M_0(t)$ is an influence function, with a square root singularity at $t=0$, which is defined and tabulated in Ref. 1.

The most general form of $g_0(x)$ to be considered here is a continuous and differentiable function, except possibly for a finite number of discontinuities.

Then, from equation (19),

$$A_0'(x_2-1) = 2\pi V\tau \int_{-\infty}^{x_2} M_0(x_2-t)\,dg_0(t), \quad . \quad . \quad . \quad (21)$$

where the integral is taken in the Stieltjes sense.

If $g_0(x)$ has its only discontinuity at $x=0$, equation (21) can be written

$$A_0'(x_2-1) = 2\pi V\tau M_0(x_2)\, g_0(0) + 2\pi V\tau \int_0^{x_2} g_0'(t)\, M_0(x_2-t)\,dt. \quad . \quad (22)$$

Equations (19) and (21) can now be used with equations (17) and (18) to give the disturbance velocities due to the upwash field in terms of the body shape.

In the special case where

$$\left.\begin{aligned} g_0(x) &= 0, & x &< 0 \\ &= g_0 \text{ (constant)}, & x &\geqslant 0 \end{aligned}\right\} \quad . \quad . \quad . \quad . \quad (23)$$

(*i.e.* $g_0(x)$ is a multiple of the Heaviside unit function, and the body shaping consists of a straight taper starting at $x=0$), we have, from (22),

$$A_0'(x_2-1) = 2\pi V\tau M_0(x_2)\, g_0$$

and equations (17) and (18) become

$$\frac{\partial \phi_2(x_1, r_1)}{\partial x_1} = g_0 V\tau \left[\frac{1-H'(\eta_1)}{\{(x_1-H(\eta_1)+1)^2 - r_1^2\}^{1/2}} \int_0^{H(\eta_1)} M_0(x_2)\, dx_2 - \right.$$

$$\left. - \int_0^{H(\eta_1)} \frac{M_0(x_2)\, dx_2}{\{(x_1-x_2+1)^2 - r_1^2\}^{1/2}} \right] \quad . \quad . \quad . \quad (24)$$

$$\left[\frac{\partial \phi_2(x_1, r_1)}{\partial r_1}\right]_{r_1=1} = g_0 V\tau \left[\frac{-H'(\eta_1) - x_1 + H(\eta_1) - 1}{\{(x_1-H(\eta_1)+1)^2 - 1\}^{1/2}} \int_0^{H(\eta_1)} M_0(x_2)\, dx_2 + \right.$$

$$\left. + \int_0^{H(\eta_1)} \frac{(x_1-x_2+1)\, M_0(x_2)\, dx_2}{\{(x_1-x_2+1)^2 - 1\}^{1/2}} \right], \quad . \quad . \quad (25)$$

where, in equation (25), $\eta_1 = x_1 + 2$. Relation (5) gives the full expression for the disturbance velocities,

$$\frac{\partial \Phi(x_1, r_1)}{\partial x_1} = \frac{\partial \phi_1(x_1, r_1)}{\partial x_1} + \frac{\partial \phi_2(x_1, r_1)}{\partial x_1}, \quad . \quad . \quad . \quad . \quad (26)$$

with a similar expression for $[\partial \Phi(x_1, r_1)/\partial r_1]_{r_1=1}$.

This section is concluded by quoting the results[1] of quasi-cylinder theory for substitution in relation (26):—

$$\frac{\partial \phi_1(x_1, r_1)}{\partial x_1} = V\tau \left[-\frac{g_0(\xi_1)}{\sqrt{(r_1)}} + \int_0^{\xi_1} g_0(t)\, W_0(\xi_1 - t, r_1)\, dt \right] . \quad . \quad (27)$$

$$\left[\frac{\partial \phi_1(x_1, r_1)}{\partial r_1}\right]_{r_1=1} = V\tau g_0(x_1), \quad . \quad . \quad . \quad . \quad . \quad . \quad . \quad . \quad (28)$$

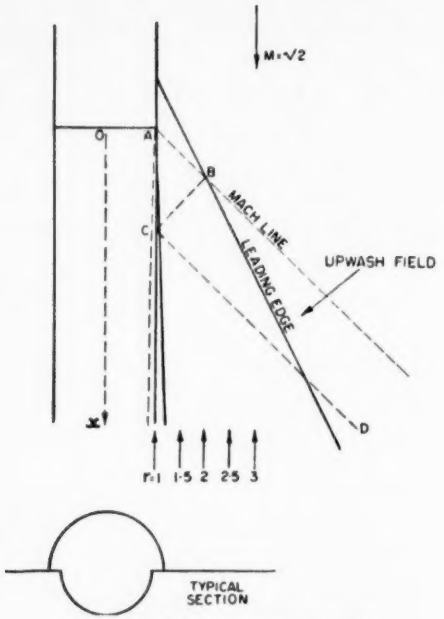

FIGURE 3. First illustrative example.

Here $\xi_1 = x_1 - r_1 + 1$ and $W_0(t, r)$ is an influence function defined and tabulated in Ref. 5.

The results of the application of the foregoing theory to the example illustrated in Fig. 3 are shown in Fig. 4. For this example $H(\eta) = (\eta - 4)/3$. The anti-symmetrical shaping is taken to be defined by conditions (23) on the upper surface. The results are expressed in terms of linearised pressure coefficient as follows:—

$$\left.\begin{aligned} P &= -\frac{2}{V}\frac{\partial \Phi(x_1, r_1)}{\partial x_1} = P_1 + P_2 \\ P_1 &= -\frac{2}{V}\frac{\partial \phi_1(x_1, r_1)}{\partial x_1}, \quad P_2 = -\frac{2}{V}\frac{\partial \phi_2(x_1, r_1)}{\partial x_1} \end{aligned}\right\} \quad . \quad . \quad (29)$$

2.6. "Nearly-Sonic" Leading Edge

The second case in which relatively simple analytical expressions for the disturbance velocities due to the upwash field can be obtained is for combinations with "nearly-sonic" leading edges. This concept is illustrated in Fig. 5. For all points R on the leading edge downstream of the line AB,

$$\tan \gamma \ll 1. \quad . \quad . \quad (30)$$

It then follows that for any point (x_0, r_0) in the upwash field

$$\frac{x_0 + 1 - r_0}{r_0} \leqslant \tan\gamma \ll 1. \quad . \quad . \quad . \quad . \quad (31)$$

We now consider anti-symmetric body shaping which is given by

$$\frac{\partial R}{\partial x} = r \sum_{n=0}^{N} g_{2n}(x) \cos 2n\theta$$

on the side on which the velocities are to be found.

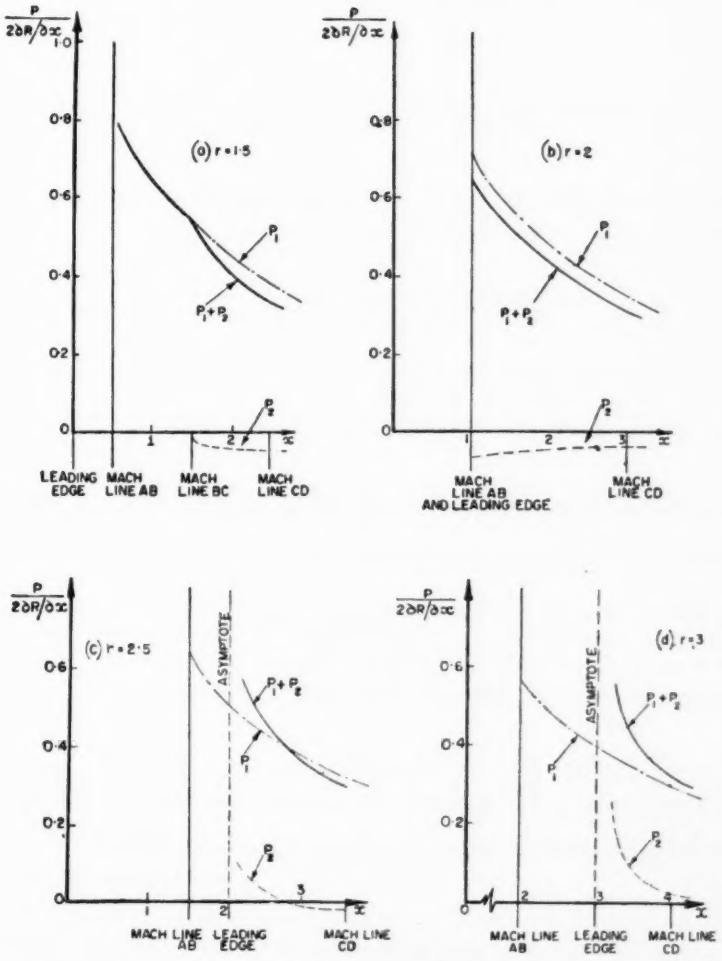

FIGURE 4. Wing pressure distributions.

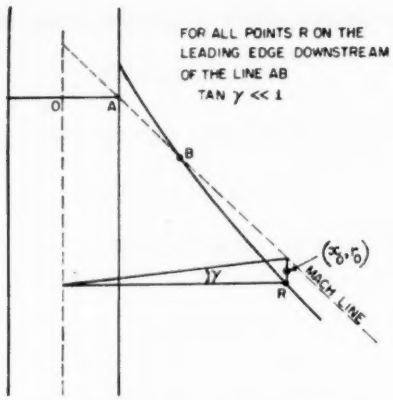

FIGURE 5. "Nearly-sonic" leading edge.

At a general point (x_0, r_0) of the upwash field the potential due to body shaping is

$$\phi_1(x_0, r_0) = \frac{1}{2\pi} \sum_{n=0}^{N} \int_{-1}^{x_0 - r_0} \frac{A_{2n}(x_2) \cosh\left[2n \cosh^{-1}\{(x_0 - x_2)/r_0\}\right] dx_2}{\{(x_0 - x_2)^2 - r_0^2\}^{1/2}} \quad . \quad . \quad . \quad (32)$$

where

$$A_{2n}(x_2 - 1) = 2\pi V \tau \int_0^{x_2} g_{2n}(t)\, M_{2n}(x_2 - t)\, dt \quad . \quad . \quad . \quad (33)$$

and $M_{2n}(t)$ is an influence function defined and tabulated up to $n = 3$ in Ref. 1.

Under condition (30), using condition (31),

$$\frac{x_0 - r_0 - x_2}{r_0} \leqslant \frac{x_0 + 1 - r_0}{r_0} \ll 1,$$

and so, to a first approximation,

$$\cosh\left[2n \cosh^{-1}\left(\frac{x_0 - x_2}{r_0}\right)\right] = \cosh\left[2n \cosh^{-1}\left(1 + \frac{x_0 - r_0 - x_2}{r_0}\right)\right] \simeq 1.$$

A first approximation to equation (32) can therefore be taken as

$$\phi_1(x_0, r_0) = \frac{1}{2\pi} \sum_{n=0}^{N} \int_{-1}^{x_0 - r_0} \frac{A_{2n}(x_2)\, dx_2}{\{(x_0 - x_2)^2 - r_0^2\}^{1/2}} = \frac{1}{2\pi} \int_{-1}^{x_0 - r_0} \frac{\sum_{n=0}^{N} A_{2n}(x_2)\, dx_2}{\{(x_0 - x_2)^2 - r_0^2\}^{1/2}}. \quad (34)$$

Equation (34) shows that over the upwash field the potential due to the multipole distribution can be approximated by that due to a simple source distribution of strength $\sum_{n=0}^{N} A_{2n}(x)$.

In this case equation (8) becomes (*cf.* equation (13))

$$0=\frac{1}{2\pi}\int_0^{\xi'}\frac{d\xi_0}{(\xi'-\xi_0)^{1/2}}\left\{\frac{\sum_{n=0}^{N}A_{2n}(\xi_0)}{(\eta_1-\xi_0)^{1/2}}+\int_{F(\xi_0)}^{\eta_1}\frac{g(\xi_0,\eta_0)\,d\eta_0}{(\eta_1-\eta_0)^{1/2}}\right\} \quad . \quad . \quad (35)$$

for all $0\leqslant\xi'\leqslant\xi''$.

Equation (35) may be regarded as an Abel integral equation of which the solution is

$$\frac{\sum_{n=0}^{N}A_{2n}(\xi_0)}{(\eta_1-\xi_0)^{1/2}}+\int_{F(\xi_0)}^{\eta_1}\frac{g(\xi_0,\eta_0)\,d\eta_0}{(\eta_1-\eta_0)^{1/2}}=0 \quad . \quad . \quad . \quad (36)$$

for all $0\leqslant\xi_0\leqslant\xi''$.

Substitution from equation (36) into equation (7) gives

$$\phi_2(x_1,r_1)=\psi_2(\xi_1,\eta_1)$$

$$=-\frac{1}{2\pi}\int_0^{\xi''}\frac{d\xi_0}{(\xi_1-\xi_0)^{1/2}}\frac{\sum_{n=0}^{N}A_{2n}(\xi_0)}{(\eta_1-\xi_0)^{1/2}}=-\frac{1}{2\pi}\int_{-1}^{H(\eta_1)-1}\frac{\sum_{n=0}^{N}A_{2n}(x_2)\,dx_2}{\{(x_1-x_2)^2-r_1^2\}^{1/2}} \quad . \quad (37)$$

From equation (37), equations can be obtained for the disturbance velocities in exactly the same way that the equations (17) and (18) were obtained from equation (15). Equation (33) can then be used to express the results in terms of body shape, exactly as relation (19) was used in Section 2.5.

3. Approximate Solution when the Upwash Field Extends to the Body Side

3.1. General Remarks

Referring to the general arrangement (Fig. 1), it was pointed out in the Introduction that the method given in this paper only applies exactly to points on the wing upstream of *CD*. When the upwash field extends right into the body side

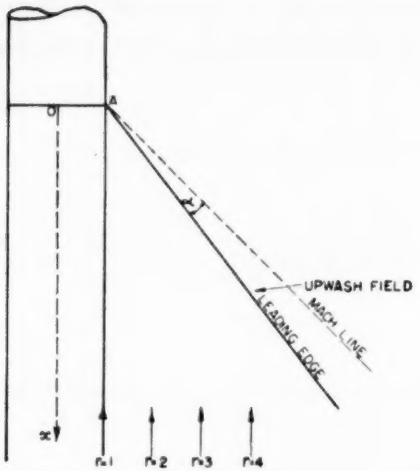

FIGURE 6. Second illustrative example.

the point C coincides with A at the wing root leading edge and the region of exact application of the theory disappears.

This case will be discussed by means of a particular example, illustrated in Fig. 6. The wing leading edge is straight and swept behind the Mach line by a small angle α (a particular case of a "nearly-sonic" edge). For this example $H(\eta)=(\eta-2)\tan\alpha$. The anti-symmetric shaping is taken to be defined by (23) on the upper surface.

The linearised pressure coefficient at a point on the wing of this configuration is now expressed in the form of an infinite series

$$P=P_1(1+a_1+a_2+\ldots)+P_2(1+b_1+b_2+\ldots), \quad . \quad . \quad (38)$$

where the a_i, b_i, as well as P_1, P_2, are functions of position and where:—

P_1 is given by quasi-cylinder theory, neglecting the flow round the leading edge, P_2 is given by the method of this paper and is due to the flow round the leading edge associated with P_1 but neglecting reflection by the body, a_1P_1 is given by quasi-cylinder theory and is obtained by cancelling the flow across the body cylinder due to the flow field associated with P_2, b_1P_2 is obtained from a_1P_1 in the same way that P_2 is obtained from P_1, and so on. P_2 has a square root singularity along the wing leading edge.

It is shown in Section 3.3 that relation (38) can be written

$$P=(P_1+P_2)(1+O(x^{3/2})). \quad . \quad . \quad . \quad . \quad (39)$$

Neglecting terms of $O(x^{3/2})$, we obtain the approximate solution

$$P\simeq P_1+P_2. \quad . \quad . \quad . \quad . \quad . \quad . \quad (40)$$

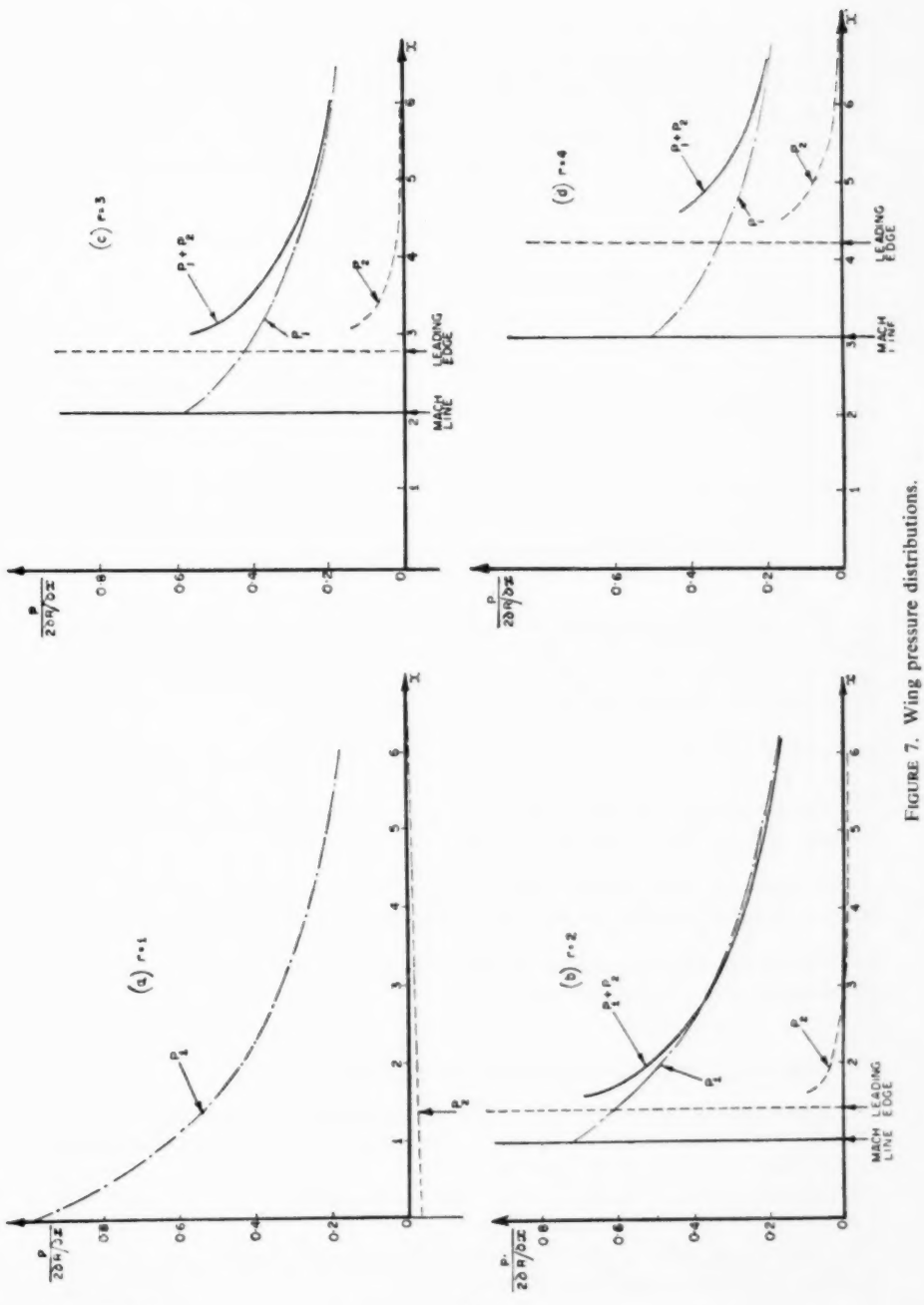

FIGURE 7. Wing pressure distributions.

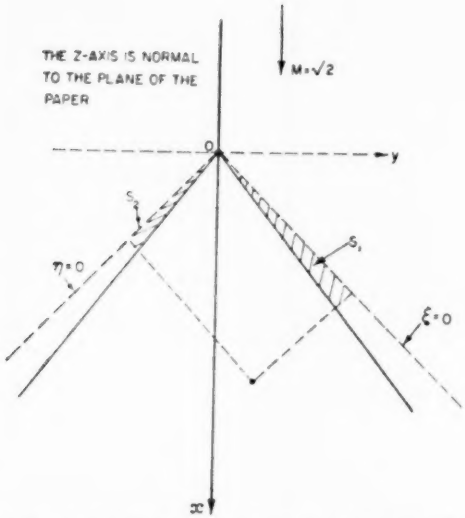

FIGURE 8. Illustration of solution at root leading edge.

This approximate equation holds all over the wing. Near the wing leading edge P_2 is the dominant term. However, in the wing root P_2 is small, in fact of the same order as $P_1a_1 = O(x^{3/2})$ (since P_1a_1 is obtained by the reflection of P_2 by the body), and so in the wing root equation (40) is replaced by

$$P \simeq P_1. \qquad . \quad . \quad . \quad . \quad . \quad . \quad . \quad (41)$$

The approximate solutions (40) and (41) are illustrated for several stations on the wing in Fig. 7, for the case $\tan \alpha = 1/6$.

At the wing root leading edge conditions become conical and it becomes possible to find higher order terms in the series (38). This is done in Section 3.2.

The results of Section 3.2 are used in Section 3.3 to estimate the errors in the approximate equations (40) and (41).

3.2. The Solution at the Wing Root Leading Edge

This section is concerned with the conical configuration illustrated in Fig. 8. The origin O is chosen at the wing apex. For $y > 0$ the configuration corresponds to conditions very near to the apex A in Fig. 6. The curved basic body side of Fig. 6 is replaced by a plane wall, $y = 0$. The body shaping, $\partial R/\partial x = \tau g_0$, for $x > 0$, is replaced by a constant deflection of the wall, $\partial y/\partial x = \tau g_0$, for $x > 0$, $z > 0$. For $z < 0$ the wall deflection is equal in magnitude and opposite in sign. The linearised boundary condition is applied in the plane $y = 0$.

For $z > 0$ the boundary conditions are satisfied by adding to the (two-dimensional) potential due to the deflected wall (which would be the complete disturbance potential if the wing leading edge were supersonic) a distribution of sources over the region S_1, in the plane $z=0$, between the leading edge and the leading Mach line, and an (equal) image distribution for $y < 0$ over the region S_2 to satisfy the boundary condition on $y=0$.

The boundary condition to be satisfied on the upwash field is

$$\Phi = 0, \quad . \quad . \quad . \quad . \quad . \quad . \quad (42)$$

where Φ is the disturbance velocity potential.

This leads to a problem of a type discussed by Evvard[2], involving interacting upwash fields.*

In terms of the Cartesian co-ordinate system illustrated in Fig. 8, the following characteristic co-ordinates are chosen :—

$$\xi = x - y, \quad \eta = x + y.$$

The (two-dimensional) potential due to the deflected wall is denoted by Φ_1.

Then $$\Phi_1(x, y) = \Psi_1(\xi, \eta) = -V g_0 \tau \xi. \quad . \quad . \quad . \quad . \quad (43)$$

Suppose the upwash distributions over S_1, S_2 (Σ_1, Σ_2 in characteristic co-ordinates) are

$$\left.\begin{aligned} t_1(x, y) &= g_1(\xi, \eta) \\ t_2(x, y) &= g_2(\xi, \eta) \end{aligned}\right\}$$

$$g_2(\xi, \eta) = g_1(\eta, \xi). \quad . \quad . \quad . \quad . \quad . \quad (44)$$

Then, at $P(x_1, y_1; \xi_1, \eta_1)$,

$$\Phi = \Phi_1 + \frac{1}{2\pi} \int_{\Sigma_1} \frac{g_1(\xi_0, \eta_0)\, d\xi_0 d\eta_0}{\{(\xi_1 - \xi_0)(\eta_1 - \eta_0)\}^{1/2}} + \frac{1}{2\pi} \int_{\Sigma_2} \frac{g_2(\xi_0, \eta_0)\, d\xi_0 d\eta_0}{\{(\xi_1 - \xi_0)(\eta_1 - \eta_0)\}^{1/2}} \quad . \quad (45)$$

*The problem, being conical, could no doubt be solved using complex variable techniques. The solution given here is more suitable for the present purpose of discussing the terms in equation (38).

In particular,

$$\Phi(x_1, 0) = \Phi_1(x_1, 0) + \frac{1}{\pi} \int_0^{x_1 \tan \alpha} \frac{d\xi_0}{(x_1 - \xi_0)^{1/2}} \int_{\xi_0 \cot \alpha}^{x_1} \frac{g_1(\xi_0, \eta_0)\, d\eta_0}{(x_1 - \eta_0)^{1/2}} \quad . \quad . \quad . \quad (46)$$

At a point (ξ_2, η_1) in the upwash field S_1, we have, combining equations (42) and (45),

$$\Psi_1(\xi_2, \eta_1) + \frac{1}{2\pi} \int_0^{\xi_2} \frac{d\xi_0}{(\xi_2 - \xi_0)^{1/2}} \left\{ \int_0^{\xi_0 \tan \alpha} \frac{g_2(\xi_0, \eta_0)\, d\eta_0}{(\eta_1 - \eta_0)^{1/2}} + \int_{\xi_0 \cot \alpha}^{\eta_1} \frac{g_1(\xi_0, \eta_0)\, d\eta_0}{(\eta_1 - \eta_0)^{1/2}} \right\} = 0 \quad (47)$$

for all $0 \leqslant \xi_2 \leqslant \eta_1 \tan \alpha$.

Equation (47) may be solved as an Abel integral equation, using relations (43) and (44), giving

$$\int_0^{\xi_0 \tan \alpha} \frac{g_1(\eta_0, \xi_0)\, d\eta_0}{(\eta_1 - \eta_0)^{1/2}} + \int_{\xi_0 \cot \alpha}^{\eta_1} \frac{g_1(\xi_0, \eta_0)\, d\eta_0}{(\eta_1 - \eta_0)^{1/2}} = 4V g_0 \tau \xi_0^{1/2}. \quad . \quad (48)$$

Equation (48) may itself be regarded as an Abel integral equation, thus reducing to

$$g_1(\xi_0, \eta_0) = \frac{1}{\pi} \frac{\partial}{\partial \eta_0} \int_{\xi_0 \cot \alpha}^{\eta_0} \frac{d\eta_1}{(\eta_0 - \eta_1)^{1/2}} \left\{ 4V g_0 \tau \xi_0^{1/2} - \int_0^{\xi_0 \tan \alpha} \frac{g_1(\eta', \xi_0)\, d\eta'}{(\eta_1 - \eta')^{1/2}} \right\}$$

$$= \frac{4V g_0 \tau \xi_0^{1/2}}{\pi (\eta_0 - \xi_0 \cot \alpha)^{1/2}} - \frac{1}{\pi (\eta_0 - \xi_0 \cot \alpha)^{1/2}} \int_0^{\xi_0 \tan \alpha} \frac{g_1(\eta', \xi_0)(\xi_0 \cot \alpha - \eta')^{1/2} d\eta'}{\eta_0 - \eta'} .$$

Introducing conical variables

$$\zeta_0 = \xi_0 / \eta_0, \quad p = \eta' / \xi_0,$$

and writing $g_1(\xi_0, \eta_0) = g_1(\zeta_0)$, we have, for $0 \leqslant \zeta_0 \leqslant \tan \alpha$,

$$g_1(\zeta_0) = \frac{4V g_0 \tau \zeta_0^{1/2}}{\pi (1 - \zeta_0 \cot \alpha)^{1/2}} \left\{ 1 - \frac{\zeta_0}{4V g_0 \tau} \int_0^{\tan \alpha} \frac{g_1(p)(\cot \alpha - p)^{1/2} dp}{1 - p\zeta_0} \right\} \quad . \quad (49)$$

Equation (49) is solved by successive substitutions, writing

$$g_1(\zeta_0) = \frac{4V g_0 \tau \zeta_0^{1/2}}{\pi (1 - \zeta_0 \cot \alpha)^{1/2}} \left\{ 1 + g_1^{(1)}(\zeta_0) + g_1^{(2)}(\zeta_0) + \ldots \right\} \quad . \quad . \quad (50)$$

$$\left.\begin{aligned} \text{where} \quad g_1^{(1)}(\zeta_0) &= -\frac{\zeta_0}{\pi}\int_0^{\tan\alpha} \frac{p^{1/2}(\cot\alpha - p)^{1/2}dp}{(1-p\cot\alpha)^{1/2}(1-p\zeta_0)} \\ \text{and} \quad g_1^{(n)}(\zeta_0) &= -\frac{\zeta_0}{\pi}\int_0^{\tan\alpha} \frac{g_1^{(n-1)}(p)\,p^{1/2}(\cot\alpha - p)^{1/2}dp}{(1-p\cot\alpha)^{1/2}(1-p\zeta_0)}, \quad \text{for } n>1 \end{aligned}\right\} \quad . \quad . \quad (51)$$

It can be shown by induction that

$$|g_1^{(n)}(\zeta_0)| \leqslant \left\{\frac{1}{2}\frac{\tan^2\alpha}{1-\tan^2\alpha}\right\}^n$$

and so, for α small enough, the solution (50) converges faster than some geometric series.

Substituting from equation (48) into equation (46), and expressing the result in conical variables, we obtain

$$\Phi(x_1, 0) = \Phi_1(x_1, 0) + \frac{x_1}{\pi}\int_0^{\tan\alpha} \frac{dp}{(1-p)^{1/2}}\left\{4Vg_0\tau p^{1/2} - p\int_0^{\tan\alpha}\frac{g_1(s)\,ds}{(1-ps)^{1/2}}\right\} . \quad . \quad (52)$$

Substitution of the solution for $g_1(\zeta_0)$ given by equations (50) and (51) gives finally

$$\frac{\partial\Phi(x_1,0)}{\partial x_1} = \frac{\partial\Phi_1(x_1,0)}{\partial x_1} + \frac{Vg_0\tau}{\pi}\left\{\frac{8}{3}(\tan\alpha)^{3/2} + \frac{4}{5}(\tan\alpha)^{5/2} - \frac{4}{7}(\tan\alpha)^{7/2} + O(\tan\alpha)^{9/2}\right\} \quad . \quad . \quad . \quad (53)$$

and hence

$$P = -\frac{2}{V}\frac{\partial\Phi(x_1,0)}{\partial x_1} = 2g_0\tau - \frac{2g_0\tau}{\pi}\left\{\frac{8}{3}\alpha^{3/2} + \frac{4}{5}\alpha^{5/2} + \frac{16}{21}\alpha^{7/2} + O(\alpha^{9/2})\right\} \quad (54)$$

This, then, is the pressure coefficient at the wing root leading edge of the configuration in Fig. 6.

The successive substitutions correspond physically to successive reflections in the plane wall, and so the result, equation (54), can be interpreted in terms of equation (38). At the wing root leading edge, where the body reflects as if a plane wall, $P_2 = P_1a_1$, $P_2b_1 = P_1a_2$, . . . and so on. Then the first term in (54) is P_1, the term in $\alpha^{3/2}$ is the first term in the expansion of $P_2 + P_1a_1$, and higher order terms in (54) successively get contributions from $P_2b_1 + P_1a_2$, . . . and so on.

3.3. Errors due to Approximation

This section is concerned with the errors in the approximations (40) and (41) to equation (38).

To find a_1P_1 (equation (38)) exactly it would be necessary to find the flow across the body cylinder due to the flow field associated with P_2, which is represented by a source distribution over the upwash field. An estimate of the magnitude of this cross flow can be obtained by finding the flow across the body cylinder in the wing plane only. This is given by equation (25). Using the series expansion of $M_0(t)$ given in Ref. 1 it can be shown that, for small α, equation (25) is equivalent to

$$\left[\frac{\partial\phi_2}{\partial r_1}\right]_{r_1=1} = g_0 V\tau \frac{2\sqrt{2}}{3\pi} \frac{3x_1+8}{(x_1+2)^{3/2}} \alpha^{3/2} + O(\alpha^{5/2}).$$

To the first order in α this function is greatest at $x_1=0$ and decreases monotonically as x_1 increases. At $x_1=10$ it has fallen to 0·32 of its value at $x_1=0$.

Taking this as an indication of the general behaviour of the flow across the body cylinder it follows that a_1 is $O(\alpha^{3/2})$ and decreases (for a fixed value of r_1) when x_1 becomes large.

b_1P_2 is obtained from a_1P_1 in the same way that P_2 is obtained from P_1. So b_1 is also $O(\alpha^{3/2})$ and decreases for large x_1.

In the wing root equation (40) is replaced by equation (41). The neglected term P_2 decreases with increasing x_1 (Fig. 7). So the error in approximation (41) decreases for large x_1. Use of equations (53) and (54) gives the error in the approximation (41) at the wing root leading edge. For example, when $\tan\alpha = 1/6$, the error is approximately 6 per cent. This will be typical of the error in the wing root for small x_1.

REFERENCES

1. NIELSEN, J. N. Quasi-Cylindrical Theory of Wing-Body Interference at Supersonic Speeds and Comparison with Experiment. N.A.C.A. Report 1252, 1955.
2. EVVARD, J. C. Use of Source Distributions for Evaluating Theoretical Aerodynamics of Thin Finite Wings at Supersonic Speeds. N.A.C.A. Report 951, 1950.
3. ROBINSON, A. and LAURMANN, J. A. *Wing Theory*. Cambridge University Press, 1956.
4. DONOVAN, A. F. and LAWRENCE, H. R. *High Speed Aerodynamics and Jet Propulsion*. Vol. VII. *Aerodynamic Components of Aircraft at High Speed*. Oxford University Press, 1957.
5. NIELSEN, J. N. Tables of Characteristic Functions for Solving Boundary-Value Problems of the Wave Equation. N.A.C.A. T.N. 3873, 1957.

Struts with Linearly Varying Axial Loading

J. S. PRZEMIENIECKI, Ph.D., A.F.R.Ae.S.

(*Bristol Aircraft Limited*)

SUMMARY: Analytical solutions for the deflections and bending moments are derived for elastic struts with linearly varying axial loading applied either (*a*) along the undeformed straight strut axis or (*b*) at the strut axis in the deflected position. The instability of struts with various end conditions is discussed and the stability criteria are given as a series of curves relating the maximum compressive axial load with the maximum distributed loading. Furthermore, explicit formulae for the deflections and bending moment distributions have been compiled for several typical cases of lateral loading combined with the axial loading of the type (*a*), which is of some practical importance in aircraft structures. A numerical example is included to show the practical application of the general analysis to a typical strut problem.

1. Introduction

Struts with linearly varying axial load can be divided, in general, into two basic types, depending on the method of application of the distributed axial loading, which may be applied either (*a*) along the *undeformed* straight strut axis or (*b*) at the strut axis in the *deflected* position (*see* Fig. 1).

The strut problems in aircraft structures can often be approximated to the type (*a*); the distributed axial loading can be taken as a constant shear flow q acting in the plane containing the undeformed strut axis, but once any flexural deformations have taken place this loading becomes equivalent to a distributed loading q applied at the strut axis in the deflected position and a distributed couple $n=qy$, where y is the flexural deflection of the strut. The type (*b*) occurs in struts loaded by their own weight, where the distributed loading q is applied at the strut axis in the deflected position.

The analysis of struts with uniformly distributed loading applied along the undeformed strut axis does not appear to have been published previously. On the other hand, struts with distributed loading applied at the strut axis in the deflected position have been analysed quite extensively in technical literature; the earliest paper on this subject is due to Greenhill[1], while a more general theory has been developed recently by Bültmann[2].

The main object of this paper is to present a general analysis of uniform elastic struts subjected to linearly varying axial loading, with particular reference to the

Received January 1959.

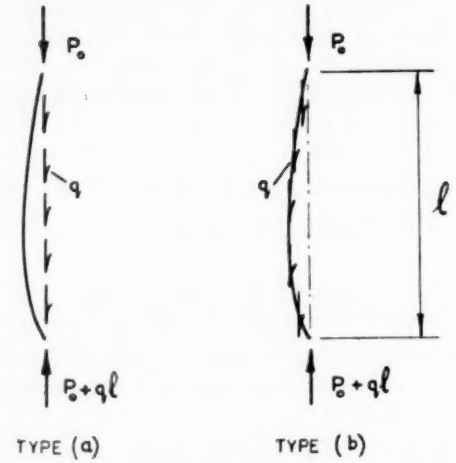

FIGURE 1. Basic types of axial loading.

two types of loading discussed earlier. The mathematical formulation of the problem and its solution present no difficulty. The derivation of the governing differential equations for the flexural deflections of struts under a general loading has already been given by Duncan[3]. The differential equations for the deflections can be solved with the aid of Bessel functions of order 1/3 but the practical application of these solutions is somewhat unwieldy. Another alternative is to use solutions in series form which can then be used directly for the calculation of deflections, slopes and bending moments. Such solutions would also allow a direct comparison with the special case of constant axial load which otherwise would not be possible with the solutions in terms of Bessel functions. In the present paper the series solution has been used as a basic solution, but the actual computation of the deflection functions and their first derivatives has been carried out via the Bessel function solution, because of slow convergence of the series solution; thus the necessity of computing a large number of terms in the series solution has been obviated. Only for the special case of a strut with zero axial load at one end, has the Bessel function solution been used directly.

The stability criteria for struts with various end conditions are given as a series of curves relating the maximum compressive axial load with the maximum distributed loading. This shows that struts with distributed loading applied along the undeformed strut axis are more stable than struts with loading applied at the strut axis in the deflected position.

Furthermore, explicit formulae for deflections and bending moment distributions have been compiled for several typical cases of lateral loading combined with axial loading of the type (*a*), which is of some practical importance in aircraft structures.

A numerical example is also included to show the practical application of the present analysis to a typical strut problem.

NOTATION

y, η flexural deflections

x distance measured along the loading axis

l strut length

e eccentricity of loading

I moment of inertia of the strut cross section

E Young's modulus

M bending moment

M_0, M_l bending moments at $x=0$ and $x=l$ respectively

S shear force

Q lateral concentrated load

$P=P_0+qx$, axial loading

P_0 axial load at $x=0$

q distributed compressive loading

w distributed lateral loading

n distributed bending couple

n_c constant distributed couple

$\mu^2=P_0/EI$

$\lambda^3=q/EI$

$\alpha=\lambda/\mu=(q^2EI/P_0^3)^{1/6}$

$\zeta=1+\alpha^3\mu x$

$z=\{2/(3\alpha^3)\}\{1+\alpha^3\mu x\}^{3/2}$

$z_0=(z)_{\mu x=0}=2/(3\alpha^3)$

$\theta=(2/3)(\lambda x)^{3/2}$

y_{CF} complementary functions

$y_1, \ldots, y_4$ complementary functions of equation (8*a*)

$\eta_1, \ldots, \eta_4$ complementary functions of equation (17)

y_5 particular integral of equation (8*a*)

η_5 particular integral of equation (17)

y_p integral defined by equation (57)

$\Phi_1(\mu x), \Phi_2(\mu x)$ Bessel function solutions of equation (44), defined by equations (46) and (47) respectively

$C_1, \ldots, C_4$ constants of integration

$A, \ldots, D$ constants of integration

a, b, c, d constant coefficients

k_1, k_2 constants

$W = \Phi_1'\Phi_2 - \Phi_2'\Phi_1$, Wronskian of equation (44)

$J_\nu(\ )$ Bessel function of the first kind of order ν

$Y_\nu(\ )$ Bessel function of the second kind of order ν

$\Gamma(\ )$ gamma function

$F(\mu x)$ function of μx

$\phi = dy/d(\mu x)$

$f(x), g(x)$ functions of x.

2. Governing Differential Equations for Deflections[3]

Consider the equilibrium of the element AB of length ds in a uniform strut subjected to distributed loading and let Ox be the axis of the strut when it is unloaded (*see* Fig. 2). The distributed loading consists of lateral loading w, compressive loading q and bending couple n; both w and q are assumed here to be constant. In the notation used in Fig. 2, P denotes the total load in the direction of xO applied to the right of the point A, while S is the total load in the direction of Oy applied to the right of A. The bending moment M at any cross section of the strut is the clockwise moment due to all external loads between x and $x=l$, where l is the strut length.

Taking moments about the point B and neglecting second-order terms,

$$P\frac{dy}{dx} + S - \frac{dM}{dx} + n = 0. \qquad (1)$$

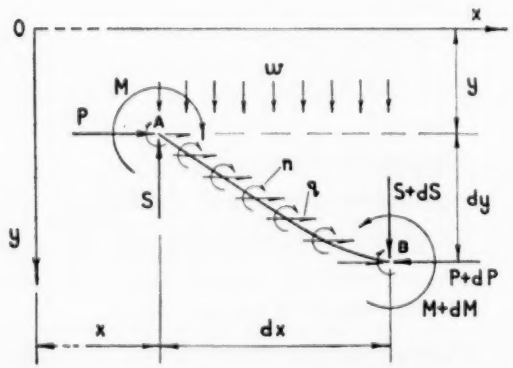

FIGURE 2. Forces and moments on element AB; for loading type (*a*), $n = n_e + qy$, while, for type (*b*), $n = n_e$, where n_e is a constant distributed couple.

Resolving forces along the y and x axes respectively,

$$\frac{dS}{dx} = -w \quad . \quad . \quad . \quad . \quad . \quad . \quad (2)$$

and $$\frac{dP}{dx} = q. \quad . \quad . \quad . \quad . \quad . \quad . \quad (3)$$

Equation (3) becomes, on integration,

$$P = P_0 + qx, \quad . \quad . \quad . \quad . \quad . \quad . \quad (4)$$

where P_0 is the axial load at $x = 0$.

From the linearised simple bending theory

$$M = -EI\frac{d^2y}{dx^2}, \quad . \quad . \quad . \quad . \quad . \quad (5)$$

where EI is the flexural rigidity of the strut. Differentiating equation (1) with respect to x, and then substituting equations (2), (4) and (5), the governing differential equation for the deflections is obtained:—

$$\frac{d^2}{dx^2}\left\{EI\frac{d^2y}{dx^2} + (P_0 + qx)\,y\right\} + \frac{d}{dx}\left\{n - qy\right\} = w. \quad . \quad . \quad (6)$$

For $q = 0$ and $n = 0$, equation (6) reduces to the well-known strut equation

$$EI\frac{d^4y}{dx^4} + P_0\frac{d^2y}{dx^2} = w. \quad . \quad . \quad . \quad . \quad (7)$$

Solutions of equation (6) are known for $n = 0$, *i.e.* for struts loaded by distributed compressive axial loading applied at the strut axis in the deflected position. An important case, however, arises in the analysis of compression members attached to shear panels. This may be represented approximately by a strut with linearly varying axial loading equilibrated by a distributed shear (shear flow) acting along the undeformed straight strut axis. This distributed shear, when transferred to the neutral axis of the deflected strut, becomes equivalent to a uniform distributed loading q and a distributed couple $n = qy$.

A constant distributed couple n_c can also be conveniently included in the general analysis, so that for the two basic types of loading the distributed couples can be taken as

(*a*) $n = n_c + qy$ and (*b*) $n = n_c$.

In Sections 3, 4 and 5, a detailed discussion of the general solution of equation (6) is given, with particular reference to these two types of loading.

3. Deflection Functions for $n=n_c+qy$ and $P_0 \neq 0$: Loading Type (a)

Substituting $n=n_c+qy$ in equation (6), the following basic equation is obtained

$$\frac{d^2}{dx^2}\left\{EI\frac{d^2y}{dx^2}+(P_0+qx)\,y\right\}=w. \quad . \quad . \quad . \quad . \quad (8)$$

Equation (8) does not involve n_c, but when this equation is solved n_c will appear in the constants of integration calculated by satisfying the end conditions at $x=0$ and $x=l$.

Introducing now two non-dimensional parameters $\mu^2=P_0/EI$ and $\alpha=\lambda/\mu$, where $\lambda^3=q/EI$, equation (8) can be re-written as

$$\frac{d^2}{d(\mu x)^2}\left\{\frac{d^2y}{d(\mu x)^2}+(1+\alpha^3\mu x)\,y\right\}=\frac{w}{\mu^2P_0}. \quad . \quad . \quad (8a)$$

Integrating this equation twice, it follows that

$$y''+(1+\alpha^3\mu x)\,y=C_3+C_4\mu x+\frac{w}{2\mu^2P_0}(\mu x)^2, \quad . \quad . \quad . \quad (9)$$

where C_3 and C_4 are arbitrary constants of integration and primes ($'$) denote derivatives with respect to μx.

The complementary functions of equation (9) can be obtained in a series form, using standard methods, so that

$$y_{CF}=C_1y_1+C_2y_2, \quad . \quad . \quad . \quad . \quad . \quad (10)$$

where C_1 and C_2 are arbitrary constants, while y_1 and y_2 are the two complementary functions. The detailed analysis used to obtain the solutions y_1 and y_2 is given separately in Appendix I, where the series solutions are derived in terms of Bessel functions.

The particular integrals of equation (9), together with the solutions y_1 and y_2, give the four complementary functions and one particular integral of equation (8*a*). Thus the complete solution of equation (9) or (8*a*) can be written as

$$y=C_1y_1+C_2y_2+C_3y_3+C_4y_4+wy_5/(2\mu^2P_0), \quad . \quad . \quad . \quad (11)$$

where y_3, y_4 and y_5 are the particular integrals of equation (9) with the right hand side equal to 1, (μx) and $(\mu x)^2$ respectively.

The solutions for the particular integrals of equation (9) are derived in Appendix I; the y_3 functions have been obtained by the method of variation of parameters, leading eventually to a numerical integration of Bessel functions of order 1/3, while the functions y_4 and y_5 have been obtained by inspection.

It is also shown that

$$y_4 = \frac{1 - y_3}{\alpha^3} + y_2, \quad . \quad . \quad . \quad . \quad . \quad (12)$$

and hence $$y_4' = \frac{-y_3'}{\alpha^3} + y_2'. \quad . \quad . \quad . \quad . \quad . \quad (13)$$

Similarly $$y_5 = -\frac{1 - y_3}{\alpha^6} + \frac{\mu x - y_2}{\alpha^5} - 2y_1 \quad . \quad . \quad (14)$$

and $$y_5' = \frac{y_3'}{\alpha^6} + \frac{1 - y_2'}{\alpha^5} - 2y_1'. \quad . \quad . \quad . \quad (15)$$

Substituting equation (11) into (5), and then using equation (9), it can be shown that the bending moment distribution in the strut is given by

$$\frac{M}{P_0} = (1 + \alpha^3 \mu x)(C_1 y_1 + C_2 y_2) + C_3\{(1 + \alpha^3 \mu x)\, y_3 - 1\} +$$

$$+ C_4\{(1 + \alpha^3 \mu x)\, y_4 - \mu x\} + \frac{w}{2\mu^2 P_0}\{(1 + \alpha^3 \mu x)\, y_5 - (\mu x)^2\}. \quad . \quad . \quad (16)$$

The functions y_1 to y_5 can be described as deflection functions for a strut with a linearly varying axial loading $P = P_0 + qx$, applied along the straight strut axis, and a distributed lateral loading w. The deflection functions y_1, y_2 and y_3, together with their first derivatives (slopes) are plotted in Figs. 3 to 8 for various values of the parameter $\alpha = (q^2 EI/P_0^3)^{1/6}$. The y_4 and y_5 functions are shown in Figs. 9 and 10, but for practical applications it is generally preferable to calculate these functions, and their first derivatives, from equations (12) to (15). In all cases the range of values of α has been restricted to $0 \leqslant \alpha \leqslant 2$. However, the special case of $\alpha = \infty$, corresponding to $P_0 = 0$, is discussed separately in Section 4.

It can be seen clearly from Figs. 3, 5, 7 and 9 that as α tends to zero the deflection functions degenerate into the general solution for the deflection of a uniform strut subjected to constant axial loading, *i.e.* $y_1 = \cos \mu x$, $y_2 = \sin \mu x$, $y_3 = 1$ and $y_4 = \mu x$.

4. Deflection Functions for $n = n_0 + qy$ and $P_0 = 0$: Loading Type (a)

If the end load $P_0 = 0$, then μx can no longer be used as an independent variable. Introducing therefore $\lambda x = (q/EI)^{1/3} x$ as the new independent variable, equation (8*a*) takes the form

$$\frac{d^2}{d(\lambda x)^2}\left\{\frac{d^2\eta}{d(\lambda x)^2} + \lambda x \eta\right\} = \frac{w}{\lambda q}, \quad . \quad . \quad . \quad (17)$$

where $\lambda^3 = q/EI$ and η is used in place of y to avoid confusion with solutions for $P_0 \neq 0$, *i.e.* for $0 \leqslant \alpha < \infty$.

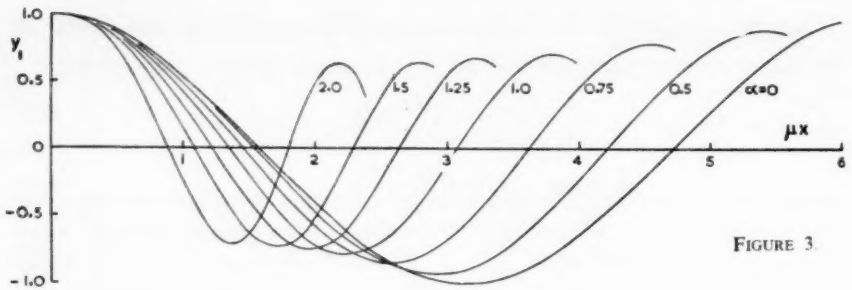

FIGURE 3.

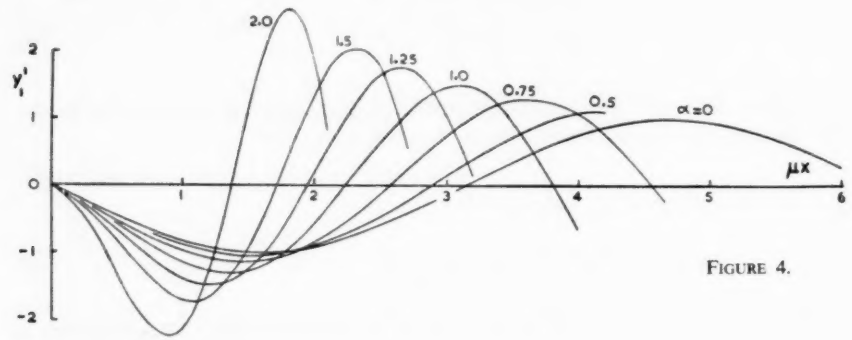

FIGURE 4.

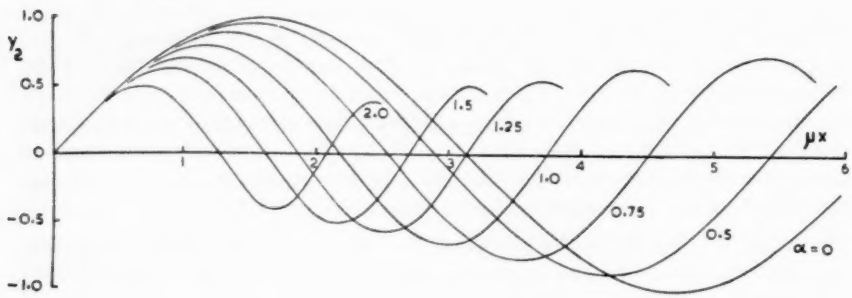

FIGURE 5.

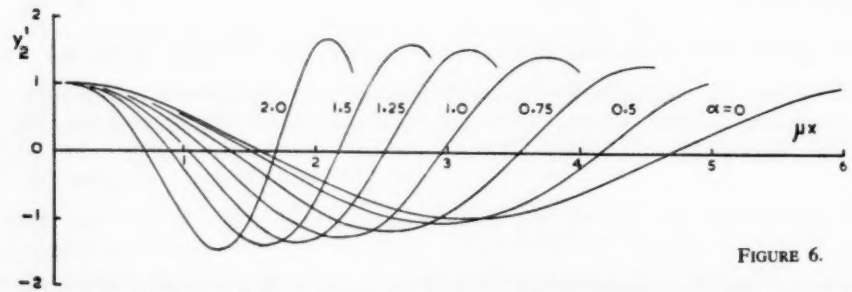

FIGURE 6.

FIGURE 3-6. Variation of the deflection functions y and their first derivatives (slopes) y' with μx and α.

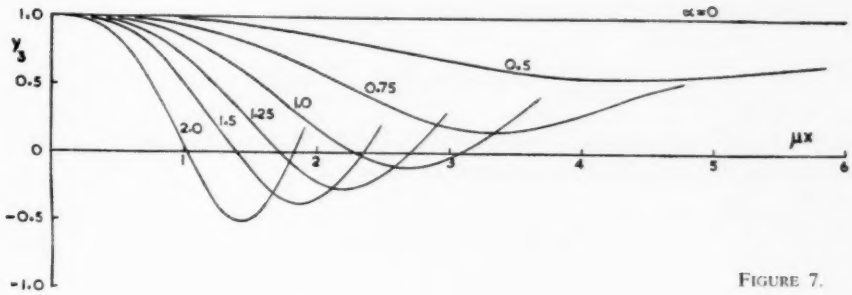

FIGURE 7.

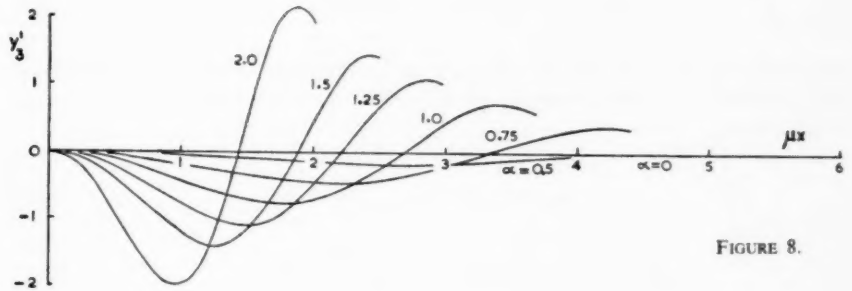

FIGURE 8.

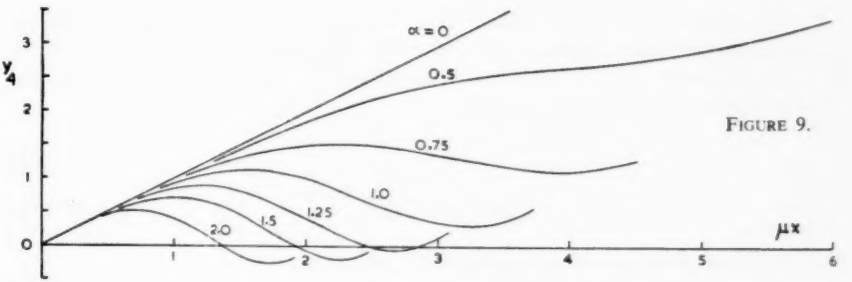

FIGURE 9.

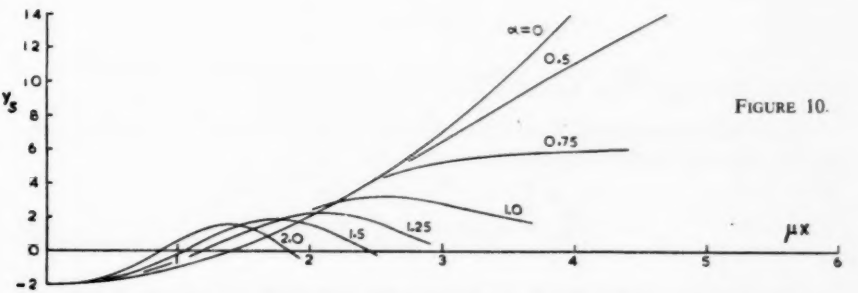

FIGURE 10.

FIGURES 7-10. Variation of the deflection functions y and their first derivatives (slopes) y' with μx and α.

Equation (17) can be integrated directly twice to give

$$\frac{d^2\eta}{d(\lambda x)^2} + \lambda x\eta = C + D\lambda x + \frac{w}{2\lambda q}(\lambda x)^2, \quad . \quad . \quad . \quad (18)$$

where C and D are arbitrary constants of integration. The complementary functions of this second-order differential equation are given by[4]

$$\eta_1 = (\lambda x)^{1/2} J_{1/3}\left[\frac{2}{3}(\lambda x)^{3/2}\right] \quad . \quad . \quad . \quad . \quad (19)$$

$$\text{and} \quad \eta_2 = (\lambda x)^{1/2} Y_{1/3}\left[\frac{2}{3}(\lambda x)^{3/2}\right], \quad . \quad . \quad . \quad (20)$$

where $J_{1/3}$ and $Y_{1/3}$ are Bessel functions of the first and second kind respectively and of order 1/3. Differentiating equations (19) and (20) with respect to (λx) it follows that

$$\eta_1' = d\eta_1/d(\lambda x) = \lambda x\, J_{-2/3}\left[\frac{2}{3}(\lambda x)^{3/2}\right] \quad . \quad . \quad . \quad (21)$$

$$\text{and} \quad \eta_2' = d\eta_2/d(\lambda x) = \lambda x\, Y_{-2/3}\left[\frac{2}{3}(\lambda x)^{3/2}\right]. \quad . \quad . \quad (22)$$

As in the previous case, the method of variation of parameters can be used to evaluate the particular integral η_3 when the right hand side of equation (18) is equal to 1 (*see* Appendix I); the other particular integrals can be obtained directly by inspection from equation (18), so that

$$\eta_4 = 1 \quad . \quad . \quad . \quad . \quad . \quad . \quad (23)$$

$$\text{and} \quad \eta_5 = \lambda x. \quad . \quad . \quad . \quad . \quad . \quad . \quad (24)$$

Hence the complete solution of equation (17) becomes

$$\eta = A\eta_1 + B\eta_2 + C\eta_3 + D + w\frac{\lambda x}{2\lambda q}, \quad . \quad . \quad . \quad (25)$$

where A, B, C, and D are arbitrary constants of integration.

Substituting equation (25) into (5), and then using equation (18), it can be shown that the bending moment distribution is given by

$$\frac{M}{q/\lambda} = \lambda x(A\eta_1 + B\eta_2) + C(\lambda x\eta_3 - 1). \quad . \quad . \quad . \quad (26)$$

The deflection functions η_1, η_2 and η_3 and their first derivatives (slopes) are shown in Figs. 11 and 12.

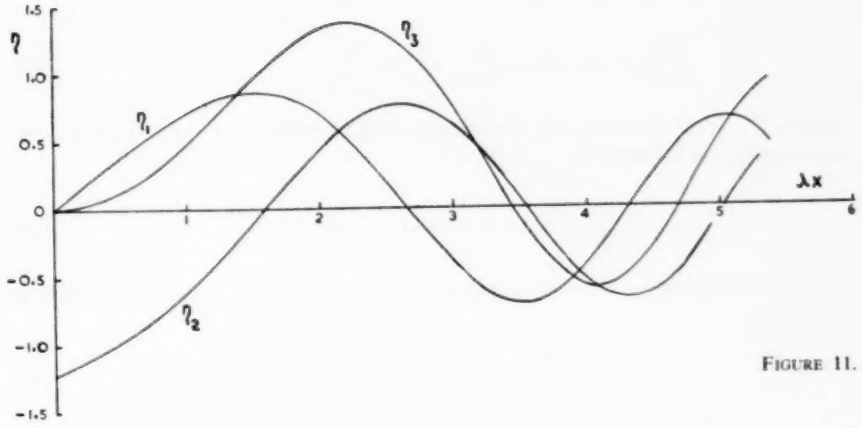

FIGURE 11.

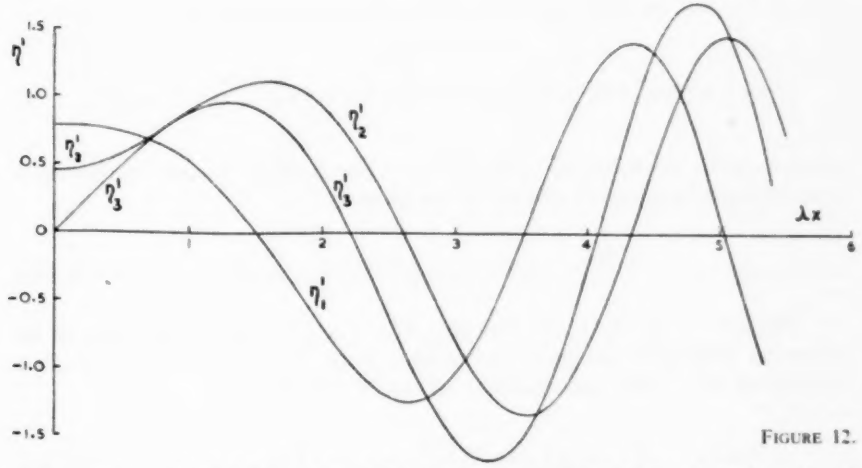

FIGURE 12.

FIGURE 11 AND 12. Variation of the deflection functions η and their first derivatives (slopes) η' with λx.

5. Deflection Functions for $n = n_c$: Loading Type (b)

For $n = n_c$ equation (6) takes the form

$$\frac{d^2}{dx^2}\left\{EI\frac{d^2y}{dx^2} + (P_c + qx)\,y\right\} - q\frac{dy}{dx} = w, \quad . \quad . \quad . \quad (27)$$

which becomes, using the non-dimensional variable μx,

$$\frac{d^2}{d(\mu x)^2}\left\{\frac{d^2y}{d(\mu x)^2} + (1 + x^3\mu x)\,y\right\} - x^2\frac{dy}{d(\mu x)} = \frac{w}{\mu^2 P_c}. \quad . \quad . \quad (27a)$$

Equation (27*a*) can be integrated immediately to give

$$\frac{d^3y}{d(\mu x)^3} + (1+\alpha^3\mu x)\frac{dy}{d(\mu x)} = C_3 + \frac{w}{\mu^2 P_0}\mu x, \quad . \quad . \quad . \quad . \quad (28)$$

where C_3 is a constant of integration. Substituting now $\phi = dy/d(\mu x)$ into equation (28) it follows that

$$\frac{d^2\phi}{d(\mu x)^2} + (1+\alpha^3\mu x)\phi = C_3 + \frac{w}{\mu^2 P_0}\mu x, \quad . \quad . \quad . \quad . \quad (29)$$

which is of the same form as equation (9) and therefore its complete solution is given by

$$\phi = \frac{dy}{d(\mu x)} = C_1 y_1 + C_2 y_2 + C_3 y_3 + \frac{w y_4}{\mu^2 P_0} \quad . \quad . \quad . \quad . \quad (30)$$

Thus in this case the deflected shape of the strut is determined by

$$y = C_1 \int_0^{\mu x} y_1\, d(\mu x) + C_2 \int_0^{\mu x} y_2\, d(\mu x) + C_3 \int_0^{\mu x} y_3\, d(\mu x) + C_4 + \frac{w}{\mu^2 P_0}\int_0^{\mu x} y_4\, d(\mu x), \quad (31)$$

where C_1 to C_4 are constants of integration. The bending moment distribution is obtained from equations (5) and (31) and is given by

$$\frac{M}{P_0} = -\left(C_1 y_1' + C_2 y_2' + C_3 y_3' + \frac{w y_4'}{\mu^2 P_0}\right). \quad . \quad . \quad (32)$$

Integrals of the deflection functions y_1, y_2 and y_3 have been obtained by numerical integration and these are shown in Figs. 13, 14, and 15. To calculate integrals of the y_4 functions, equation (12) can be used and gives

$$\int_0^{\mu x} y_4 d(\mu x) = \frac{\mu x}{\alpha^3} - \frac{1}{\alpha^3}\int_0^{\mu x} y_3 d(\mu x) + \int_0^{\mu x} y_2 d(\mu x) \ldots \quad . \quad . \quad (33)$$

Similarly, if the end load $P_0 = 0$ and λx is used as an independent variable, it can be shown that

$$\eta = A\int_0^{\lambda x} \eta_1 d(\lambda x) + B\int_0^{\lambda x} \eta_2 d(\lambda x) + C\int_0^{\lambda x} \eta_3 d(\lambda x) + D + w\frac{\lambda x}{\lambda q} \quad . \quad . \quad (34)$$

and

$$\frac{M}{q/\lambda} = -(A\eta_1' + B\eta_2' + C\eta_3'), \quad . \quad . \quad . \quad . \quad (35)$$

where primes (′) denote here derivatives with respect to λx. Integrals occurring in equation (34) have been obtained by numerical integration and are shown in Fig. 16.

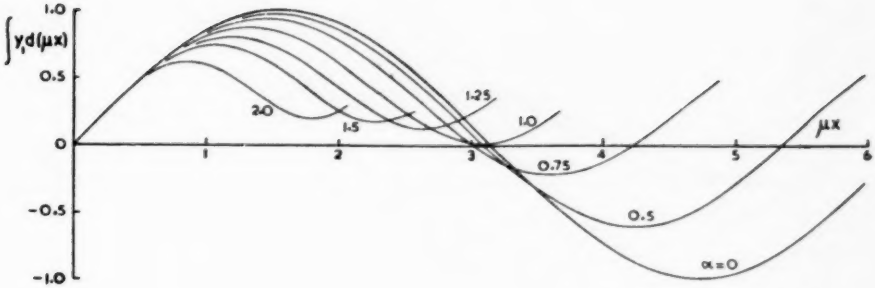

FIGURE 13.

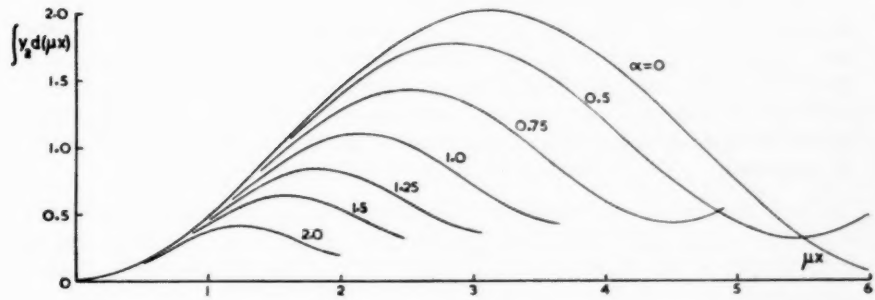

FIGURE 14.

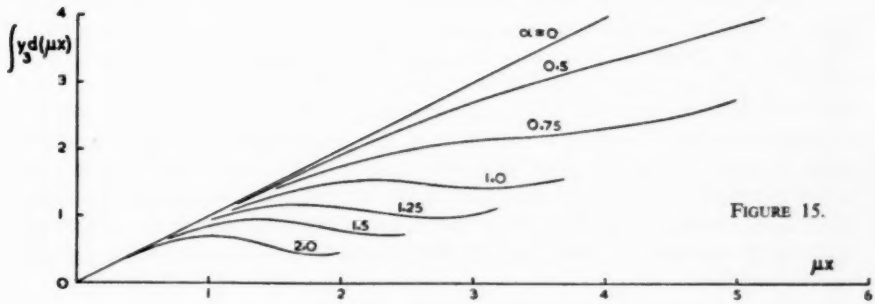

FIGURE 15.

FIGURES 13-15. Variation of integrals $\int_0^{\mu x} y d(\mu x)$ with μx and α.

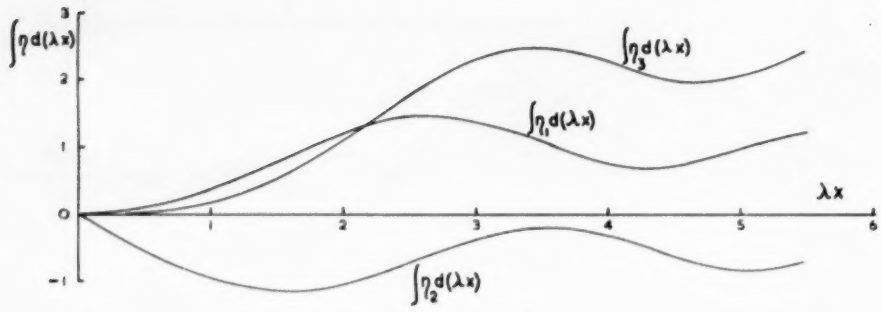

FIGURE 16. Variation of integrals $\int_0^{\lambda x} \eta d(\lambda x)$ with λx.

6. Statically Determinate Problems

If a strut is subjected to lateral loading or end bending moments, then it is possible to determine deflections, and hence bending moment distributions, for given end conditions. In such cases the end conditions provide a sufficient number of equations, at least one of which is non-homogeneous, to determine the unknown constants of integration in the general solution for deflections. Multi-bay struts present no difficulty, apart from the increase in the number of unknown constants of integration.

Several common cases occurring in the analysis of aircraft structures for which $n = n_c + qy$, *i.e.* type (*a*), have been compiled in Appendix III. Furthermore, to facilitate the calculation of bending moments for the case of eccentrically loaded struts, which is usually the most common case in practice, the y_1 and y_2 functions have also been plotted in a carpet form in Figs. 17 and 18.

7. Instability Loads

If no external lateral loading or bending moments are applied to the strut then it is not possible to determine the deflections from the corresponding kinematic boundary conditions at the ends of the strut. The boundary conditions give then only a set of four homogeneous linear equations for the deflection functions y_1 to y_4 with a trivial solution $y = 0$. For the deflections to have values other than zero, the determinant formed by the coefficients from the simultaneous equations must be equal to zero. When expanded, this determinant yields a transcendental equation which constitutes the required stability criterion for the compressive load P_0 and the distributed loading q, and the roots of this transcendental equation give a functional relationship between P_0 and q which determines the stability boundary for the applied loading.

The stability boundaries have been calculated for typical end conditions and are plotted in Fig. 19 as a series of curves relating the maximum compressive axial load P_0 with the maximum distributed loading q which, when applied simultaneously, produce flexural instability of the strut. This shows that struts with

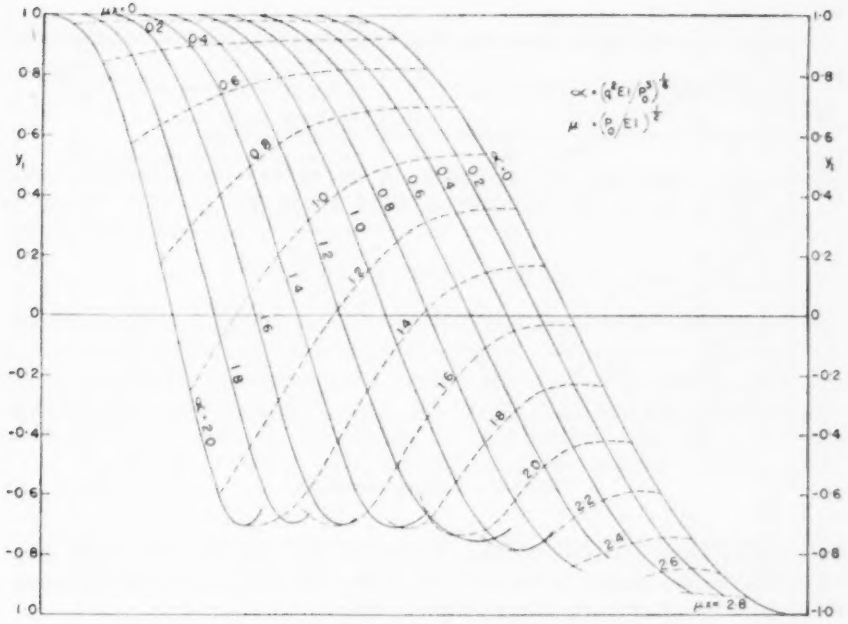

FIGURE 17. Carpet plot for the y_1 functions.

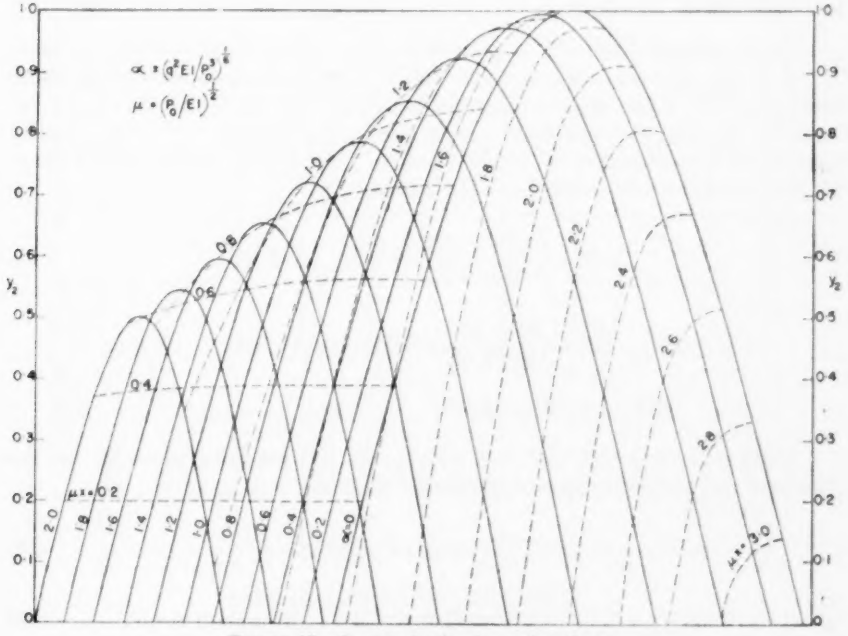

FIGURE 18. Carpet plot for the y_2 functions.

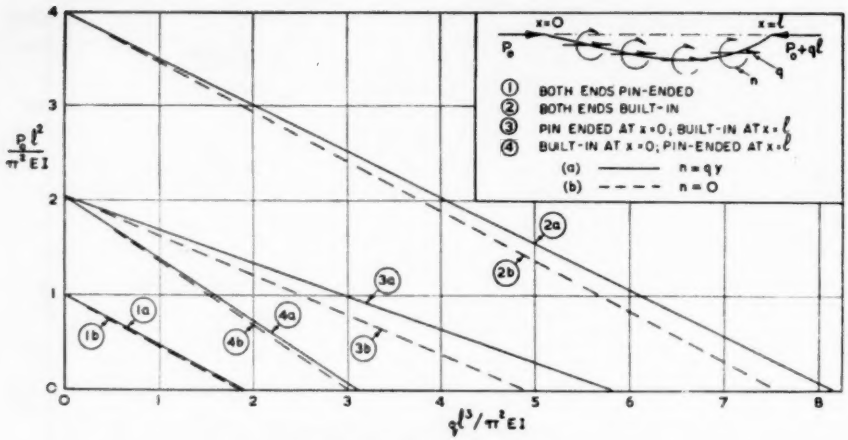

FIGURE 19. Stability boundaries.

distributed loading applied along the undeformed strut axis are more stable than struts with loading applied at the strut axis in the deflected position; the difference between the two cases is a maximum when $P_0=0$.

8. Numerical Example

As an example, consider a pin-ended strut subjected to bending moments $M_0=P_0e$ and $M_l=(P_0+ql)e$ at $x=0$ and $x=l$ respectively, a distributed shear loading $q=800$ lb./in. applied along the strut axis, and axial load $P_0=20{,}000$ lb. Thus for this case the distributed couple $n=n_0+qy$, where $n_0=qe$, and e can be regarded as the eccentricity of applied loading. The flexural rigidity $EI=1{\cdot}673\times10^6$ lb.in.^{2} and the strut length $l=20$ in. Hence

$$(\mu l)^2=\frac{20{,}000\times20^2}{1{\cdot}673\times10^6}=4{\cdot}782,\quad \mu l=2{\cdot}187,$$

$$(\lambda l)^3=\frac{800\times20^3}{1{\cdot}673\times10^6}=3{\cdot}826,\quad \lambda l=1{\cdot}564,$$

and $$\alpha=\lambda/\mu=0{\cdot}715.$$

Using equations (11) and (16) with $w=0$, the general expressions for the deflection and bending moment distributions become

$$y=C_1y_1+C_2y_2+C_3y_3+C_4y_4 \quad . \quad . \quad . \quad . \quad (36)$$

$$\frac{M}{P_0}=(1+\alpha^3\mu x)(C_1y_1+C_2y_2)+C_3\left[(1+\alpha^3\mu x)\,y_3-1\right]+C_4\left[(1+\alpha^3\mu x)\,y_4-\mu x\right]. \quad . \quad (37)$$

These equations are to be solved subject to the boundary conditions

$$\left.\begin{aligned} y=0,\quad M&=P_0 e \qquad \text{at } x=0 \\ y=0,\quad M&=(P_0+ql)\,e \qquad \text{at } x=l \end{aligned}\right\} \quad . \quad . \quad . \quad . \quad . \quad (38)$$

Using these boundary conditions to determine the unknown constants of integration C_1 to C_4, and noting from equation (12) that $y_4=(1-y_3)/\alpha^2+y_2$, it follows finally that

$$M=P_0\,e\,(1+\alpha^2\mu x)\,[y_1-(y_{1l}-1)\,y_2/y_{2l}], \quad . \quad . \quad . \quad (39)$$

where the additional suffix l denotes the values of y_1, y_2 at $x=l$. Variation of the bending moment with x/l, calculated from equation (39), is shown in Fig. 20. To illustrate the difference between the distributed and constant loading cases the bending moment distributions for $P=P_0$ and $P=P_0+ql$ are also included in Fig. 20, which shows clearly that in this case the use of a constant axial load $P=P_0+ql$, *i.e.* $P=36{,}000$ lb., would overestimate the maximum bending moment by a large factor.

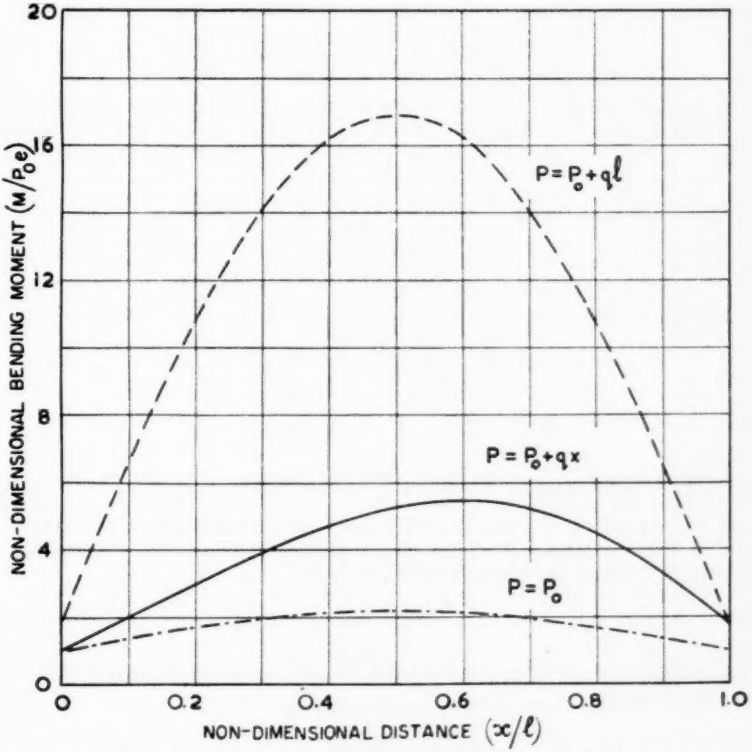

FIGURE 20. Numerical example: bending moment distribution.

ACKNOWLEDGMENT

The author wishes to acknowledge the permission of Bristol Aircraft Limited to publish this paper. Grateful thanks are also due to Miss M. W. Gadge for computing the deflection functions.

Appendix I

GENERAL SOLUTION OF EQUATIONS (9) AND (18)

The governing differential equation for calculating the deflected shape of a loaded strut is of the form (*see* equation (9))

$$y''+(1+\alpha^3\mu x)\,y=F(\mu x), \qquad (40)$$

where $F(\mu x)$ is a function of the independent variable μx. The two complementary functions of this equation can be obtained by the well-known method of series integration. It can be shown easily that this leads to

$$y_{CF}=C_1y_1+C_2y_2, \qquad (10)$$

where C_1 and C_2 are arbitrary constants of integration and y_1 and y_2 are given by

$$y_1=\cos\mu x+\alpha^3\left\{-\frac{1}{3!}(\mu x)^3+\frac{4}{5!}(\mu x)^5-\frac{9}{7!}(\mu x)^7+\ldots.\right\}+$$

$$+\alpha^6\left\{\frac{4}{6!}(\mu x)^6-\frac{28}{8!}(\mu x)^8+\ldots.\right\}+$$

$$+\ldots. \qquad (41)$$

and

$$y_2=\sin\mu x+\alpha^3\left\{-\frac{2}{4!}(\mu x)^4+\frac{6}{6!}(\mu x^6)-\frac{12}{8!}(\mu x)^8+\ldots.\right\}+$$

$$+\alpha^6\left\{\frac{10}{7!}(\mu x)^7-\frac{52}{9!}(\mu x)^9+\ldots.\right\}+$$

$$+\ldots. \qquad (42)$$

These expressions can be used for small values of μx, but for $\mu x>1$ the convergence of the series is not satisfactory. For $\alpha=0$, *i.e.* for constant axial loading, the two solutions become simply $y_1=\cos\mu x$ and $y_2=\sin\mu x$. An alternative solution can be obtained in terms of Bessel functions of the first and second kind by changing the independent variable μx into a new variable ζ given by

$$\zeta=1+\alpha^3\mu x. \qquad (43)$$

Hence, provided that α is finite and not equal to zero, equation (40) with $F(\mu x)=0$ can be transformed into

$$\frac{d^2y}{d\zeta^2}+\frac{\zeta y}{\alpha^6}=0. \qquad (44)$$

The solution of equation (44) is given by[4]

$$y_{cr}=A\Phi_1(\mu x)+B\Phi_2(\mu x), \quad . \quad . \quad . \quad . \quad . \quad (45)$$

where A and B are arbitrary constants and

$$\Phi_1(\mu x)=\left(\frac{\zeta}{x^2}\right)^{1/2} J_{1/3}\left[\frac{2}{3}\left(\frac{\zeta}{x^2}\right)^{3/2}\right]=\left(\frac{3z}{2}\right)^{1/3} J_{1/3}(z) \quad . \quad (46)$$

$$\Phi_2(\mu x)=\left(\frac{\zeta}{x^2}\right)^{1/2} Y_{1/3}\left[\frac{2}{3}\left(\frac{\zeta}{x^2}\right)^{3/2}\right]=\left(\frac{3z}{2}\right)^{1/3} Y_{1/3}(z) \quad . \quad . \quad (47)$$

and $$z=\frac{2}{3}\left(\frac{\zeta}{x^2}\right)^{3/2}=\frac{2}{3x^3}(1+x^3\mu x)^{3/2}. \quad . \quad . \quad . \quad . \quad (48)$$

Differentiating equations (46) and (47) with respect to μx it follows that

$$\Phi_1'(\mu x)=x\left(\frac{3z}{2}\right)^{2/3} J_{-2/3}(z) \quad . \quad . \quad . \quad . \quad (49)$$

and $$\Phi_2(\mu x)=x\left(\frac{3z}{2}\right)^{2/3} Y_{-2/3}(z). \quad . \quad . \quad . \quad . \quad (50)$$

The series solutions y_1 and y_2 must obviously be linear combinations of the Bessel function solutions $\Phi_1(\mu x)$ and $\Phi_2(\mu x)$, because the latter are solutions of the same differential equation (40). Hence

$$\begin{bmatrix} y_1 \\ y_2 \end{bmatrix}=\begin{bmatrix} a & b \\ c & d \end{bmatrix}\begin{bmatrix} \Phi_1 \\ \Phi_2 \end{bmatrix}; \quad \begin{bmatrix} y_1' \\ y_2' \end{bmatrix}=\begin{bmatrix} a & b \\ c & d \end{bmatrix}\begin{bmatrix} \Phi_1' \\ \Phi_2' \end{bmatrix}, \quad (51)$$

where a, b, c and d are constant coefficients. From equations (41) and (42) it follows immediately that

$$\left.\begin{aligned} y_1(0)&=1 \; ; \quad & y_1'(0)&=0 \\ y_2(0)&=0 \; ; \quad & y_2'(0)&=1 \end{aligned}\right\} \quad . \quad . \quad . \quad . \quad . \quad (52)$$

The unknown coefficients from equation (51) can now be determined from (52) and it is found that

$$\left.\begin{aligned} a&=-\Phi_2'(0)/W \\ b&=\Phi_1'(0)/W \\ c&=\Phi_2(0)/W \\ d&=-\Phi_1(0)/W, \end{aligned}\right\} \quad . \quad . \quad . \quad . \quad . \quad (53)$$

where $$W=\Phi_1'(0)\,\Phi_2(0)-\Phi_2'(0)\,\Phi_1(0). \quad . \quad . \quad . \quad (54)$$

The expression (54) for W is the Wronskian determinant of equation (44) and it can be shown that it is equal to $-3\alpha/\pi$ (*see* Appendix II).

Bessel functions of the first and second kind of order $1/3$ and $-2/3$, occurring in equations (46), (47), (49) and (50), have already been tabulated[5, 6] and therefore it has been possible to compute the y_1 and y_2 functions and their derivatives (slopes) from equations (51), (53) and (54).

It remains now to determine the particular integrals of equation (40) which, together with the solutions y_1 and y_2, will give four complementary functions and one particular integral of equation (8*a*). The particular integrals of equation (40) can be best found by means of the method of variation of parameters. This method gives the general solution of equation (40) in the form[7]

$$y=y_1\int_{k_1}^{\mu x}\frac{F(\mu x)\,y_2 d(\mu x)}{(y_1'y_2-y_2'y_1)}-y_2\int_{k_2}^{\mu x}\frac{F(\mu x)\,y_1 d(\mu x)}{(y_1'y_2-y_2'y_1)}, \qquad (55)$$

where the lower limits k_1 and k_2 are arbitrary and they introduce constant multipliers of y_1 and y_2, while the upper limits give the required particular integrals. It is shown in Appendix II that the Wronskian determinant of equations (40) or (9) is given by $y_1'y_2-y_2'y_1=-1$. Hence the calculation of the particular integrals of equation (9) reduces to the integration of

$$y_p=-y_1\int_0^{\mu x}F(\mu x)\,y_2 d(\mu x)+y_2\int_0^{\mu x}F(\mu x)\,y_1 d(\mu x), \qquad (56)$$

where, for $F(\mu x)$, the values 1, μx, and $(\mu x)^2$ are substituted in turn. For the purpose of computing integrals in equation (56) it has been assumed arbitrarily that $k_1=k_2=0$. Thus equation (56) represents the particular integral, together with some undetermined parts of the complementary functions y_1 and y_2.

Changing the independent variable μx into z in equation (56) by means of equation (48), substituting $F(\mu x)=1$, and then using equations (46), (47), (51), (53) and (54), it follows that

$$y_p=\frac{1}{\alpha W}\left(\frac{3z}{2}\right)^{1/3}\left\{-Y_{1/3}(z)\int_{z_0}^{z}J_{1/3}(z)\,dz+J_{1/3}(z)\int_{z_0}^{z}Y_{1/3}(z)\,dz\right\}$$

$$=Ay_1+By_2+y_3, \qquad (27)$$

with $$z_0=(z)_{\mu x=0}=2/(3\alpha^3), \qquad (48a)$$

where A and B are constants and y_3 is the particular integral of equation (40) with $F(\mu x)=1$. The constants A and B are determined from the condition that when α tends to zero, y_3 should tend to one, which is the correct particular integral for $y''+y=1$. Substituting $y_1=\cos\mu x$ and $y_2=\sin\mu x$ into equation (56) with $k_1=k_2=0$, integrating the resulting equation and then using equation (57), it can be shown that

$$y_3=y_p+y_1. \qquad (58)$$

Differentiating equation (58) with respect to μx,

$$y_3' = y_p' + y_1', \quad . \quad . \quad . \quad . \quad . \quad . \quad . \quad (59)$$

where $$y_p' = \frac{1}{W}\left(\frac{3z}{2}\right)^{2/3} \left\{ J_{-2/3}(z) \int_{z_0}^{z} Y_{1/3}(z)\,dz - Y_{-2/3}(z) \int_{z_0}^{z} J_{1/3}(z)\,dz. \right\} \quad . \quad (60)$$

Functions represented by equations (57) and (60) have been computed by numerical integration of $\int J_{1/3}(z)\,dz$ and $\int Y_{1/3}(z)\,dz$, since no simple expressions could be derived in terms of known tabulated functions.

For $F(\mu x)=\mu x$ and $F(\mu x)=(\mu x)^2$, there is no need to calculate the particular integrals separately, since the results for $F(\mu x)=1$, *i.e.* the y_3 functions, can be directly used for that purpose without any additional numerical integration. The method used becomes apparent from Table I.

TABLE I

TABLE OF PARTICULAR INTEGRALS

Equation No.	*Differential Equation*	*Particular Integral*
(*i*)	$y''+(1+x^3\mu x)\,y=1$	y_3
(*ii*)	$y''+(1+x^3\mu x)\,y=\mu x$	y_4
(*iii*)	$y''+(1+x^3\mu x)\,y=(\mu x)^2$	y_5
(*iv*)	$y''+(1+x^3\mu x)\,y=1+x^3\mu x$	1
(*v*)	$y''+(1+x^3\mu x)\,y=\mu x+x^3(\mu x)^2$	μx

The particular integrals for equations (*iv*) and (*v*) in Table I have been obtained by inspection. Substituting now appropriate particular solutions into the differential equations (*i*), (*ii*) and (*iii*), and then adding equation (*i*) to x^3 times equation (*ii*),

$$(y_3''+x^3y_4'')+(1+x^3\mu x)(y_3+x^3y_4)=1+x^3\mu x.$$

Hence, using the particular solution for equation (*iv*), it follows that

$$y_4=\frac{1-y_3}{x^3}.$$

Comparing now the functional behaviour of this equation at the origin $x=0$ with the particular solution for $x=0$, *i.e.* $y_4=\mu x$, it is found necessary to modify it by adding the complementary function y_2 so that

$$y_4=\frac{(1-y_3)}{x^3}+y_2 \quad . \quad . \quad . \quad . \quad . \quad . \quad . \quad (12)$$

and hence $$y'_4=-\frac{y_3'}{x^3}+y_2'. \quad . \quad . \quad . \quad . \quad . \quad . \quad (13)$$

Similarly it can be shown that for $F(\mu x)=(\mu x)^2$ the particular solution y_5 is given by

$$y_5=\frac{\mu x-y_4}{\alpha^3}-2y_1$$

$$=-\frac{1-y_3}{\alpha^6}+\frac{\mu x-y_2}{\alpha^3}-2y_1 \quad . \quad . \quad . \quad (14)$$

and $$y_5'=\frac{y_3'}{\alpha^6}+\frac{1-y_2'}{\alpha^3}-2y_1'. \quad . \quad . \quad . \quad . \quad . \quad (15)$$

Now from equations (9) and (8*a*) it follows that the functions y_1, y_2, y_3 and y_4 are the four complementary functions of equation (8*a*), while y_5 is the particular integral for uniformly distributed lateral loading w. Thus the complete solution of equation (8*a*) can be written as

$$y=C_1y_1+C_2y_2+C_3y_3+C_4y_4+\frac{wy_5}{2\mu^2P_0}. \quad . \quad . \quad . \quad (11)$$

For the case of $P_0=0$, *i.e.* $\alpha=\infty$, the governing differential equation is

$$\frac{d^2\eta}{d(\lambda x)^2}+\lambda x\eta=C+D\lambda x+\frac{w}{2\lambda q}(\lambda x)^2. \quad . \quad . \quad . \quad . \quad (18)$$

To evaluate the particular integrals of this equation the method of variation of parameters can also be used. For the right hand side of equation (18) equal to one, the particular integral is given by

$$\eta_3=\eta_1\int_0^{\lambda x}\frac{\eta_2 d(\lambda x)}{\eta_1'\eta_2-\eta_2'\eta_1}-\eta_2\int_0^{\lambda x}\frac{\eta_1 d(\lambda x)}{\eta_1'\eta_2-\eta_2'\eta_1}, \quad . \quad . \quad (61)$$

where the lower limits have been chosen arbitrarily. In this case the Wronskian determinant is given by $\eta_1'\eta_2-\eta_2'\eta_1=-3/\pi$ (*see* Appendix II) so that, substituting equations (19) and (20) into (61), it follows that

$$\eta_3=-\frac{\pi}{3}(\lambda x)^{1/2}\left\{J_{1/3}\left[\frac{2}{3}(\lambda x)^{3/2}\right]\int_0^{\lambda x}(\lambda x)^{1/2}Y_{1/3}\left[\frac{2}{3}(\lambda x)^{3/2}\right]d(\lambda x)-\right.$$

$$\left.-Y_{1/3}\left[\frac{2}{3}(\lambda x)^{3/2}\right]\int_0^{\lambda x}(\lambda x)^{1/2}J_{1/3}\left[\frac{2}{3}(\lambda x)^{3/2}\right]d(\lambda x)\right\} \quad . \quad . \quad (62)$$

and thence

$$\eta_3'=\frac{d\eta_3}{d(\lambda x)}=-\frac{\pi}{3}\lambda x\left\{J_{-2/3}\left[\frac{2}{3}(\lambda x)^{3/2}\right]\int_0^{\lambda x}(\lambda x)^{1/2}Y_{1/3}\left[\frac{2}{3}(\lambda x)^{3/2}\right]d(\lambda x)-\right.$$

$$\left.-Y_{-2/3}\left[\frac{2}{3}(\lambda x)^{3/2}\right]\int_0^{\lambda x}(\lambda x)^{1/2}J_{1/3}\left[\frac{2}{3}(\lambda x)^{3/2}\right]d(\lambda x)\right\} \quad . \quad . \quad (63)$$

Integrals occurring in equations (62) and (63) can be transformed into integrals $\int J_{1/3}(\theta)\,d\theta$ and $\int Y_{1/3}(\theta)\,d\theta$ by the substitution $\theta=(2/3)(\lambda x)^{3/2}$. Since these integrals had to be calculated for equations (57) and (60), no additional computation is required for the calculation of the η_3 and η_3' functions. The remaining particular integrals can be obtained by inspection; for the right hand side of equation (18) equal to λx,

$$\eta_4=1, \quad . \quad . \quad . \quad . \quad . \quad . \quad . \quad . \quad (23)$$

while for $(\lambda x)^2$ the particular integral

$$\eta_5=\lambda x. \quad . \quad . \quad . \quad . \quad . \quad . \quad . \quad . \quad (24)$$

The deflection functions η_1, η_2, η_3 and η_4 are the four complementary functions of equation (18), while η_5 is the particular integral for uniformly distributed lateral loading w. Hence the general solution of equation (18) becomes simply

$$\eta=A\eta_1+B\eta_2+C\eta_3+D\eta_4+w\,\frac{\lambda x}{2\lambda q}. \quad . \quad . \quad . \quad . \quad . \quad (25)$$

Appendix II

WRONSKIANS OF EQUATIONS (9), (18) AND (44)

Let y_1 and y_2 be two solutions of the second-order differential equation

$$\frac{d^2y}{dx^2}+f(x)\frac{dy}{dx}+g(x)=0, \quad . \quad . \quad . \quad . \quad . \quad (64)$$

where $f(x)$ and $g(x)$ are functions of an independent variable x. The Wronskian W of the two independent solutions y_1 and y_2 is defined as

$$W=-\begin{vmatrix} y_1 & y_2 \\ \dfrac{dy_1}{dx} & \dfrac{dy_2}{dx} \end{vmatrix}=\frac{dy_1}{dx}y_2-\frac{dy_2}{dx}y_1. \quad . \quad . \quad . \quad (65)$$

This determinant can be obtained, except for a constant factor, directly from the differential equation by means of the relationship

$$W=A\exp\left[-\int^x f(x)\,dx\right], \quad . \quad . \quad . \quad . \quad . \quad (66)$$

where A is a constant factor. Hence the Wronskians for equations (9), (18) and (44) are independent of x, since in all three equations $f(x)=0$.

Consider now the Wronskian of equation (44), which is given by

$$\begin{aligned} W&=\Phi_1'\Phi_2-\Phi_2'\Phi_1 \\ &=-\frac{3xz}{2}\left[J_{1/3}(z)\,Y_{-2/3}(z)-J_{-2/3}(z)\,Y_{1/3}(z)\right] \\ &=-\sqrt{3}\,xz\left[J_{1/3}(z)\,J_{2/3}(z)+J_{-1/3}(z)\,J_{-2/3}(z)\right]. \quad . \quad . \quad . \quad (67) \end{aligned}$$

Here $$z=\frac{2}{3\alpha^3}(1+\alpha^3\mu x)^{3/2} \quad . \quad . \quad . \quad . \quad . \quad . \quad . \quad . \quad (48)$$

and primes (′) denote derivatives with respect to μx. The last expression in equation (67) is obtained by means of the following identity for Bessel functions of the second kind:—

$$Y_\nu(z)=\frac{\{J_\nu(z)\cos\nu\pi-J_{-\nu}(z)\}}{\sin\nu\pi} \quad . \quad . \quad . \quad . \quad . \quad . \quad . \quad . \quad (68)$$

Since in this case the Wronskian is independent of μx and z, W can conveniently be calculated at $z=0$. Substituting therefore approximate expressions for Bessel functions when z is small, and then letting z tend to zero, it can be shown that

$$W=-\frac{2\sqrt{3}\,\alpha}{\Gamma(2/3)\,\Gamma(1/3)} \quad . \quad . \quad . \quad . \quad . \quad . \quad (69)$$

Using now the property of the gamma function that

$$\Gamma(x)\,\Gamma(1-x)=\frac{\pi}{\sin\pi x}, \quad . \quad . \quad . \quad . \quad . \quad . \quad . \quad (70)$$

equation (69) becomes

$$W=-3\alpha/\pi. \quad . \quad . \quad . \quad . \quad . \quad . \quad . \quad (71)$$

Similarly the Wronskians of equations (9) and (18) can be evaluated at $x=0$.

This gives $$y_1'y_2-y_2'y_1=-1 \quad . \quad . \quad . \quad . \quad . \quad . \quad . \quad (72)$$

and $$\eta_1'\eta_2-\eta_2'\eta_1=-3/\pi. \quad . \quad . \quad . \quad . \quad . \quad . \quad (73)$$

Appendix III

Bending Moments and Deflections

The formulae for the deflections and bending moments in Table II may be applied to any strut with constant cross section, in which the elementary formula connecting curvature and bending moment holds and the distributed axial loading is applied along the straight loading axis, *i.e.* loading type (*a*).

The formulae for the deflections and bending moments in Table II, with the exception of Cases 3 and 8, have been derived directly from the basic equations (11) and (16) or (25) and (26), using appropriate boundary conditions. For Cases 3 and 8, where a concentrated lateral load Q is applied, two separate sets of basic equations with eight arbitrary constants must be considered, corresponding to the two regions for $0\leqslant x\leqslant l_1$ and $l_1\leqslant x\leqslant l$. Some simplification, however, may be achieved by considering the differential equations for the bending moment in a pin-ended strut subjected to a concentrated lateral load.

TABLE II

SUMMARY OF FORMULAE FOR BENDING MOMENTS AND DEFLECTIONS

(Bars over functions denote the values at $x=l$)

Mode of Support and Loading	*Deflection and Bending Moment*
1. Ends pin-ended. Compression end loads, distributed shear and end couples 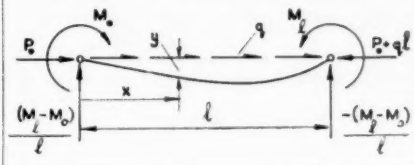	$y=\frac{M_0}{P_0}\left\{y_1+(\bar{y}_3-\bar{y}_1)\frac{y_2}{\bar{y}_2}-y_3\right\}+$ $+\frac{(M_1-M_0)}{P_0\mu l}\left\{\frac{\bar{y}_4}{\bar{y}_2}y_2-y_4\right\}$ $M=M_0\left\{1+(1+\alpha^3\mu x)\left(y_1+\frac{\bar{y}_3-\bar{y}_1}{\bar{y}_2}y_2-y_3\right)\right\}+$ $+\frac{(M_1-M_0)}{\mu l}\left\{\mu x-(1+\alpha^3\mu x)\left(-\frac{\bar{y}_4}{\bar{y}_2}y_2+y_4\right)\right\}$
2. Ends pin-ended. Compression end loads, distributed shear and uniform lateral loading 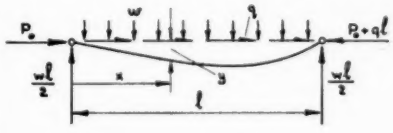	$y=\frac{w}{\mu^2P_0}\left\{y_1-\left(\bar{y}_1-\frac{\mu l}{2}\bar{y}_4+\frac{1}{2}\bar{y}_5\right)\frac{y_2}{\bar{y}_2}-\right.$ $\left.-\frac{\mu l}{2}y_4+\frac{1}{2}y_5\right\}$ $M=\frac{w}{\mu^2}(1+\alpha^3\mu x)\left\{y_1-\left(\bar{y}_1-\frac{\mu l}{2}\bar{y}_4+\frac{1}{2}\bar{y}_5\right)\frac{y_2}{\bar{y}_2}-\right.$ $\left.-\frac{\mu l}{2}y_4+\frac{1}{2}y_5\right\}+\frac{w}{\mu^2}\left\{\frac{\mu l}{2}\mu x-\frac{1}{2}(\mu x)^2\right\}$
3. Ends pin-ended. Compression end loads, distributed shear and concentrated lateral load 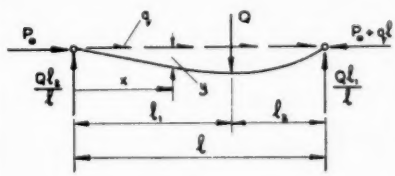	$y=Ay_1+By_2-\frac{Ql_2}{\mu lP_0}y_4$ for $0\leqslant\mu x\leqslant\mu l_1$ $y=Cy_1+Dy_2-\frac{Ql_1}{P_0}\left(y_3-\frac{y_4}{\mu l}\right)$ for $\mu l_1\leqslant\mu x\leqslant\mu l$ $\frac{M}{P_0}=(1+\alpha^3\mu x)\left\{Ay_1+By_2-\frac{Ql_2}{\mu lP_0}y_4\right\}+\frac{Ql_2}{\mu lP_0}\mu x$ for $0\leqslant\mu x\leqslant\mu l_1$ $\frac{M}{P_0}=(1+\alpha^3\mu x)\left\{Cy_1+Dy_2-\frac{Ql_1}{P_0}\left(y_3-\frac{y_4}{\mu l}\right)\right\}+$ $+\frac{Ql_1}{P_0}\left(1-\frac{x}{l}\right)$ for $\mu l_1\leqslant\mu x\leqslant\mu l$, where A, B, C and D are constants determined from the conditions that $y=0$ at each end, and the conditions that y and y' should be continuous at $x=l_1$.
4. Ends pin-ended. Eccentrically applied compression end loads and distributed shear 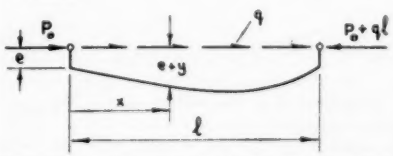	$y+e=e\left\{y_1+\frac{(1-\bar{y}_1)}{\bar{y}_2}y_2\right\}$ $M=eP_0(1+\alpha^3\mu x)\left\{y_1+\frac{(1-\bar{y}_1)}{\bar{y}_2}y_2\right\}$

TABLE II

(continued)

Mode of Support and Loading	*Deflection and Bending Moment*
5. **Arbitrary end conditions. Compression end loads, distributed shear, end couples, and uniformly distributed lateral loading**	$y = C_1 y_1 + C_2 y_2 + C_3 y_3 + C_4 y_4 + \frac{w}{2\mu^2 P_0} y_5$ $\frac{M}{P_0 l} = (1+\alpha^3\mu x)(C_1 y_1 + C_2 y_2) + C_3\{(1+\alpha^3\mu x) y_3 - 1\} +$ $+ C_4\{(1+\alpha^3\mu x) y_4 - \mu x\} +$ $+ \frac{w}{2\mu^2 P_0}\{(1+\alpha^3\mu x) y_5 - (\mu x)^2\},$ where $C_1 \ldots C_4$ are arbitrary constants determined from the boundary conditions.
6. **Ends pin-ended. Distributed shear and end couples** 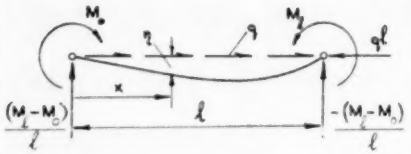 	$\eta = \frac{M_0}{ql}\left\{-(1+0{\cdot}813\bar{\eta}_2 - \lambda l\bar{\eta}_3)\frac{\eta_1}{\bar{\eta}_1} + 0{\cdot}813\eta_2 - \right.$ $\left. -\lambda l\eta_3 + 1\right\} + \frac{M_1}{ql}\left\{(1+0{\cdot}813\bar{\eta}_2)\frac{\eta_1}{\bar{\eta}_1} - 0{\cdot}813\eta_2 - 1\right\}$ $M = M_0\left\{-(1+0{\cdot}813\bar{\eta}_2 - \lambda l\bar{\eta}_3)\left(\frac{x}{l}\right)\frac{\eta_1}{\bar{\eta}_1} + \right.$ $\left. + 0{\cdot}813\left(\frac{x}{l}\right)\eta_2 - \lambda x\eta_3 + 1\right\} +$ $+ M_1\left\{(1+0{\cdot}813\bar{\eta}_2)\left(\frac{x}{l}\right)\frac{\eta_1}{\bar{\eta}_1} - 0{\cdot}813\left(\frac{x}{l}\right)\eta_2\right\}$
7. **Ends pin-ended. Distributed shear and uniform lateral loading** 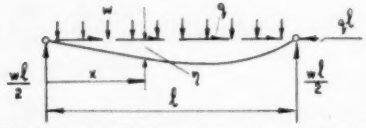 	$\eta = \frac{wl}{2q}\left\{0{\cdot}813\frac{\bar{\eta}_2}{\bar{\eta}_1}\eta_1 - 0{\cdot}813\eta_2 + \left(\frac{x}{l}\right) - 1\right\}$ $M = 0{\cdot}406wl^2\left(\frac{x}{l}\right)\left\{\frac{\bar{\eta}_2}{\bar{\eta}_1}\eta_1 - \eta_2\right\}$
8. **Ends pin-ended. Distributed shear and concentrated lateral load** 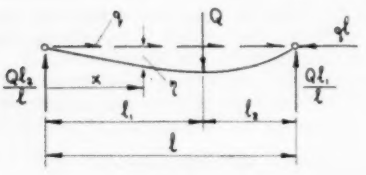 	$\eta = A\eta_1 + B\eta_2 - \frac{Ql_2}{ql}$ for $0 \leqq \lambda x \leqq \lambda l_1$ $\eta = C\eta_1 + D\eta_2 - \frac{Ql_1}{ql}\left(\lambda l\eta_3 - 1\right)$ for $\lambda l_1 \leqq \lambda x \leqq \lambda l$ $\frac{M}{q/\lambda} = \lambda x\,(A\eta_1 + B\eta_2)$ for $0 \leqq \lambda x \leqq l_1$ $\frac{M}{q/\lambda} = \lambda x\left(C\eta_1 + D\eta_2 - \frac{Ql_1}{ql}\lambda l\eta_3\right) + \frac{Ql_1}{ql}\lambda l$ for $\lambda l_1 \leqq \lambda x \leqq \lambda l$, where A, B, C and D are constants determined from the conditions that $\eta = 0$ at each end and the conditions that η and η' should be continuous at $x = l_1$.

TABLE II

(continued)

Mode of Support and Loading	*Deflection and Bending Moment*
9. Ends pin-ended. Eccentrically applied distributed shear 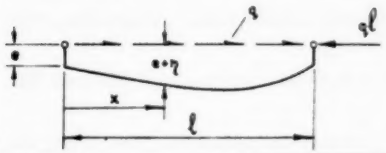	$\eta+e=e\left\{(1+0{\cdot}813\bar{\eta}_2)\frac{\eta_1}{\bar{\eta}_1}-0{\cdot}813\eta_2\right\}$ $M=eqx\left\{(1+0{\cdot}813\bar{\eta}_2)\frac{\eta_1}{\bar{\eta}_1}-0{\cdot}813\eta_2\right\}$
10. Arbitrary end conditions. Distributed shear, end couples, and uniformly distributed lateral loading	$\eta=A\eta_1+B\eta_2+C\eta_3+D+\frac{w}{2q\lambda}\ (\lambda x)$ $\frac{M}{q/\lambda}=\lambda x\,(A\eta_1+B\eta_2)+C\,(\lambda x\eta_3-1),$ where A, B, C and D are arbitrary constants determined from the boundary conditions.

For Case 3 these equations are given by

$$M=-EI\frac{d^2y}{dx^2}=(P_0+qx)y+Q\frac{l_2}{l}x, \qquad 0\leqslant x\leqslant l_1 \quad . \quad (74)$$

and

$$M=-EI\frac{d^2y}{dx^2}=(P_0+qx)\,y+Q\frac{l_2}{l}\,x-Q\,(x-l_1), \quad l_1\leqslant x\leqslant l. \quad . \quad (75)$$

Writing these equations in non-dimensional form as

$$y''+(1+\alpha^3\mu x)\,y=-\frac{Ql_2\mu x}{\mu lP_0}, \qquad 0\leqslant\mu x\leqslant\mu l_1 \quad . \quad (76)$$

and

$$y''+(1+\alpha^3\mu x)\,y=-\frac{Ql_1}{P_0}+\frac{Ql_1}{P_0}\,\frac{\mu x}{\mu l}, \qquad \mu l_1\leqslant\mu x\leqslant\mu l \quad . \quad (77)$$

it becomes clear that the general solutions for the deflections are given by (*see* equation (9))

$$y=Ay_1+By_2-\frac{Ql_2}{\mu lP_0}\,y_4, \qquad 0\leqslant\mu x\leqslant\mu l_1 \quad . \quad (78)$$

and

$$y=Cy_1+Dy_2-\frac{Ql_1}{P_0}\left(y_3-\frac{y_4}{\mu l}\right), \qquad \mu l_1\leqslant\mu x\leqslant\mu l. \quad . \quad (79)$$

Thus only four, instead of eight, arbitrary constants appear in the equations for deflections. These constants are determined from the conditions that $y=0$ at each end and the conditions that y and dy/dx should be continuous at $x=l_1$. The bending moment equation then follows simply from equation (5).

References

1. GREENHILL, A. G. On Height Consistent with Stability. *Proceedings of Cambridge Philosophical Society*, Vol. 4, 1881.

2. BÜLTMANN, W. Die Knickfestigkeit des geraden Stabes mit veränderlicher Druckkraft. *Der Stahlbau*, Vol. 17, pp. 49-50, May 1944, and Vol. 20, pp. 50-52, April 1951.

3. DUNCAN, W. J. Multiply-Loaded and Continuously Loaded Struts. *Engineering*, Vol. 174, pp. 180-182, 202-203, August 1952.

4. VON KÁRMÁN, T. and BIOT, M. A. *Mathematical Methods in Engineering*, McGraw-Hill, 1st Edition, p. 67, 1940.

5. WATSON, G. N. *Theory of Bessel Functions*. Cambridge University Press, Table III, Functions of order one-third, pp. 714-729, 1922.

6. KARAS, K. Tabellen für Besselsche Funktionen erster und zweiter Art mit den Parametern $\nu = \pm 2/3, \pm 1/4, \pm 3/4$. *Zeitschrift für Angewandte Mathematik und Mechanik*, Vol. 16, No. 4, pp. 248-252, August 1936.

7. JEFFREYS, H. and JEFFREYS, B. S. *Methods of Mathematical Physics*. Cambridge University Press, 2nd Edition, pp. 493-494, 1950.

Some Properties of the Admittances of Dynamical Chains

W. J. DUNCAN

(University of Glasgow)

SUMMARY: Simple relations among the coefficients appearing in the admittances of dynamical chains are obtained by considering the initial motions which follow the application of certain impulses.

1. Introduction

This paper is a sequel to Ref. 1 and relations among the coefficients appearing in the impulsive or indicial admittances of the simple dynamical chains considered there are obtained from an examination of the initial motions which follow the application of certain single impulses or systems of impulses. The reader may be reminded that the dynamical chains considered consist of a set of masses (or generalised masses) linearly arranged and with "elastic" connections between adjacent elements. The masses are $m_1, m_2 \ldots\ldots m_n$ and the corresponding displacements $x_1, x_2 \ldots\ldots x_n$ respectively. The stiffness of the connection between m_r and m_{r+1} is denoted by $c_{r,\,r+1}$ while that of the connection between m_1 and "earth" is c_{01}; the stiffness of the connection between m_n and earth is c_{n0}. When both c_{01} and c_{n0} are zero the system is called *unanchored*: otherwise it is *anchored*. For anchored systems with n degrees of freedom the typical impulsive admittance is

$$\alpha_{rs}(t) = \sum_{p=1}^{n} A_{rsp} \sin \omega_p t, \qquad (1)$$

where $\omega_1 \ldots\ldots \omega_n$ are the roots of the characteristic equation. An unanchored system with n degrees of freedom has the typical impulsive admittance

$$\alpha_{rs}(t) = A_0 t + \sum_{p=1}^{n-1} A_{rsp} \sin \omega_p t, \qquad (2)$$

where A_0 is the reciprocal of the sum of the masses of the system, while $\omega_1, \ldots\ldots, \omega_{n-1}$ are the roots of the reduced characteristic equation. The equations for determining the coefficients A_{rsp} were given in the earlier paper, together with explicit expressions for the impulsive admittances for two- and three-mass anchored and unanchored systems.

Received January 1960.

2. Unit Impulse Applied to r^{th} Mass

The system is initially at rest and all the displacements zero (elastic connections unstrained). Unit impulse is then applied to m_r at the instant $t=0$, so it acquires the initial velocity $1/m_r$. Consequently, *if we pay attention at present only to the lowest power of t appearing in the displacement*, we shall have

$$x_r = \frac{t}{m_r} . \qquad (3)$$

Now consider the adjacent mass m_{r+1}. Its neighbour m_{r+2} exerts no force upon it initially but, on account of (3), the mass m_r exerts a force upon it given by

$$F = x_r c_{r,r+1} = \frac{c_{r,r+1} t}{m_r} . \qquad (4)$$

Hence the initial motion of m_{r+1} is governed by the equation

$$m_{r+1} \ddot{x}_{r+1} = \frac{c_{r,r+1} t}{m_r} . \qquad (5)$$

while $x_{r+1} = \dot{x}_{r+1} = 0$ when $t=0$. Thus when t is very small

$$x_{r+1} = \frac{c_{r,r+1} t^3}{3! m_r m_{r+1}} . \qquad (6)$$

When the system is anchored the complete expression for this displacement is

$$x_{r+1} = z_{r,r+1}(t) = \sum_{p=1}^{n} A_{r,r+1,p} \sin \omega_p t, \qquad (7)$$

where n is the number of masses or degrees of freedom. Now expand the sines in powers of t and compare with (6). We get

$$\sum_{p=1}^{n} \omega_p A_{r,r+1,p} = 0 \qquad (8)$$

and

$$\sum_{p=1}^{n} \omega_p^3 A_{r,r+1,p} = -\frac{c_{r,r+1}}{m_r m_{r+1}} . \qquad (9)$$

For an unanchored system with n masses we obtain similarly

$$A_0 + \sum_{n-1}^{p=1} \omega_p A_{r,r+1,p} = 0 \qquad (10)$$

and

$$\sum_{p=1}^{n-1} \omega_p^3 A_{r,r+1,p} = -\frac{c_{r,r+1}}{m_r m_{r+1}} . \qquad (11)$$

Next consider the motion of m_{r+2}. The mass m_{r+3} initially exerts no force on m_{r+2}, but m_{r+1} exerts the force

$$x_{r+1}C_{r+1,r+2}=\frac{C_{r,r+1}C_{r+1,r+2}t^3}{3!m_rm_{r+1}}$$

on account of (6). Hence the expression for x_{r+2} with only the lowest power of t retained is

$$x_{r+2}=\frac{C_{r,r+1}C_{r+1,r+2}t^5}{5!m_rm_{r+1}m_{r+2}}. \quad . \quad . \quad . \quad . \quad . \quad (12)$$

On comparison with the complete expression for x_{r+2}, namely $\alpha_{r,r+2}(t)$, we obtain the following results.

For an Anchored System

$$\sum_{p=1}^{n}\omega_p A_{r,r+2,p}=0 \quad . \quad . \quad . \quad . \quad . \quad (13)$$

$$\sum_{p=1}^{n}\omega_p{}^3A_{r,r+2,p}=0 \quad . \quad . \quad . \quad . \quad . \quad (14)$$

$$\sum_{p=1}^{n}\omega_p{}^5A_{r,r+2,p}=\frac{C_{r,r+1}C_{r+1,r+2}}{m_rm_{r+1}m_{r+2}} \quad . \quad . \quad . \quad (15)$$

$$A_0+\sum_{p=1}^{n-1}\omega_p A_{r,r+2,p}=0 \quad . \quad . \quad . \quad . \quad (16)$$

For an Unanchored System

$$\sum_{p=1}^{n-1}\omega_p{}^3A_{r,r+2,p}=0 \quad . \quad . \quad . \quad . \quad . \quad (17)$$

$$\sum_{p=1}^{n-1}\omega_p{}^5A_{r,r+2,p}=\frac{C_{r,r+1}C_{r+1,r+2}}{m_rm_{r+1}m_{r+2}}. \quad . \quad . \quad (18)$$

Evidently the argument can be extended to the $(r+k)^{\text{th}}$ mass (where $r+k \not> n$) and zero summations similar to (13), (14), (16) and (17) will be obtained. The first non-vanishing summation will be

$$\Sigma\,\omega_p{}^{2k+1}A_{r,r+k,p}=(-1)^k\,\frac{C_{r,r+1}C_{r+1,r+2}\cdots C_{r+k-1,\,r+k}}{m_rm_{r+1}\cdots m_{r+k}}. \quad . \quad . \quad (19)$$

On account of the symmetry of the admittances we have

$$A_{rsp}=A_{srp}. \quad . \quad . \quad . \quad . \quad . \quad . \quad (20)$$

By use of this relation summations containing A_{rsp} with s less than r can be obtained from those already given.

It only remains to consider the initial motion of the mass itself. Its initial velocity is $1/m_r$, so we have for an anchored system

$$\sum_{p=1}^{n} \omega_p A_{rrp} = \frac{1}{m_r}, \qquad . \quad . \quad . \quad . \quad . \quad (21)$$

while for an unanchored system

$$A_0 + \sum_{p=1}^{n-1} \omega_p A_{rrp} = \frac{1}{m_r}. \qquad . \quad . \quad . \quad . \quad . \quad (22)$$

When t is very small the force on this mass is

$$-(c_{r-1,r} + c_{r,r+1})\, x_r.$$

It follows that

$$m_r \Sigma\ \omega_p{}^3 A_{rrp} = (c_{r-1,r} + c_{r,r+1})\ \Sigma\ \omega_p A_{rrp} \qquad . \quad . \quad . \quad (23)$$

All the foregoing equations may be checked and exemplified by the results given in the earlier paper for two- and three-mass systems.

For an anchored system with n masses the greatest value of k is $(n-1)$. Then there are n linear equations (terminating with (19)) for the n coefficients involved in the admittance and these may therefore be found. Thus the admittance

$$\alpha_{1n}(t) = \alpha_{n1}(t)$$

is obtained completely. For an unanchored system there are only $(n-1)$ unknown coefficients in each admittance, since A_0 is known. Hence the coefficients can be found from equations similar to the set (16)–(18) when $k = n-2$ and when $k = n-1$.

3. Impulses Proportional to the Respective Masses Applied Simultaneously

Impulses are applied simultaneously to all the masses in the same sense and the measure of the impulse applied to any mass is equal to the measure of this mass. Then all the masses initially have unit velocity. Moreover, when the system is unanchored the masses will continue to move uniformly with unit velocity and therefore without relative displacement. Hence, for an unanchored system,

$$\sum_{s=1}^{n} m_s \alpha_{rs}(t) = t. \qquad . \quad . \quad . \quad . \quad . \quad (24)$$

For an anchored system the condition that the initial velocity of m_r is unity yields

$$\sum_{s=1}^{n} \sum_{p=1}^{n} m_s \omega_p A_{rsp} = 1. \quad . \quad . \quad . \quad . \quad . \quad . \quad (25)$$

In this motion the extreme masses m_1 and m_n are subject to accelerations initially proportional to t, while the accelerations of the other masses are initially proportional to higher powers of t. Relations among the coefficients can be obtained by detailed arguments conducted along the lines of those given in Section 2, but these do not appear to be of much interest and will not be quoted.

REFERENCE

1. DUNCAN, W. J. Impulsive and Indicial Admittances of Simple Dynamical Chains. *Aeronautical Quarterly*, Vol. IX, p. 1, February 1958.

Correspondence

Impulsive and Indicial Admittances of Simple Dynamical Chains

At the end of the paper by PROFESSOR DUNCAN, published in the February 1958 issue of *The Aeronautical Quarterly* (Vol. IX, p. 1), the author writes that it has not so far been proved that all the coefficients A_{rrp} occurring in the *direct* admittances $\alpha_{rr}(t)$ are positive. A correspondent, MR. ROBERT J. FITZGERALD, of Massachusetts Institute of Technology, has now supplied a proof of this, as follows.

If we express the forced-vibration mode shape $[A]$ of a system as a sum of the natural mode shapes $[A_i]$ $(i=1, 2, \ldots, n)$ we get

$$[A] = \sum_{i=1}^{n} \frac{[A_i]^T [F] [A_i]}{[A_i]^T [M] [A_i]} \frac{1}{\omega_i^2 - \omega^2}$$

where $$[A] = \begin{bmatrix} a_1 \\ a_2 \\ . \\ . \\ a_n \end{bmatrix}, \qquad [A_i] = \begin{bmatrix} a_{1i} \\ a_{2i} \\ . \\ . \\ a_{ni} \end{bmatrix},$$

$$[F] = \begin{bmatrix} f_1 \\ f_2 \\ . \\ . \\ f_n \end{bmatrix}$$ is the set of applied force amplitudes at frequency ω,

and $[M]$ is the inertia matrix. The superscript "T" denotes that a matrix is to be transposed.

In the case of the direct admittance, $\alpha_{rr}=a_1/f_1$, we let $f_2=f_3=\ldots=f_n=0$, and obtain

$$\alpha_{rr}(\omega)=\frac{a_1}{f_1}=\sum_{i=1}^{n}\frac{a_{1i}^2}{[A_i]^T[M][A_i]}\frac{1}{\omega_i^2-\omega^2}=\sum_{i=1}^{n}\frac{C_i}{\omega_i^2-\omega^2},$$

in which $C_i>0$ $(i=1, 2, \ldots, n)$, since the denominators are positive due to the positive definite nature of $[M]$.

If we replace ω^2 by $-s^2$ in $\alpha_{rr}(\omega)$, we get the Laplace transform of the impulse response

$$\alpha_{rr}(s)=\sum_{i=1}^{n}\frac{C_i}{s^2+\omega_i^2},$$

as can be shown by taking Laplace transforms in the original matrix dynamic equation.

Taking the inverse transform, the impulse response becomes

$$\alpha_{rr}(t)=\sum_{i=1}^{n}\frac{C_i}{\omega_i}\sin\omega_i t$$

in which all the coefficients are positive.

BRISTOL
Aircraft

EXPANDING COMMITMENTS LEAD TO AN EXPANDING GUIDED WEAPON TEAM

there are opportunities for—

ADVANCED WORK ON HYPERSONIC PROJECTS

AERODYNAMICS—
Aeronautical Engineers or Mathematicians

A1. Advanced problems of hypersonic flow and their application to configuration design.

A2. Unsteady flow aerodynamics.

A3. Stability and response.

A4. Supersonic project aerodynamics.

A5. Hypersonic flutter.

STRUCTURES—
Engineers or Mathematicians

S1. Project design of advanced missiles.

S2. Heat transfer problems.

INSTRUMENTS—
Physicists

P1. Optical devices, including mosaic systems, colour densitometry and flight camera installations.

P2. Gyroscopes, pressure measuring devices and electro-mechanical instruments.

FLIGHT SYSTEMS—

F1. **Mathematicians or Engineers** for theoretical studies and development on missile servo-control systems.

F2. **Mechanical Engineers** for theoretical studies and development on hydraulic and fuel systems.

F3. **Physicists or Electronic Engineers** for radome development.

F4. **Physicists or Electronic Engineers** for aerial development.

ELECTRONIC TECHNIQUES—
Physicists

E1. Development of techniques associated with advanced electronic devices.

WEAPON SYSTEMS—
Mechanical and Electrical Engineers

W1. Liaison with manufacturers of the Bloodhound Weapon System in connection with overseas sales.

These extremely interesting opportunities are offered by a member of Europe's largest guided weapon consortium, which has recently received large orders for Bloodhound.

Applicants should have a degree or similar qualifications and 2 or 3 years' experience in related fields. Salaries will match the high standards required and assistance will be given with housing and removal expenses.

Please write to Mr J. Raimes, giving full details of age, qualifications and experience and quote the reference numbers of the posts in which you are interested. Further information on these posts will be supplied on request.

J. Raimes, Personnel Manager,
Bristol Aircraft Ltd, Room AEO/60/AQ,
Filton, Bristol.

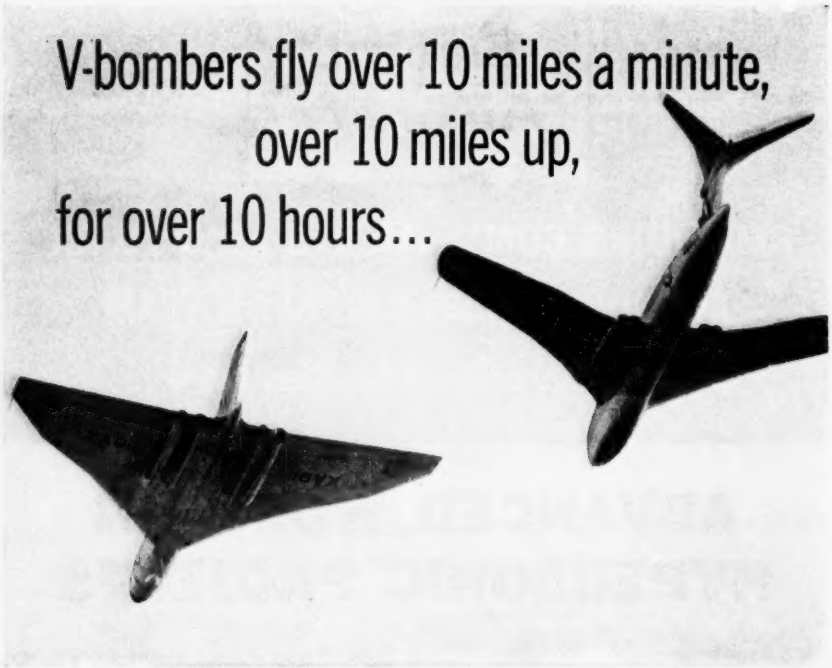

...AND BRISTOL SIDDELEY SUPPLY THE POWER

One of the largest manufacturers of motive power units in the world, Bristol Siddeley Engines Limited produce two outstanding high-thrust turbojet engines—the Olympus and the Sapphire. Between them these two engines power the major part of the RAF's strategic V-bomber force. The Olympus, which delivers 17,000 lb thrust dry (other versions are rated at 33,000 lb), powers the Avro Vulcan Mk 1 and 2. The Sapphire powers the Handley Page Victor Mk 1. These engines give the V-bombers sonic capability—long range—great altitude—superior performance to any other aircraft of their type in the world.

Bristol Siddeley products currently in production include:—

AERO

TURBOJETS: Olympus, Sapphire, Orpheus, Viper.
TURBOPROPS: Proteus, Double Mamba.
ROCKETS: Gamma.
RAMJETS: Thor.

INDUSTRIAL & MARINE

DIESELS: Maybach.
GAS TURBINES: Proteus.
CARS: Armstrong Siddeley Star Sapphire, Bristol 406.
OTHER PRODUCTS: Gas bearing compressors, Beaver ball screws and splines.

BRISTOL SIDDELEY ENGINES LIMITED

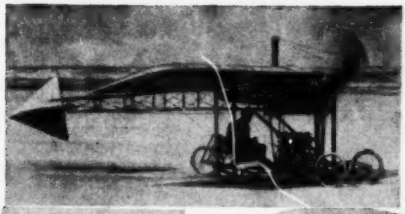

50

50 years of experience are behind the Blackburn NA.39

1909 Robert Blackburn designed, built and flew his first aircraft at Marske Sands in Yorkshire.

1959 Latest of a long line, the Blackburn NA.39 Strike Aircraft which first flew on its target date in April, 1958, is now in production. Of this aircraft the Ministry of Defence has stated "In the low-level strike role, the NA.39 is ahead of any aircraft in the world"

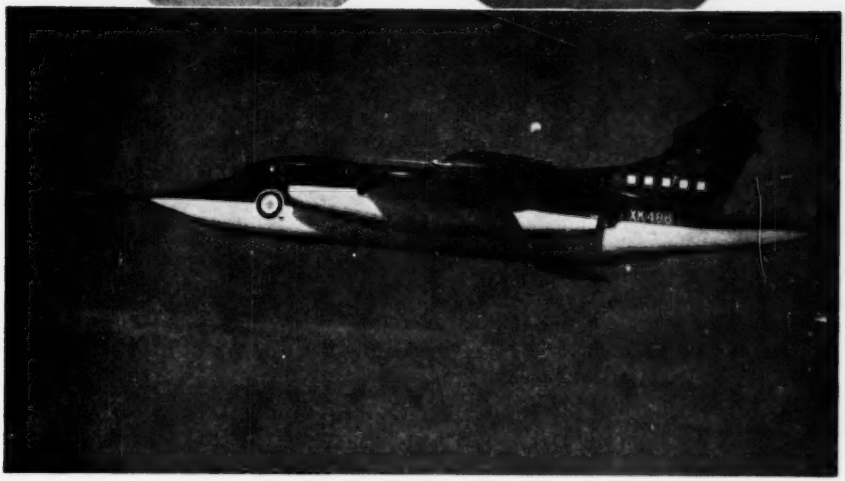

If you are an A.F.R.Ae.S. or possess an equivalent qualification, please write to the Technical Staff Manager, when we shall be pleased to give you details of the opportunities available to experienced men within our technical organisation.

Blackburn Aircraft Limited, Brough, Yorkshire

A128/d

CHAPMAN AND HALL

Published under the authority of the
Royal Aeronautical Society

AIRCRAFT HYDRAULICS

edited by

H. G. CONWAY

Volume I—Hydraulic Systems

Size 10 in. x 6 in. 146 pages 107 illustrations

35s. net

Volume II—Component Design

Size 10 in. x 6 in. 216 pages 120 illustrations

45s. net

INSTRUMENTATION IN TESTING AIRCRAFT

by C. N. JAQUES

Size 8¾ in. x 5½ in. 292 pages 117 illustrations

45s. net

LANDING GEAR DESIGN

by H. G. CONWAY

Size 10 in. x 6 in. 342 pages 366 illustrations

56s. net

AIRCRAFT ELECTRICAL ENGINEERING

edited by

G. G. WAKEFIELD

Size 10 in. x 6 in. 350 pages 201 illustrations

50s. net

37 ESSEX STREET - LONDON WC2

NOTICE TO CONTRIBUTORS

1. All communications should be addressed to the Editor, The Aeronautical Quarterly, 4 Hamilton Place, London, W.1.

2. Papers for consideration should be typewritten with double spacing and be accompanied by a summary of not more than 250-300 words. *Papers must be as short as possible*, otherwise considerable delay in publication will result, and in any case they should not be longer than twenty foolscap pages. Full descriptions and complete results of work, as written for an internal report, are not suitable for publication in *The Aeronautical Quarterly*, and such reports need to be rewritten in concise form. Only necessary equations should be included in the text; routine mathematics should be omitted or given as an Appendix to the Paper. Illustrations should be reduced to a minimum. The titles of papers should be kept short—with sub-titles if necessary.

3. Only simple symbols and formulae should be typewritten. All others should be written clearly in ink. Greek letters should be indicated and a clear distinction drawn between capital and small letters. Particular attention should be paid to the use of alpha and *a*, kappa and *k*, mu and *u*, nu and *v*, eta and *n*. The letter *l* must be distinguished from the numeral 1, and the letter *O* from the zero 0.

   The use of dots, bars, and so on, over letters, or the use of dots as multiplication signs and bars for brackets should be avoided as far as possible.

   Suffixes and prefixes must be indicated clearly and complicated suffixes and prefixes should be avoided.

4. A list of *all* symbols used, both in the illustrations and text, *must* be given at the end of the paper whether they are standard or not.

5. *Clear* diagrams or sketches must be submitted for redrawing by the Society's draughtsman.

   Photographs must be not less than half plate size and must be clear black and white glossy prints.

6. References should be given in the form:—
   WARD, G. N. Calculation of Downwash Behind a Supersonic Wing. *The Aeronautical Quarterly*, Vol. I, pp. 35-38, May 1949.

7. The copyright of every paper printed in *The Aeronautical Quarterly* is the property of The Royal Aeronautical Society. Permission to reprint or to use any paper will not be unreasonably refused.

8. It is a condition of publication that the author shall have obtained consent where necessary to use any material in his paper which is copyright or the property of any other person or his employers.

9. Authors will be entitled to 20 reprints of their papers free of charge. This number will be shared between joint authors.

The Aeronautical Quarterly is published at the Offices of The Royal Aeronautical Society, 4 Hamilton Place, Piccadilly, London, W.1, at 15s. 0d. net for a single number to non-members and 7s. 6d. net for a single number to members of The Royal Aeronautical Society. Instructions for Contributors are given above. None of the papers must be taken as expressing the opinion of the Council of The Royal Aeronautical Society unless such is definitely stated to be the case. All communications for publication or advertisement in The Quarterly should be addressed to—The Editor, The Aeronautical Quarterly, 4 Hamilton Place, W.1.

Telephone: Grosvenor 3515 (5 lines). Telegraphic Address: Didaskalos, Audley, London

CHAPMAN AND HALL

Published under the authority of the
Royal Aeronautical Society

AIRCRAFT HYDRAULICS

edited by

H. G. CONWAY

Volume I—Hydraulic Systems

Size 10 in. x 6 in. 146 pages 107 illustrations

35s. net

Volume II—Component Design

Size 10 in. x 6 in. 216 pages 120 illustrations

45s. net

INSTRUMENTATION IN TESTING AIRCRAFT

by C. N. JAQUES

Size 8¾ in. x 5½ in. 292 pages 117 illustrations

45s. net

LANDING GEAR DESIGN

by H. G. CONWAY

Size 10 in. x 6 in. 342 pages 366 illustrations

56s. net

AIRCRAFT ELECTRICAL ENGINEERING

edited by

G. G. WAKEFIELD

Size 10 in. x 6 in. 350 pages 201 illustrations

50s. net

37 ESSEX STREET - LONDON WC2

NOTICE TO CONTRIBUTORS

1. All communications should be addressed to the Editor, The Aeronautical Quarterly, 4 Hamilton Place, London, W.1.

2. Papers for consideration should be typewritten with double spacing and be accompanied by a summary of not more than 250-300 words. *Papers must be as short as possible*, otherwise considerable delay in publication will result, and in any case they should not be longer than twenty foolscap pages. Full descriptions and complete results of work, as written for an internal report, are not suitable for publication in *The Aeronautical Quarterly*, and such reports need to be rewritten in concise form. Only necessary equations should be included in the text; routine mathematics should be omitted or given as an Appendix to the Paper. Illustrations should be reduced to a minimum. The titles of papers should be kept short—with sub-titles if necessary.

3. Only simple symbols and formulae should be typewritten. All others should be written clearly in ink. Greek letters should be indicated and a clear distinction drawn between capital and small letters. Particular attention should be paid to the use of alpha and *a*, kappa and *k*, mu and *u*, nu and *v*, eta and *n*. The letter *l* must be distinguished from the numeral 1, and the letter *O* from the zero 0.

   The use of dots, bars, and so on, over letters, or the use of dots as multiplication signs and bars for brackets should be avoided as far as possible.

   Suffixes and prefixes must be indicated clearly and complicated suffixes and prefixes should be avoided.

4. A list of *all* symbols used, both in the illustrations and text, *must* be given at the end of the paper whether they are standard or not.

5. *Clear* diagrams or sketches must be submitted for redrawing by the Society's draughtsman.

   Photographs must be not less than half plate size and must be clear black and white glossy prints.

6. References should be given in the form:—
   WARD, G. N. Calculation of Downwash Behind a Supersonic Wing. *The Aeronautical Quarterly*, Vol. I, pp. 35-38, May 1949.

7. The copyright of every paper printed in *The Aeronautical Quarterly* is the property of The Royal Aeronautical Society. Permission to reprint or to use any paper will not be unreasonably refused.

8. It is a condition of publication that the author shall have obtained consent where necessary to use any material in his paper which is copyright or the property of any other person or his employers.

9. Authors will be entitled to 20 reprints of their papers free of charge. This number will be shared between joint authors.

The Aeronautical Quarterly is published at the Offices of The Royal Aeronautical Society, 4 Hamilton Place, Piccadilly, London, W.1, at 15s. 0d. net for a single number to non-members and 7s. 6d. net for a single number to members of The Royal Aeronautical Society. Instructions for Contributors are given above. None of the papers must be taken as expressing the opinion of the Council of The Royal Aeronautical Society unless such is definitely stated to be the case. All communications for publication or advertisement in The Quarterly should be addressed to—The Editor, The Aeronautical Quarterly, 4 Hamilton Place, W.1.

Telephone: Grosvenor 3515 (5 lines). Telegraphic Address: Didaskalos, Audley, London

THE AERONAUTICAL QUARTERLY

It is the aim of *The Aeronautical Quarterly* to attract not only original papers contributing to aeronautical science and engineering, and papers developing new or improved methods of analysis and experimental techniques, but also papers on allied sciences which have a bearing on aeronautical problems. *The Aeronautical Quarterly* is open to authors of any nationality and is not restricted to members of the Society.

VOLUME XI

Volume XI of *The Aeronautical Quarterly* will be published in four parts, in February, May, August and November 1960. The prices, *including postage and packing*, are:—

	To Members of the Society		*To Non-Members*	
	£ s. d.		£ s. d.	
Per Part	8 0	($1.15)	15 6	($2.20)
Subscription (4 parts)	1 12 0	($4.50)	3 2 0	($8.70)

Papers to be published in forthcoming issues include:—

M. D. Wood, J. H. Horlock and E. K. Armstrong—Experimental Investigations of the Stalled Flow of a Single-Stage Axial Flow Compressor.

R. Hicks—The Bending and Twisting of a Flat Elastic Plate with a Reinforced Circular Hole.

W. S. Coleman—A Theoretical Approach to the Aerodynamically Significant Characteristics of Roughness from Insects.

C. Bourque and B. G. Newman—Reattachment of a Two-Dimensional, Incompressible Jet to an Adjacent Flat Plate.

D. B. Spalding—Heat and Mass Transfer in Aeronautical Engineering.

PRINTED BY THE LEWES PRESS, WIGHTMAN & CO. LTD., LEWES, SUSSEX, ENGLAND, AND PUBLISHED BY THE ROYAL AERONAUTICAL SOCIETY, 4 HAMILTON PLACE, LONDON, W.1, ENGLAND.